MORPHOLOGICAL AND PHYSIOLOGICAL PROPERTIES OF AMACRINE CELLS LOCATED IN THE GANGLION CELL LAYER OF THE FERRET RETINA

by

Sally Wahba Aboelela

A DISSERTATION

Presented to the Department of Physiology and Pharmacology

and the Oregon Health & Science University

School of Medicine

in partial fulfillment of
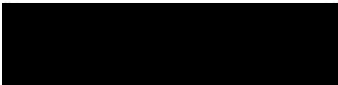
the requirements for the degree of

Doctor of Philosophy

September 2003

School of Medicine
Oregon Health & Science University

CERTIFICATE OF APPROVAL

This certifies that the Ph.D. thesis of

Sally Wahba Aboelela

has been approved

David W. Robinson Ph.D

Charles Allen Ph.D

Craig Jahr Ph.D

Henrique VonGersdoff Ph.D

John Williams Ph.D.

TABLE OF CONTENTS

List of Illustrations

List of Abbreviations

AHP	After Hyperpolarization
DAB	3,3'-Diaminobenzidine
DAC	Displaced Amacrine Cell
DSGC	Direction-Selective Ganglion Cell
EMEM	Eagle's Minimum Essential Media
GCL	Ganglion Cell Layer
Glu	Glutamate
HRP	Horseradish Peroxidase
INL	Inner Nuclear Layer
IPL	Inner Plexiform Layer
K(Ca)	Calcium-Mediated Potassium Channel
mGLUR	Metabotropic Glutamate Receptor
ONL	Outer Nuclear Layer
OPL	Outer Plexiform Layer
PDE	Phosphodiesterase
TTX	Tetrodotoxin
VS_N	Dendritic Normalized Vector Sum

Acknowledgments

There are many people who have contributed to the completion of this thesis. My gratitude first goes to my advisor Dr. David W. Robinson. When I joined Dr. Robinson's laboratory I knew nothing about the retina and had never done any electrophysiology. He patiently spent several months training me and making himself available to answer my many questions. The trait I value most in Dr. Robinson as a teacher, advisor, and friend is his ability to take on challenges as they arise, never lose his sense of humor, and come out successful in the end.

My sincere gratitude also goes to my lab mate and friend, Erin Warren. Erin has made invaluable intellectual contributions to my work through formal and informal lab meeting conversations. Also, her diligence and commitment has served as a source of inspiration for me on many occasions. She is an outstanding scientist and I am honored to have had an opportunity to work with her. Personally, she has also been an invaluable source of support and comic relief. I will always cherish the time we spent together as students in Dr. Robinson's lab.

I would also like to thank the members of the Andresen lab, especially Dr. Timothy Bailey, for the material and intellectual contributions they generously made on many occasions. Dr. Timothy Bailey has also been a valuable friend to me and has graciously given me personal and professional advice whenever I asked for it. I would also like to thank Dr. William Cameron for the generous use of his lab equipment and lab space for the entire duration of my career with Dr. Robinson.

Finally, I would like to extend my deepest gratitude to my family. They have always given me unconditional love and support without which I would not be who I am.

Abstract

This thesis examines Displaced Amacrine Cells (DACs) of the ferret retina for their physiological and morphological diversity. The two main goals were to gather information and then find correlations between anatomy and physiology as a means of compiling enough data to identify potential functional groups. Patch-clamp recordings were made on a total of 185 DACs in whole-mount ferret retina. Included in the recording pipette were lucifer yellow (for immediate post-recording visualization) and biocytin for later tissue processing using a DAB reaction, which produces a light-stable product. Three-dimensional anatomical reconstructions were made for a total of 55 neurons using Neuolucida software. The passive (resting membrane potential, input resistance, and spontaneous activity) and excitable membrane properties (spiking activity and whole cell currents) were examined using both current and voltage clamp techniques. A total of 6 physiological groups were identified and discussed, including: non-spiking cells, transiently spiking cells, continuously spiking cells, cells that are quiet at rest, cells that are synaptically active at rest, and cells that are spontaneously oscillatory. When observed under voltage-clamp conditions, there were two clear patterns for spontaneous oscillations. Fluctuations in activity observed in "summating" oscillatory cells seemed to be composed of unitary synaptic events that often summated at peak, while "baseline" oscillatory cells seemed to experience periodic fluctuations in baseline current. Both patterns of oscillatory behavior among DACs represent a previously unidentified and therefore novel pattern of amacrine cell activity in the adult ferret retina. This activity was blocked in 10 out of 10 DACs using the potent gap junction blocker, Carbenoxolone.

1

A model of the circuitry underlying DAC oscillations (included gap junction synapses between some DACs) was proposed. A total of eight morphological groups of DACs were also identified and discussed. Six of those groups emerged as a result of rigorous statistical analysis of data from several functionally relevant anatomical characteristics. By compiling and comparing the data from dendritic extent size, distribution index, circularity index, and number of nodes, two morphological groups emerged: the **"small-circular-complex"** (30% of population) DACs and the **"Large-non-circular-simple"** (30% of population) DACs. The examination of depth of stratification resulted in the identification of both the **"ON"-layer stratifying** and **"OFF"-layer stratifying** DACs. A combination of degree of symmetry and dendritic distribution index was used to identify the **"radially symmetric"** and **"non-radially symmetric"** DACs. Finally, the **"orientation-biased"** DACs and the **"Direction or/Approach – Biased"** DACs were identified based on their anatomical resemblance to previously identified physiological amacrine cell types.

The physiological and morphological cell types described above lay the foundation for further DAC study. Any or all of the cell types can now become functionally defined through rigorous examinations. Complete comparisons between the physiological and anatomical groups will be useful to determine potential roles in retinal circuitry. Moreover, more detailed investigations of the physiological properties uncovered in this study will contribute a great deal to our understanding of the DAC population. The present study represents an important step in the discovery of the contribution DACs make to retinal circuitry, which may prove to increase our more general understanding of the role all amacrine cells play in retinal processing.

Chapter 1

Introduction

There are many motivations behind the study of the retina. In addition to providing insight into the first stages of vision, the retina has served as a manageable model in which to study information processing by neuronal circuits. Since the retina is a portion of the central nervous system, and therefore has the same basic neuronal organization, an understanding of retinal processing may shed light on how information is handled by less approachable parts of the brain. Vision has also been an attractive system to work in from a sensory perspective due to the ease of stimulation using light and the particularly accessible and long optic nerve running from the retina to higher brain centers.

The retina is located in front of the pigment epithelium that lines the back of the eye. The rest of the eye is designed to focus the visual image on the retina with the least amount of optical distortion. Light enters the eye, is focused by the cornea and the lens, and then passes through the vitreous humor until it reaches the retina (Figure 1.1). Light must travel through the thickness of the transparent retina until it reaches the photoreceptors that are imbedded in the pigment epithelium layer in the most distal portion of the eye. The cells of the pigment epithelium are rich in black melanin, which absorb any light not captured by the retina that would otherwise reflect back and degrade the visual image. There is an area on the mammalian retina called the fovea, or area centralis in cat and visual streak in rabbit, where visual acuity is at its highest. During vision, the position of the eyes is continuously readjusted to reflect the visual object onto the fovea (32).

The retina is the first stage of vision and must code all the qualities of light that higher visual centers will use for visual perception. This remarkable task is accomplished

4

by a layer of neuronal tissue with a thickness half that of a credit card. In order to understand how this is done, is it necessary to investigate the cellular structure and organization of the retina.

Cellular Composition and Organization

The greatest contribution to the study of retinal neurons has been the application of the Golgi silver-impregnation staining method to the retina, first by Tartuferi in 1887 and extensively later by Santiago Ramón y Cajal in 1892 (Figure 1.2)(32). This method was capable of staining, although sporadically, entire nerve cells from the finest dendritic branches to the axonal terminals with remarkable resolution. The majority of what is known about retinal cell types and their distribution is based on light microscopic examinations of Golgi stained retina.

The organization of all vertebrate retinas consists of two synaptic layers, the inner and outer plexiform layers, and three cellular layers: the outer and inner nuclear layer and the ganglion cell layer (Figure 1.3). This organization is similar to the gray (somal) and white (axonal) matter in other regions of the CNS. There are six major classes of retinal neurons (photoreceptors, horizontal cells, bipolar cells, amacrine cells, interplexiform cells, and ganglion cells) and one type of retinal glial cell (the Müller glial cell). The somas of the photoreceptors lie in the Outer Nuclear Layer (ONL), while the somas of the horizontal, bipolar, interplexiform, and a significant subset of the amacrine cells lie in the Inner Nuclear Layer (INL).
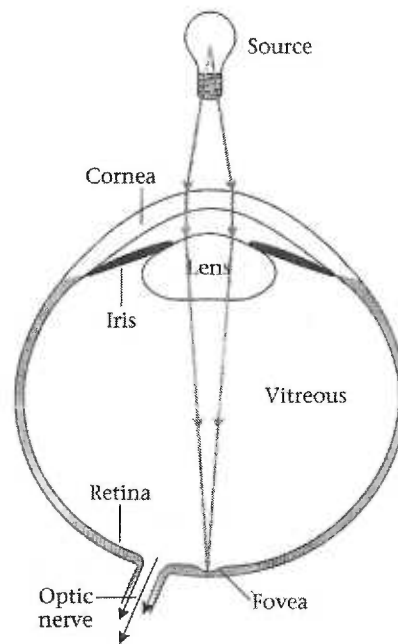
Figure 1.1. The Anatomy of the Eye – A schematic drawing of the path light takes as it enters the eye. Light passes through the Cornea, Lens, and the Vitreous fluid before it reaches the Retina.

(32)
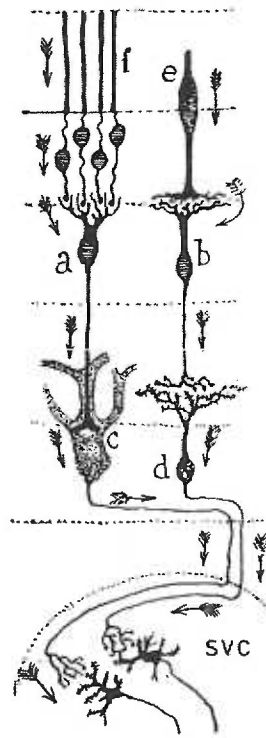
Figure 1.2. Cajal's Work in The Retina – Drawings by Ramón y Cajal (1889) of the retinal neurons (ox retina) he encountered in his studies using the Golgi-impregnation method. (61)

a.

R
olm
ONL
OPL
INL
M   M
IPL
GCL
ilm

30 µm

b.

R   R
H
B
B
A
M
I
G
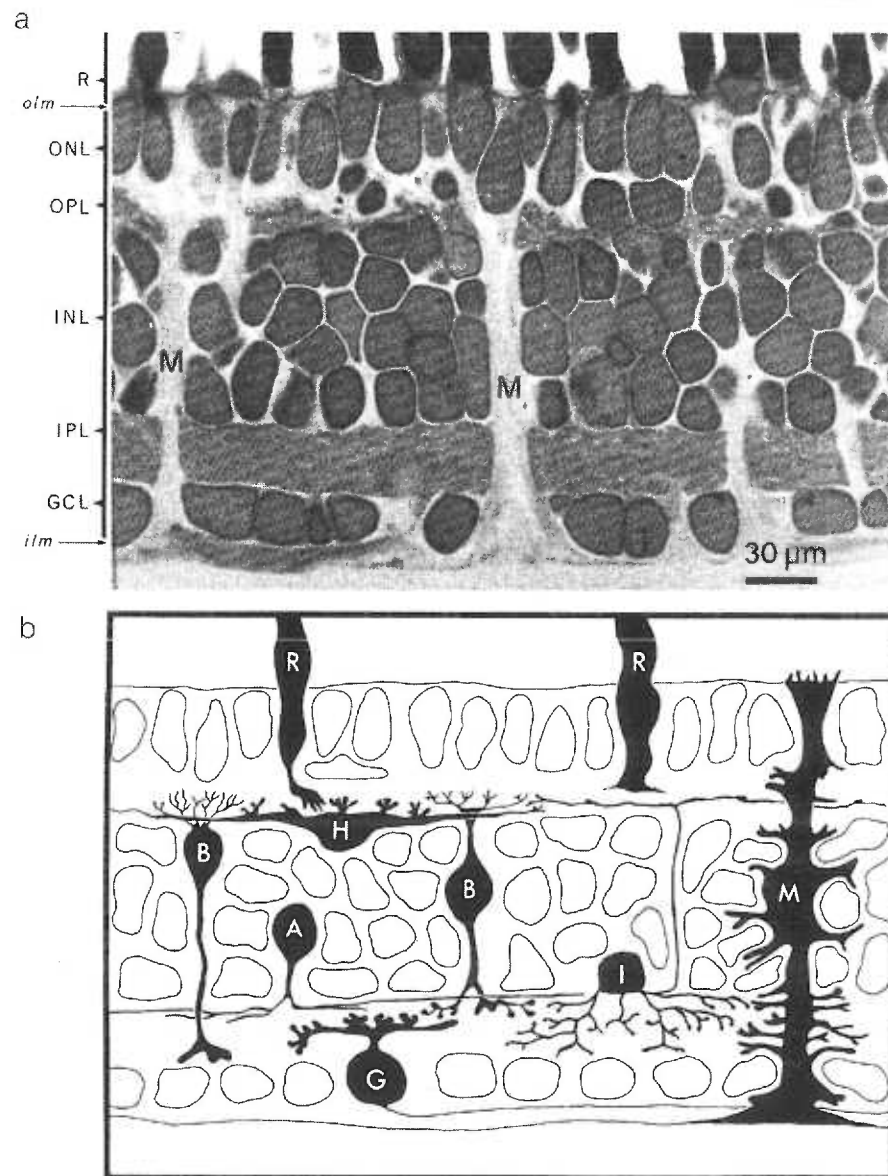
Figure 1.3. Retinal Layers and Cellular Components - **a.** A light micrograph of Mudpuppy retina, M = Muller cell. **b.** Drawing of golgi stained mudpuppy retina; R = photoreceptors, H = horizontal cells, B = bipolar cells, A = amacrine cells, I = interplexiform layer cells, M = Muller cells. (32)

The somas of the ganglion cells and a second subset of the amacrine cells occupy the Ganglion Cell Layer (GCL). The Müller glial cells extend vertically throughout the retina, from the distal margin of the ONL to the outer border of the GCL. The junctions of all Müller cell terminals seam together to form the Inner Limiting Membrane.

Present in the Outer Plexiform Layer (OPL) are synaptic connections between the photoreceptor terminals, the horizontal cells, and the bipolar dendritic projections. Conversely, in the Inner Plexiform Layer (IPL) there are synaptic interactions among the bipolar axon terminals, the dendritic projections of both subsets of amacrine cells and the dendritic projections of the ganglion cells.

Before a full understanding can be reached regarding the flow of light information through this organization of neurons, it is important to understand the unique properties of each cell type.

Photoreceptors

The photoreceptors are the primary light sensors; they convert light that enters the eye into a neuronal signal via a process termed phototransduction. There are two major classes of photoreceptors; the rods that are sensitive to very low light intensities and the cones that respond to higher light intensities and mediate color vision. Each photoreceptor is composed of an outer segment containing the phototransduction machinery, an inner segment containing the cell body, and a synaptic terminal that makes contact with bipolar and horizontal cells. Rods and cones are easily differentiated anatomically through the shape of their outer segments, logically: one has an oblong rod shape and the other is more conical (Figure 1.4). Mammals have only one type of rod cell

9

but three distinct cone cell types based on their visual pigment and its respective optimal wavelength of light absorption: green, blue, and red (32; 44).

Located along the membrane of the photoreceptor outer segments are sodium channels gated by the cyclic nucleotide, cGMP. In the absence of light, cGMP levels are high and the Na+ channels are open. This phenomenon produces what is called the dark current; the absence of light causes photoreceptors to be depolarized. Light stimulation causes a decrease in cGMP levels and results in an attenuation of the dark current, a hyperpolarization (Figure 1.5). Light alters intracellular cGMP levels, and therefore the number of open sodium channels, by regulating the activating of Phosphodiesterase (PDE) responsible for the breakdown of cGMP to GMP (44). In darkness, PDE is in its inactive form, a result of an inhibitory constraint imposed by one of the protein's own subunits (69).

Light causes a photoisomerization of the chromophore, rhodopsin. Activated rhodopsin then interacts with the G protein, transducin, catalyzing the release of bound GDP and the binding of GTP. Transducin, in its GTP-bound form, is then capable of binding to and activating PDE. Active PDE then breakdowns cGMP, causing a decrease in the concentration of intracellular cGMP and the closing of cyclic nucleotide gated Na+ channels (Figure 1.6). As a result, light, in an intensity-dependent manner, causes the attenuation of the dark current and a hyperpolarization of the photoreceptor (44; 69).

Photoreceptors are not capable of generating action potentials. These cells respond to light in a graded fashion that is dependent upon the stimulus intensity.
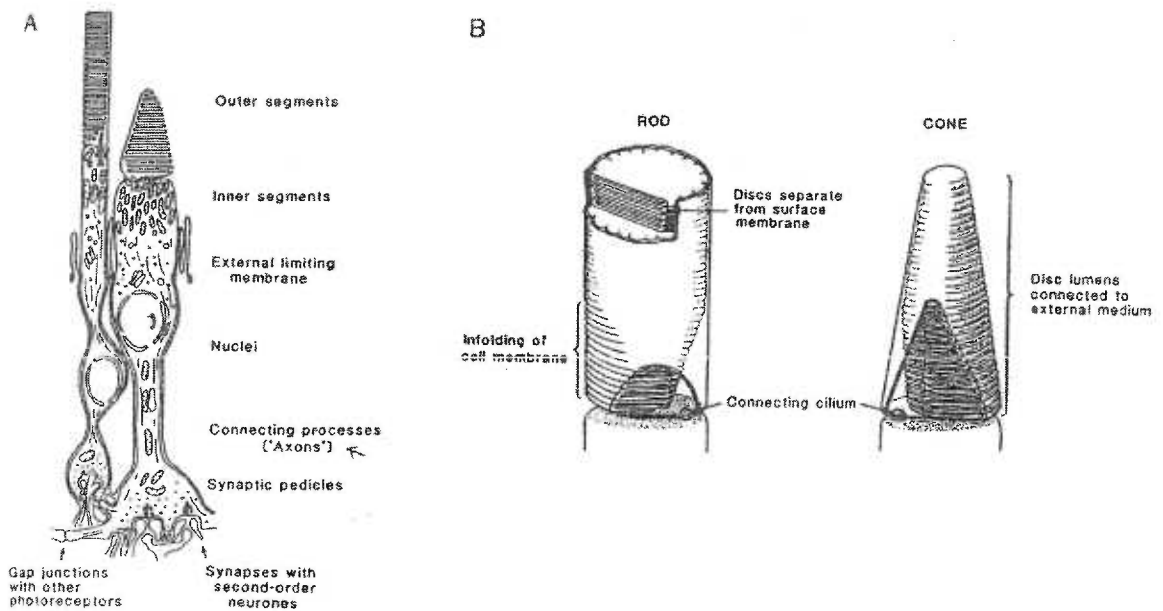
Figure 1.4. Rod and Cone Photoreceptor Anatomy – Structural diagram of vertebrate rods and cones. **A** - rods on the left and cones on the right. **B** - Outer segments of both rod and cone photoreceptors. Visible are the membranous disks that house the phototransduction machinery.

(44)
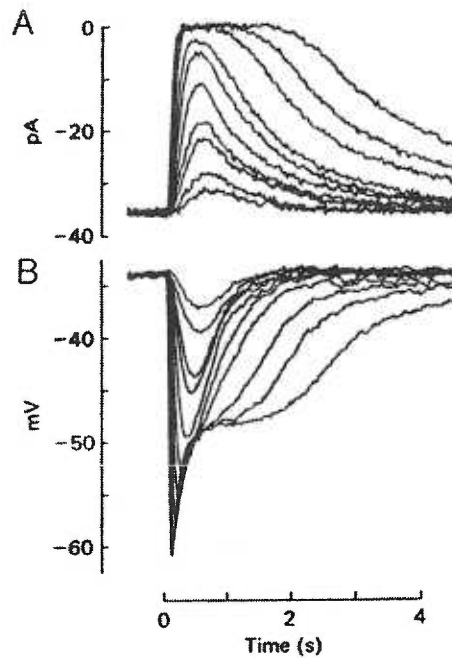
Figure 1.5. Photoreceptor Light Responses - Light responses of red rod outer

segments. Light flashes were of increasing intensity, approximately double.

Outer segment current was recorded using a suction electrode and membrane

potential was recorded with a microelectrode inserted into the inner segment.

A. membrane current, **B.** internal potential

Each trace represents a different light intensity.

(44)
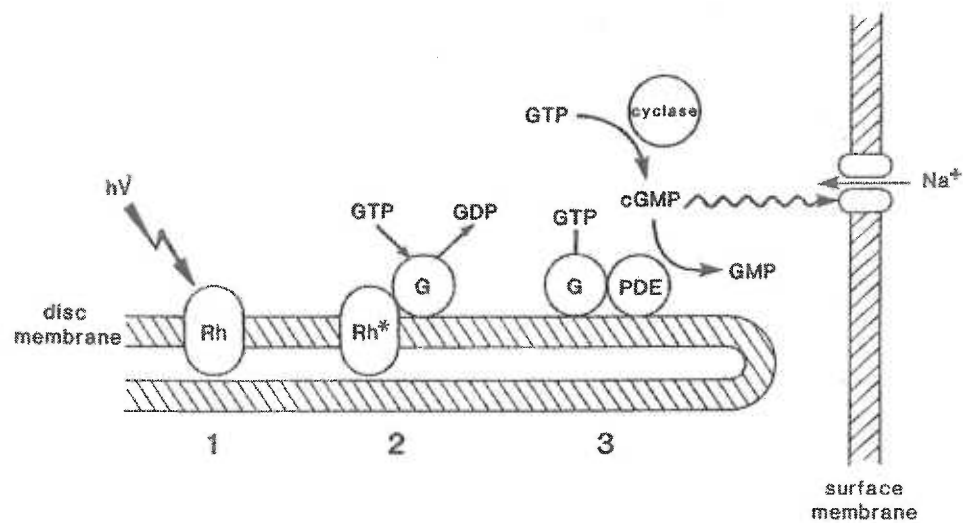
Figure 1.6. Phototransduction Cascade – Diagram of the Phototransduction Cascade that occurs at the membranous disks. **1** – The Chromophore, Rhodopsin (Rh), undergoes a photoisomerization in response to light. **2** – Active Rhodopsin (Rh*) binds to the G-protein, Transducin (G), which in turn catalyzes the binding of GTP and the release of GDP. **3**- Transducin, in its GTP-bound form, can activate Phosphodiesterase (PDE). Active PDE then catalyzes the breakdown of cGMP to GMP. The intracellular concentrations of cGMP then decrease, which cause the closing of cyclic nucleotide gated sodium channels and an attenuation of the dark current

(44)

This property is essential to code for the dynamic changes in light levels presented to our visual system by our environments. The all or nothing response property associated with action potentials is inappropriate for converting the spectrum of light levels that lie between full brightness and total darkness into a neuronal signal.

Horizontal Cells

There are two basic types of horizontal cells, one without an axon and one with a short axon (~400μm) (Figure 1.7). Horizontal cells have somas that reside in the outer margin of the INL and make synaptic connections with predominately photoreceptors. These cells receive synaptic input from a "primary" light sensor and send projections to neighboring photoreceptors. In the cat retina, there is a clear synaptic segregation between the two types of horizontal cells. The axon-less horizontal cells receive inputs and send projections to cone terminals. While the short-axon horizontal cells also receive input from cones, these cells only send projections to rod terminals. This clear segregation is not the case in other mammalian and non-mammalian retinas.

Illumination of the retina cause horizontal cells to respond with a graded depolarization; no action potential generating horizontal cells have been observed. Horizontal cells are GABAergic neurons and, when stimulated via photoreceptor input, have an inhibitory effect on the surrounding photoreceptors to which they project. This horizontal cell function is the basis for the receptive field surround response observed in ganglion cells that will be discussed later.

Bipolar Cells

There are three predominant classes of bipolar cells that have been identified in the mammalian retina. One type connects exclusively to rod photoreceptors, the rod

14

bipolar cell (Figure 1.8). The other two types connect to cone photoreceptors but differ in their responses to light stimulation. The ON cone bipolar cell depolarizes in response to light, while the OFF cone bipolar cell hyperpolarizes in response to light. The rod bipolar cell also depolarizes in response to light and has a distinct morphology characterized by a thick dendritic tuft that invaginates the rod terminal and a long axon that terminates deep in the IPL. The OFF cone bipolar cell is also termed the flat bipolar cell due to the flat contact its dendrites make onto the base of the cone terminal. The ON cone bipolar cell is referred to as the invaginating bipolar cell because of the invaginating contact its dendrites make into the cone terminal (see types of retinal synapses). The somas of all the bipolar cells are located in the approximate center of the INL and make synaptic contact with amacrine cells and ganglion cells in designated regions of the IPL.

Bipolar cells are relay neurons that convey the light signal received from the photoreceptors vertically onto the next cell in the retinal circuit. As will be discussed later, the bipolar cell is an important initial participant in the processing of the light signal; it is where the ON and OFF segregation of light stimulus originates.

Amacrine cells

Amacrine cells are an extremely diverse group of interneurons in the retina. These cells engage in a multitude of synaptic arrangements and contain a wide variety of neuropeptides. Because the research presented here is focused on amacrine cells, I will delay a lengthy discussion of them so the topic can be presented later in a more complete manner.

15

a   cell perikaryon

100 μm

axon terminals

b
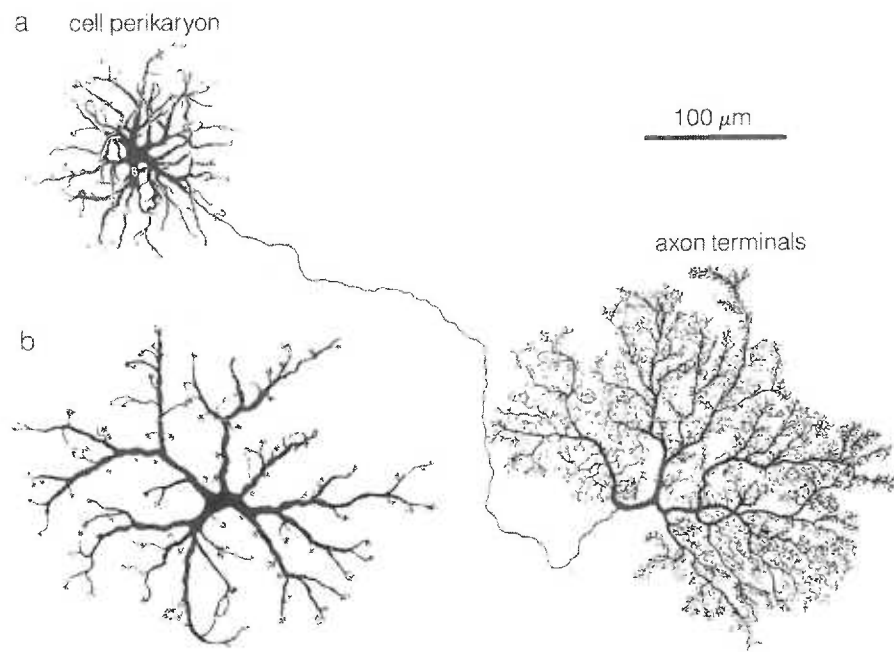
Figure 1.7. Horizontal Cell Anatomy - Light micrograph of golgi stained horizontal

cells. **a.** short axon horizontal cell. **b.** axon-less horizontal cell.

(32)

A
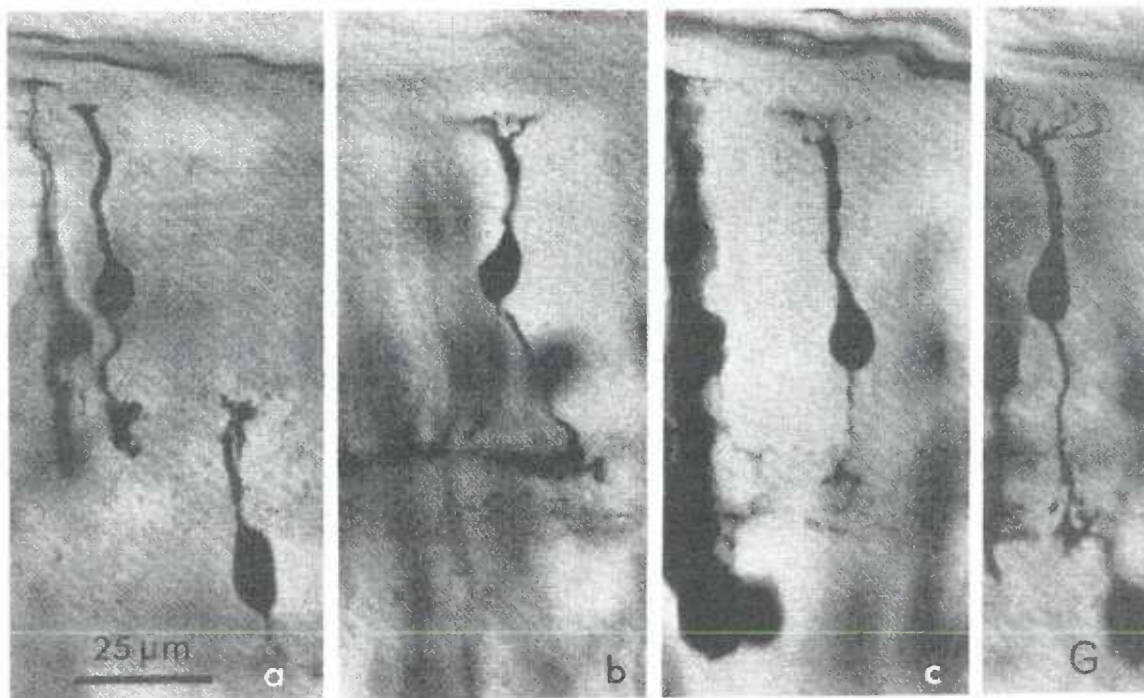
B
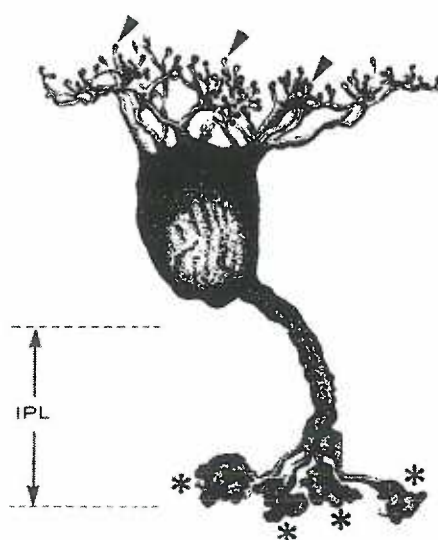
Figure 1.8. Retinal Bipolar Cells – Cone and Rod Bipolar Cells.

A - Bipolar cells from Rhesus Monkey stained using Golgi method.

a. Invaginating cone bipolar cell. **b.** and **c.** Cone related flat bipolar cell. **d.** rod related bipolar cell. (32)

B - Cameral Lucida drawing (x1900) of a Rod bipolar cell in the periphery of the rabbit retina, impregnated with the Golgi method. The dendrites give rise to a multitude of terminal branchlets (arrowheads), which end with a tiny swelling at the level of the rod spherules in the OPL. The axon is characterized by a small number of large, irregular terminals (asterisks), which are situated at the vitreal boundary of the IPL. (11)

Ganglion cells

Ganglion cells were first characterized physiologically by Hamille in 1938, when he described them as having an ON or an OFF response to light stimulation based on his recordings of individual optic nerve fibers. Characteristically, ON cells were found to be relatively quiet in darkness and respond to light with spiking activity, while OFF cells fire spikes continuously in darkness and respond to light with quiescence. He also found that each ganglion cell only responded when light was shown onto an isolated region of retina, which he described as the cell's "receptive field". Later, in 1953, Kufler discovered that the receptive fields of ganglion cells were organized into an antagonistic-concentric-center-surround arrangement; the light-evoked response of the center of the receptive field is opposite to that of the surround.

In 1966 Enroth-Cugell and Robson classified two categories of ganglion cells, X and Y (recorded intracellularly), based on the physiological characteristics of their light responses (16; 86). While both X and Y cells contained an ON and OFF subpopulation, the X cells had a sustained response to the entire duration of the light stimulus, while the Y cells responded transiently to the onset of light. The X cells had smaller average receptive fields that were thought to "summate linearly". This was based on the observation that if sinusoidal gratings of light were positioned on the cell's receptive field such that the amount of darkness and light at any given point was equal, the cell would have a "null" or no response. The Y cells had larger average receptive fields that were thought to summate "non-linearly" based on the absence of a "null" response to any position of the same sinusoidal light grating.

An anatomical study done by Boycott and Wassle in 1974 classified ganglion cells based on somal and dendritic morphologies over many degrees of retinal eccentricities (distance from the fovea or area centralis). This study described three morphological classes of ganglion cells; the "Alpha (α) cell", "Beta (β) cell", and "Gamma (γ) cell" (Figure 1.9) (7). The α-cell was characterized by having a large soma and a dendritic field diameter of about 180-1000μm, while the β-cell had a medium sized soma and a dendritic field diameter of 25-300 μm, and finally, the γ-cell had a smaller soma and a dendritic diameter of about 180-800 μm. The α-cells and β-cells were found to have dendritic diameters that increased with eccentricity (distance from the area centralis), while the dendritic diameters of γ-cells varied within its range at any point in the retina. Based solely on comparisons between previous reports and their own anatomical observations, these authors suggested that morphologically classified alpha/beta/gamma cell types correspond to the physiological Y/X/W cell types respectively. Fukuda et al in 1984 confirmed through both physiological measurements and anatomical techniques that indeed the above mentioned morphological cell types correlate to the previously identified physiological cell types (22; 23). These three ganglion cell types account for nearly 99% of the ganglion cells in the retina. In the cat retina, the X and W cells are far more numerous than the Y cells. With respect to the total number of ganglion cells present in the GCL of the cat retina, W cells make up 40%, X cells make up 50-60%, and Y cells make up 1-2% near the area centralis and nearly 10% in the periphery (22; 23).

The ultimate goal of a retinal circuit is to form the properties of a ganglion cell's receptive field. There are several different receptive field properties that incorporate

20

dynamic response properties to many spatial and/or temporal characteristics of light stimulus. The Y (α-cells) and the X (β-cells) both have receptive fields that conform to the antagonistic concentric center-surround organization first described by Kufler. The Y (α-cells) respond very rapidly to light stimulation in a transient (or phasic) manner, while the X (β-cells) respond more slowly but in a sustained (or tonic) manner. The W (γ-cells) have receptive fields that are non-concentric and contain subpopulations with a variety of response properties. Among the W ganglion cell group, there are members with the following light response properties: ON-tonic, OFF-tonic, ON-phasic, OFF-phasic, and ON-OFF-phasic (Figure 1.10) (22).

There have also been ganglion cell types identified based solely on their response properties to light. Some ganglion cells are sensitive to motion and some only spike when light moves across their receptive fields in a particular direction; "direction selective" ganglion cells (82). There are also ganglion cells that only respond to light presented in a select spatial orientation (2). The receptive fields of these cells are still usually arranged in an antagonistic center-surround manner. It has been the ongoing goal of much of retinal research to understand how the same classes of retinal neurons described above organize into the many circuits that underlie the multitude of ganglion cell receptive fields (Figure 1.11).

Retinal Synapses

The synaptic connections of the OPL and IPL between retinal neurons have been investigated using several anatomical techniques. Light microscopic examinations of retinas stained with the Golgi method and other methods such as horseradish peroxidase

21
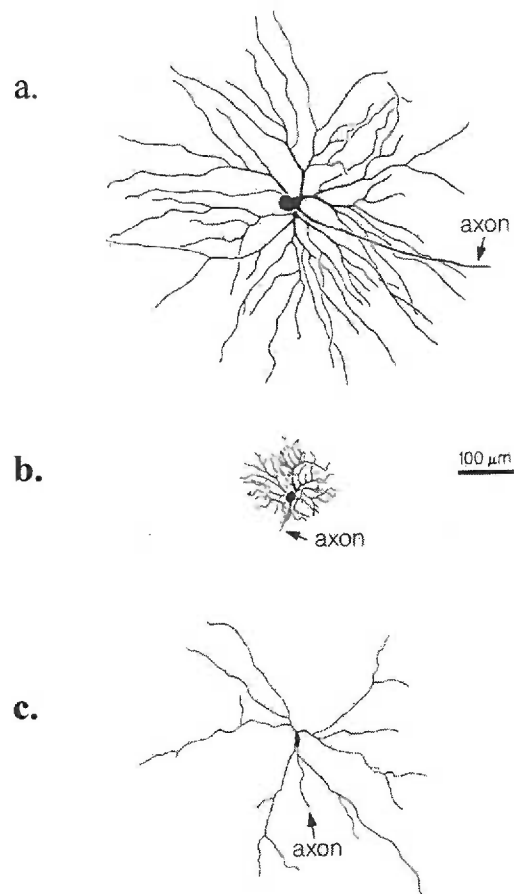
Figure 1.9. Three Major Classes of Ganglion Cells–
Drawings from Golgi-stained whole-mount cat retina.
a. an Alpha (α)-ganglion cell. b. a Beta (β)-ganglion
cell. c. a Gamma (γ)-ganglion cell. All three cells
originated from near the area centralis.
(7)

Responses   Receptive field maps

ON-CENTER CELL

stimulus

center

surround

center and
surround

OFF-CENTER CELL

stimulus

center

surround

center and
surround
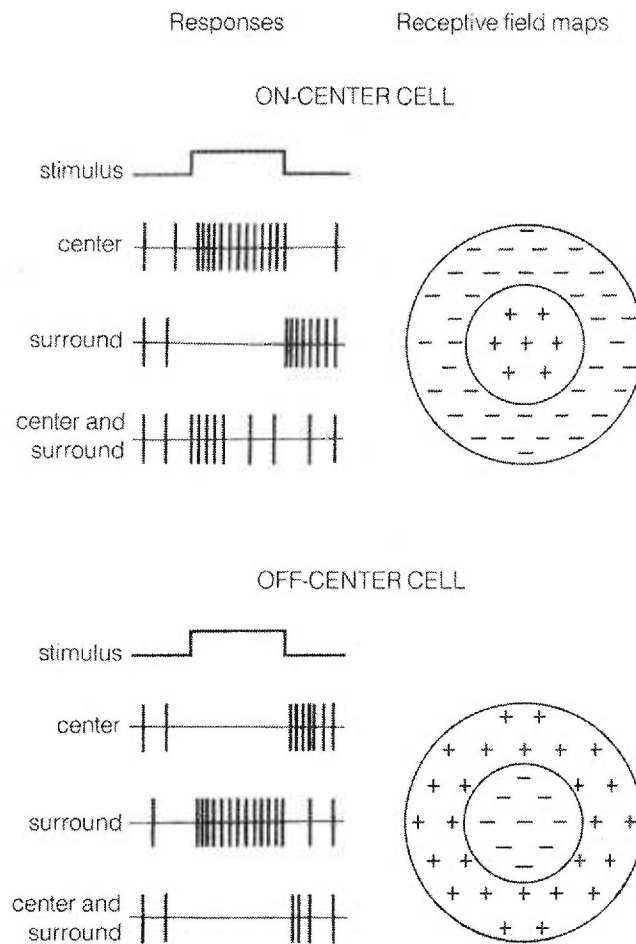
Figure 1.10. Basic Receptive field Responses and Organization – Idealized responses and receptive field maps for ON and OFF center contrast-sensitive ganglion cells. On the left are example intracellular responses on ON-Center (top) and OFF-Center (bottom) ganglion cells. Vertical line represents an action potential. Diagrams on the right represent the antagonistic center-surround arrangement of the ganglion cells' receptive field. The (+) signs are regions of excitatory responses, while the (-) signs are regions of inhibitory responses to light stimulation. (32)

23
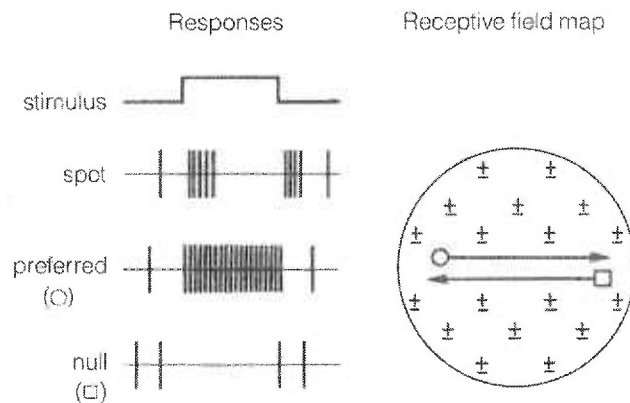
Figure 1.11. Receptive Field of The Direction-Selective Ganglion Cell -

Idealized responses and receptive field maps for direction-selectivity.

The (±) signs represent the fact that these cells respond to both the onset

and offset of a spot of light. Open circle = movement in preferred direction

Open square = movement in the null direction

(32)

(HRP) have been very useful in establishing possible synaptic connections between cells. These techniques however are limited to revealing cells that have closely apposing processes. In order to firmly establish, however, the presence of a synaptic connection between any given points of contact the resolution available via electron microscopy must be employed.

Based on light microscopic analysis of Golgi stained or HRP stained retina, interactions between several cell types have been reported in the OPL and the IPL (33; 34). The processes of photoreceptor terminals, horizontal cell dendrites and terminals, and bipolar cell dendrites have been found to come in close contact in the OPL. On the other hand, the processes of amacrine cell dendrites, bipolar cell terminals, and ganglion cell dendrites have been observed closely opposing one another in the IPL. The presence of actual synaptic interactions was later established using electron microscopy techniques.

The careful examination of electron micrographs discovered the presence of several types of synapses in the mammalian retina. Chemical synapses similar to those observed elsewhere in the brain, termed conventional synapses, are widely present in the IPL. An assemblage of synaptic vesicles near the presynaptic membrane characterizes these conventional synapses, as well as some electron dense material on both the pre and postsynaptic membrane and some filamentous material in the synaptic cleft (Figure 1.12A) (32).

Another type of chemical synapse called the Ribbon Synapse is found at multiple synaptic sites in the retina, especially in the OPL. The Ribbon Synapse typically contains
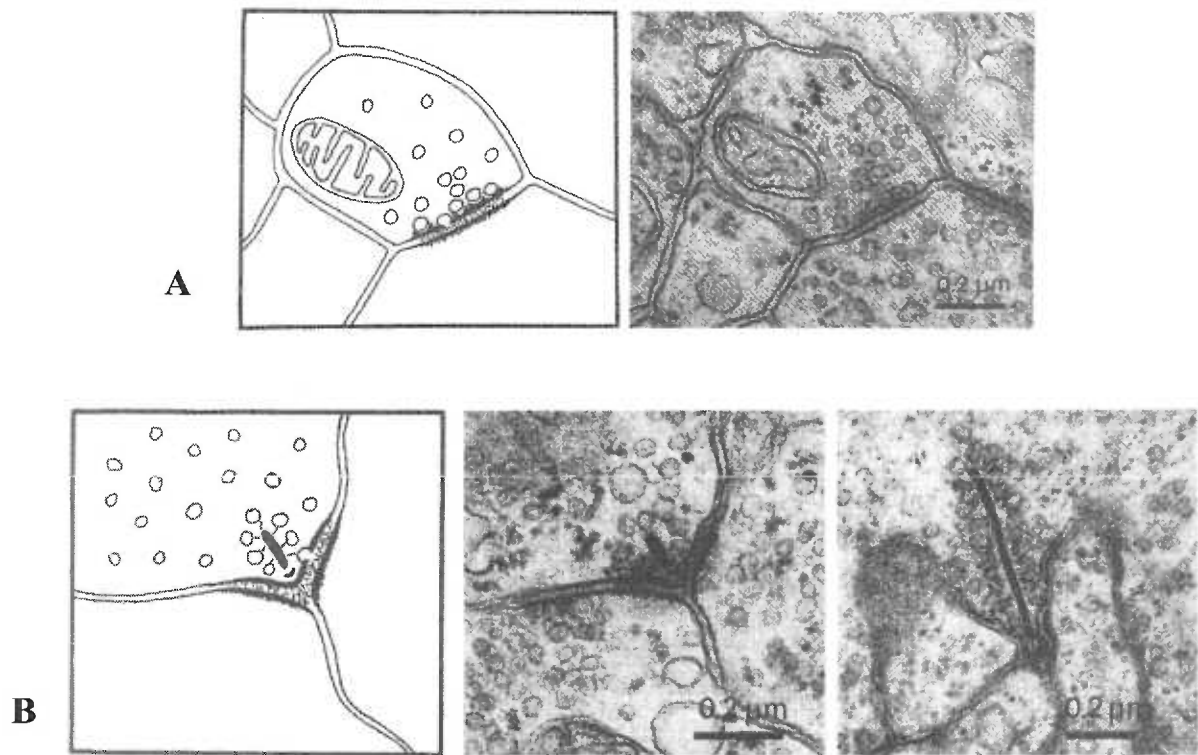
Figure 1.12. Conventional and Ribbon Synapses – **A.** Drawing (left) and electron micrograph (right) of a conventional synapse observed in the frog retina. **B.** Drawing and electron micrograph of a ribbon synapse. The micrograph on the far right is the larger ribbon synapses common in the outer retina, as opposed to the smaller ribbons (left side of panel B) commonly observed in the inner retina.

(32)

an electron-dense "ribbon" that sits above the invaginating ridge of the presynaptic terminal (Figure 1.12B) (32). Below the ribbon is a dense band called the acriform density that is thought to anchor the ribbon to the terminal membrane. Several synaptic vesicles that are attached via thin filaments surround the ribbon. The axon terminals of the photoreceptors are characterized in part by the presence of this type of chemical synapse. The cone axon terminal, also referred to as the cone pedicule, is arranged in what is called a synaptic triad (Figure 1.13). Centered around a single large presynaptic ribbon, the processes of three different cells make invaginating postsynaptic contacts; one bipolar and two horizontal cell processes. Four other bipolar processes have been found to make flat conventional synapses onto the cone pedicule surrounding the triad. The rod axon terminal, also referred to as the rod spherule, has a synaptic organization that is similar to that of the cone pedicule. The processes of two horizontal cells and two bipolar cells invaginates the rod spherule and lie postsynaptically to a large presynaptic ribbon. Ribbon synapses, when observed in the IPL, are smaller in size to those observed in the OPL (32).

Gap junctions have also been found between retinal neurons. The membranes of two gap-junctioned neurons come into close contact (~2-4nm) and a fluffy electron-dense material bridges the junction (Figure 1.14). The contacting cells are thought to form connecting channels that allow the passage of ions and small molecules up to ~1000 Daltons in weight (32). There are large gap junctions between adjacent horizontal cells and very small gap junctions between adjacent photoreceptors (14; 89). There have also been reports of gap junctions among select types of amacrine cells (49; 66; 68).

27
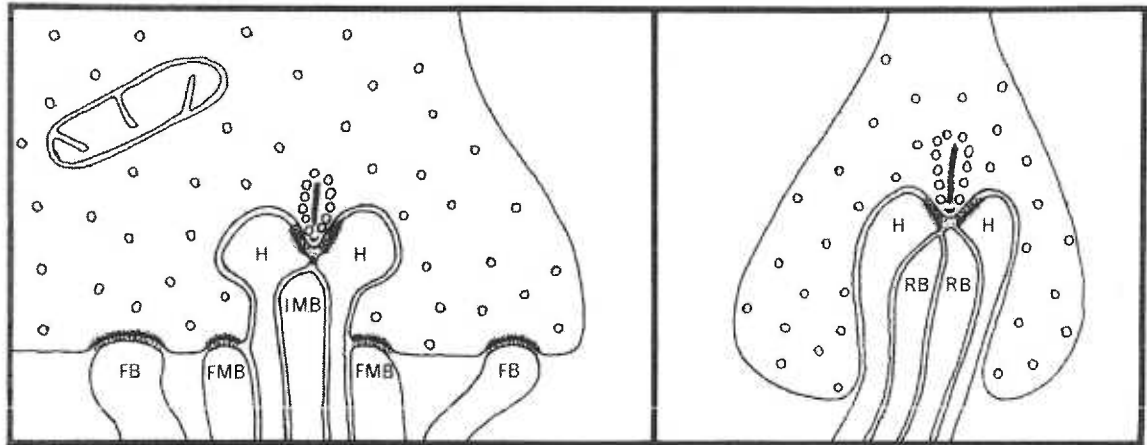
Figure 1.13. Rod and Cone Axon Terminal Organization - Schematic drawings
showing the arrangement of synaptic junctions made by bipolar and horizontal cells
onto cone (left) and rod (right) axon terminals in the primate retina. **H** - horizontal cell
dendrite. **FB** - flat bipolar cell dendrite. **FMB** - flat midget bipolar cell dendrite (not
termed midget in non primate retina). **IMB** - invaginating midget bipolar cell (not
termed midget in non primate retina).

(32)
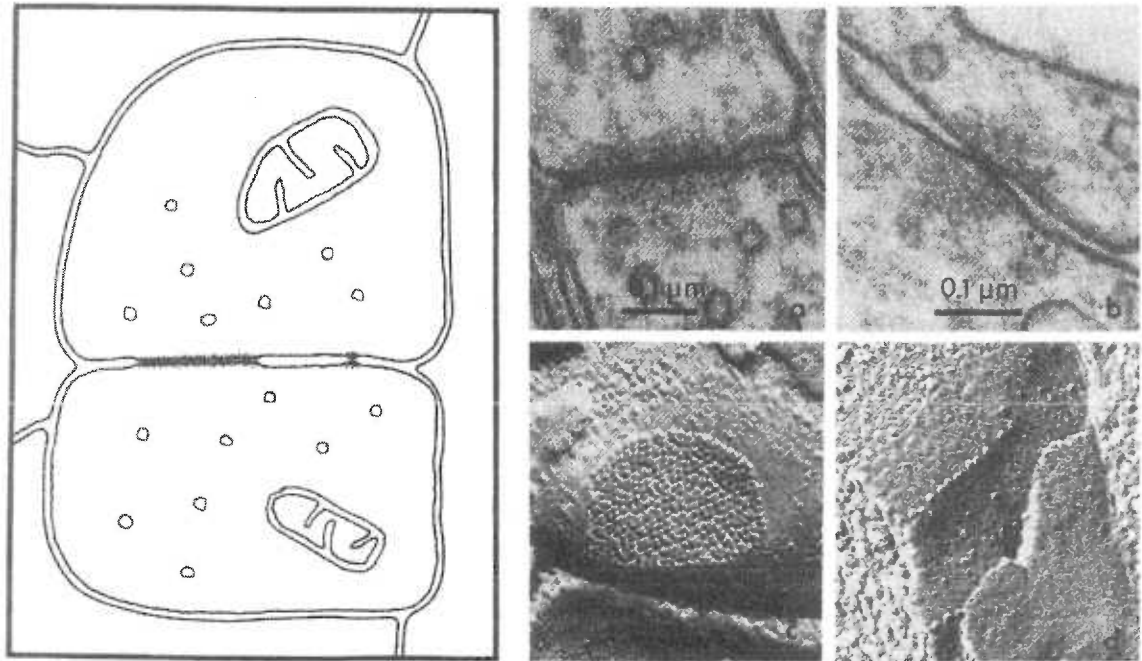
Figure 1.14. Gap Junctions in the Retina – Drawing (left) and electron micrograph (right) of a typical large and small gap junction. **c** and **d** - show the particles that bridge the gap junction membranes, these particles are shown only in profile in **a** and **b**.

(32)

All of these electrical junctions observed among retinal neurons are thought to be modulated by light levels via the release of dopamine (4; 26). In dim light conditions the gap junctions are near fully open, but during bright light condition the gap junctions are less conductive.

Retinal Circuitry and Processing

The mammalian retina is thought to have a basic circuitry and format for light processing that is somewhat conserved among species (Figure 1.15). This framework is based on anatomical evidence, physiological investigations and theoretical postulation.

Physiological studies of ganglion cells first revealed the most basic receptive field organization, the ON response and OFF response to light with an antagonistic center-surround arrangement. The circuitry behind the formation of these response properties all begins with the photoreceptors. In darkness, the photoreceptors are depolarized and the presynaptic ribbons at the photoreceptor terminals continuously release glutamate. In response to light stimulation, the photoreceptors hyperpolarize and glutamate release is attenuated (see Figure 1.15). Postsynaptic to the photoreceptors are the bipolar cells that respond to light (and the subsequent absence of glutamate) in one of two ways: by depolarizing or hyperpolarizing (Figure 1.16) (101). The type of glutamate receptor present on the bipolar cell dendrites determines how a cell responds. Bipolar cells that have ionotropic glutamate receptors on their dendritic processes respond to light (a decrease in photoreceptor driven glutamate release) by hyperpolarizing, which translates to an OFF response (32; 89).

Bipolar cells with metabotropic glutamate receptors respond to light by depolarizing, which translates to an ON response. These cells possess sodium channels
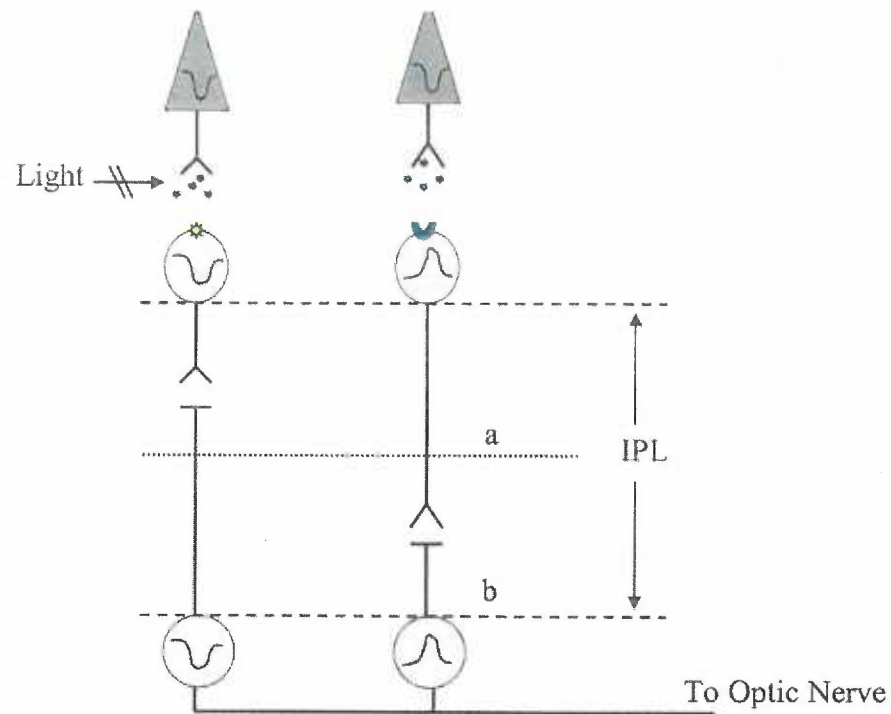
Figure 1.15. Basic Retinal Circuit – A schematic drawing of a basic retinal circuit,
highlighting the sign-conserving and the sign-inversing synapse. The triangles represent
photoreceptors that hyperpolarize in response to light (downward deflection). Glutamate
(black-filled circles) is continuously released in darkness and attenuated in light.
Postsynaptically are the bipolar cells (gray ovals). OFF-Bipolar cells that with ionotropic
glutamate receptors (yellow star) hyperpolarize (downward deflection) in the absence of
glutamate, the sign-conserving synapse. ON-Bipolar cells that possess metabotropic
glutamate receptors (green half-circle) depolarize (upward deflection) in the absence of
glutamate, the sign-conserving synapse. OFF-Bipolar cells project to sublamina a of the IPL
terminating onto OFF ganglion cells, while ON-bipolar cells project to sublamina b of the
IPL terminating onto ON-Ganglion cells.

31
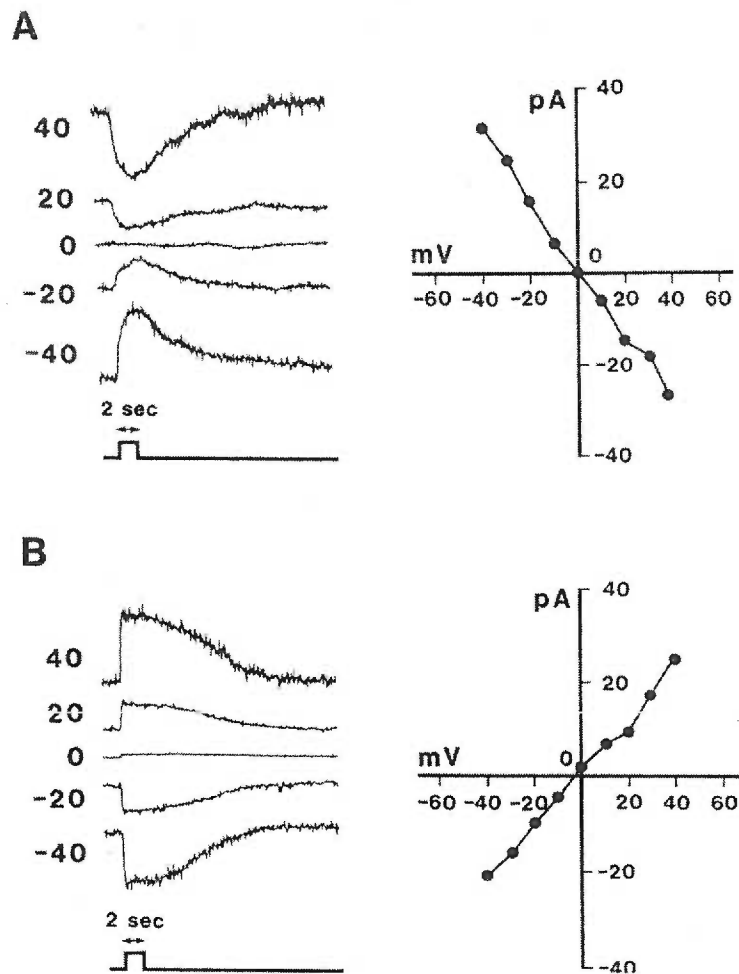
Figure 1.16. Bipolar Cells responses to Glutamate - Two types of Glu-induced membrane currents in bipolar cells from the cat retina. Responses were obtained via a 2 sec pressure application of 100 μM Glu. Left, the raw current traces of glutamate responses at different holding potentials. Right, the graphed I-V relationship of glutamate-induced current. **A.** One type on bipolar cell responds to Glu with a slow outward current at –40 mV (left); this current reverses near 0 mV (right). **B.** Another type of bipolar cell responds to Glu with a more rapid inward current at –40 mV; this current also reverses near 0 mV (right). (13)

32

that are gated by cGMP (similar to those on the photoreceptor outer segment) and regulated by the metabotropic glutamate receptor (Figure 1.17). In darkness glutamate is bound to its receptor, which initiates a G-protein cascade involving G_o keeping the sodium channels closed (17; 51; 73; 84). The details of this signaling cascade have yet to be fully elucidated. In the presence of light, glutamate is no longer bound to its receptor and the channel is free to be opened by cGMP, which in turn causes a depolarizing response.

The hyperpolarizing (OFF) bipolar cell response to light is called the **sign-conserving** response while the bipolar cell depolarization (ON) is referred to as **sign inverting**. This terminology is in reference to the photoreceptor hyperpolarizing response to light (32). Through this synaptic mechanism, the bipolar cells create the first segregation of the ON and OFF responses that are observable at the level of the ganglion cells (see Figure 1.15). These functionally divergent bipolar cells send axonal projections to separate regions of the IPL. The ON bipolar cells terminate deep within the IPL in what is called sublamina b, closest to the ganglion cell layer. The OFF bipolar cells terminate in sublamina a of the IPL, nearest to the ONL (62).

Studies that paired physiological recordings and anatomical analysis found that all cells stratifying in sublamina a of the IPL either attenuated spiking or hyperpolarized in response to light stimulation, while the cells that stratified in sublamina b responded to light by initiating spiking or depolarizing (3; 5; 40; 62). These data clearly demonstrate a functional stratification pattern present in the IPL of the mammalian retina. Sublamina a of the IPL is referred to as the OFF layer and sublamina b the ON layer.

With some exception, the ON and OFF bipolar terminals make synaptic contact with the dendritic projections of ON and OFF ganglion cells in their respective IPL sublamina (see Figure 1.15). The many retinal circuits, composed of photoreceptors terminating onto bipolar cells then synapsing onto ganglion cells, are thought of as parallel vertical channels (Figure 1.18). A lateral pathway is also thought to exist involving horizontal cells and amacrine cells. Horizontal cells are thought to provide lateral inhibition in the OPL, while amacrine cells provide lateral modulation in the IPL (6; 35; 42; 55; 63).

Horizontal dendritic processes make synaptic contact with photoreceptor terminals and send GABAergic projections to neighboring photoreceptors. Horizontal cells are also extensively gap junctioned to one another, so an inhibitory signal can be spread over many neighboring photoreceptors. This unique connectivity has been demonstrated to underlie the antagonistic center-surround receptive field property observed in many ganglion cells (32; 89).

Amacrine cells have been found to shape several spatial and temporal characteristics of receptive fields observed at the ganglion cell level. Amacrine cells engage in a myriad of synapses within the IPL, including connections with bipolar cells, other amacrine cells, and ganglion cells. Amacrine cells not only provide lateral modulation onto parallel retinal circuits, but in some cases have also been observed participating in vertical information flow through the retina. I will discuss this in greater detail in the amacrine cell section.
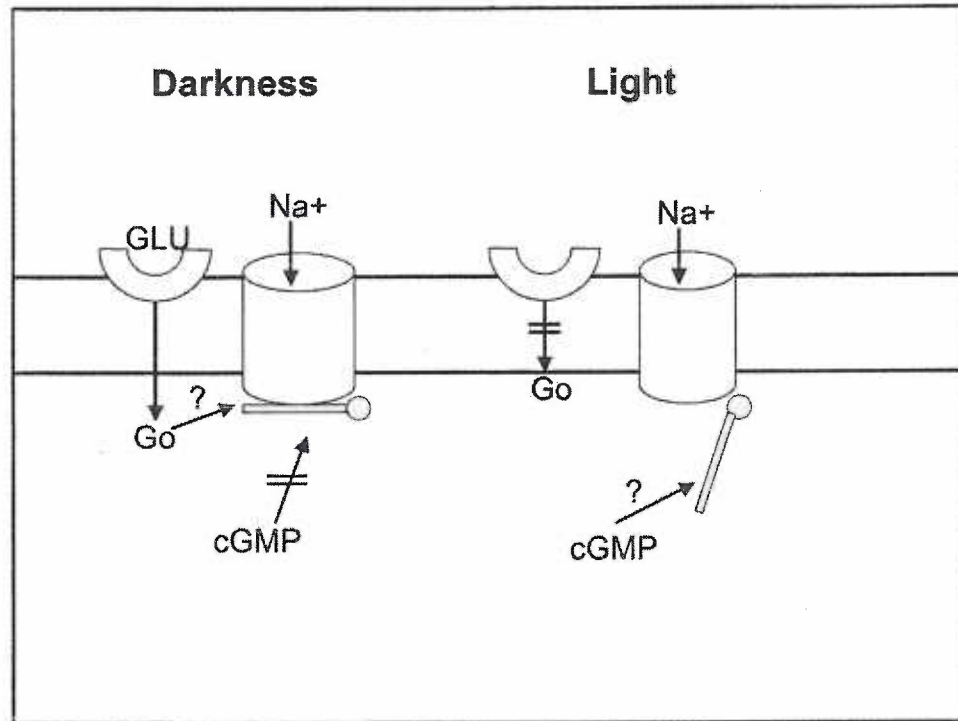
Figure 1.17. Mechanism Behind the Sign-Inverting Synapse – A schematic drawing of the mechanism of action for the metabotropic glutamate receptor (mGLUR), which are located on the ON-bipolar cells. In darkness, (left) glutamate is continuously released from the photoreceptor and bound to its postsynaptic receptor. The G-protein receptor, in its bound form, activates a signaling cascade that is initiated by Go and causes the closing of cyclic nucleotide gated sodium channels at the membrane. Upon light stimulation, glutamate is no longer available and the receptor, in-turn, sits in its inactive form. The sodium channels at the membrane are now free to be opened by intracellular cGMP. The cells then depolarize.
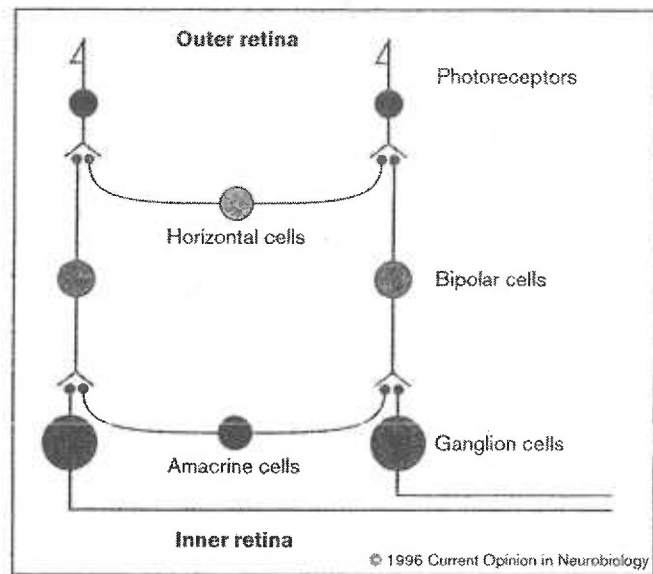
Figure 1.18. Information Flow Through the Retina – A schematic drawing of the major channels on information flow through the mammalian retina. The vertical channels include photoreceptors onto bipolar cells and finally onto ganglion cells. The lateral flow of information come from the horizontal cells in the Outer retina and the Amacrine cells in the Inner retina.

(42)

The Rod Pathway as a Model Retinal Circuit

The rod circuits leading to the ON and the OFF ganglion cell responses in the mammalian retina is a great model to observe the mechanisms by which a ganglion cell receptive field is formed (Figure 1.19). Over the past several years, the cellular components, their physiological properties, and the synaptic interactions of the mammalian rod pathway have been well established.

Compared to the cone circuitry, the circuit connecting rod photoreceptors to ganglion cells is relatively indirect. The rod pathway leading to an OFF ganglion cell response involves the use of the cone circuitry via an amacrine cell (AII). In dim light conditions, the rod photoreceptors hyperpolarize and the continuous release of glutamate at the axon terminal is attenuated (see Figure 1.15). The rod photoreceptor terminates onto the ON-rod bipolar cell in a sign-inverting synapse. The dendritic processes of the ON-rod bipolar cell possess the metabotropic glutamate receptor, which causes the opening of sodium channels and depolarization in the absence of glutamate (see Figure 1.15). The ON-rod bipolar cell makes two terminating synapses located in sublamina b of the IPL. One reciprocal synapse is made onto an indoleamine-accumulating-wide-field amacrine cell called the A17 cell. A second synaptic contact is made with the narrow-field-bistratified AII amacrine cell, also called the rod amacrine cell (see Figure 1.19) (9; 11; 12; 14; 36; 50; 64; 67; 79; 80; 83; 93; 102). The reciprocal connection with the A17 cell is thought to be excitatory and responsible for quickening the time course of the rod bipolar cell response. This claim is supported by the fact that recordings in the AII amacrine cell have demonstrated that it responds to light more rapidly than does the upstream rod bipolar cell (52-54).

The AII amacrine cell makes two terminating contacts. Tracer studies found that the AII amacrine cell is gap junctioned to the dendritic processes of the cone-ON-bipolar cell in the rabbit retina and to the ON ganglion cell in the cat retina. In all mammalian retinas, the AII amacrine cell makes a second synaptic contact with the OFF cone bipolar cell located in sublamina a of the IPL. This synapse was found to be inhibitory and mediated by glycine (68). The OFF cone bipolar cell hyperpolarizes in response to light and conveys that signal to the OFF ganglion cell (see Figure 1.15). The AII amacrine cell was the first amacrine cell found to engage in the vertical circuitry from photoreceptors to ganglion cells.

Amacrine Cells

Müller in 1851 first observed that the cell bodies lying at the vitreal border of the INL formed a distinct sublayer; these cells were termed spongioblasts by Tartuferi in 1887. Further examinations of Golgi stained retina by Dogiel in 1891 and Cajal in 1893 discovered that spongioblasts did not give rise to axons. This led Cajal to name these cells "amacrine cells" based on a Greek term (a-makrós-inos) meaning "without long fibers" (32). He was also the first to attempt to anatomically characterize amacrine cells. Cajal used vertical serial sections and divided cells into three general groups based on pattern of dendritic stratification (Figure 1.20). The first group was the diffusely stratifying cells, which he further divided into small and large cell types. The second group Cajal described was the "stratified" amacrine cells, which confined their projections to a strict region of the IPL.

38
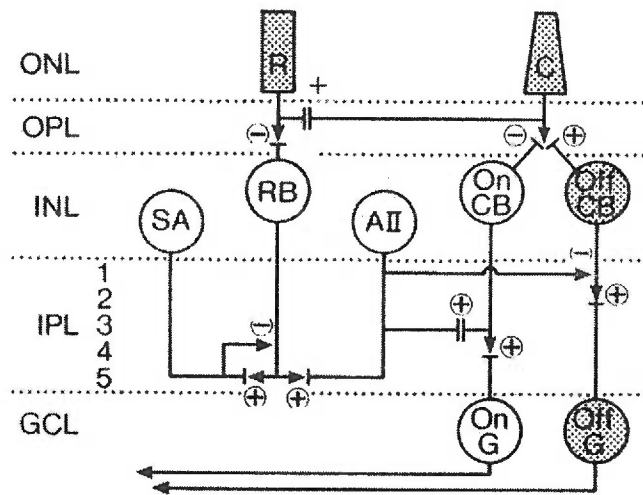
Figure 1.19. The Rod Pathway - Wiring diagram of the direct neuronal pathways serving rod and cone vision in the rabbit retina. Cells in the diagram with somata that are shaded are the cells that depolarize in response to light (ON), while non-shaded cells hyperpolarize in response to light (OFF).

R = rod photoreceptor, **C** = cone photoreceptor, **RB** = rod bipolar cell, **SA** = serotonin accumulating amacrine cell (A17), **AII** = AII amacrine cell,

ON/CB = ON-cone bipolar cell, **OFF/CB** = OFF-come bipolar cell,

ON/G = ON-Ganglion cell, **OFF/G** = OFF-Ganglion cell.

Symbols next to synaptic contacts: **(+)** = a sign-conserving synapse

(-) = a sign-inverting synapse

(83)
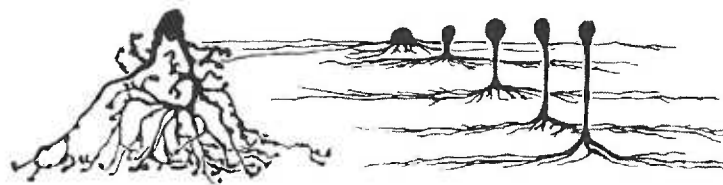
Figure 1.20. Cajal's Amacrine Cell Classification - Reproductions of

drawings made by Cajal of two general types of amacrine cells from ox and

dog retina. Left = diffuse amacrine cell. Right = five stratified amacrine cells.

(32)

Finally, he identified the bistratified cells that, along with the "stratified" cells, were also sub-grouped based on the size of the dendritic tree. Medium and very wide field amacrine cells were often missed in these early studies due to the constraints of analyzing vertical serial sections. These cell types were undiscovered until retinal whole mount staining techniques were developed some eighty years later.

Kolb et al did the first comprehensive anatomical study of amacrine cells using the Golgi-impregnated method in whole-mount retina in the cat retina in 1981. Cells were first sorted by dendritic field size, then by details of branching patterns, and finally by depth of stratification (37). A total of 22 anatomical cell types were identified. Later, Masland and Mariani developed a visualization method that was less sporadic than the Golgi-impregnation method and applied it to the study of amacrine cell anatomy. In this method, focal irradiation is applied to the nuclei of a cell, producing a fluorescent product. This technique, termed "photofilling", had the advantage of visualizing all cells in a given retinal region lending itself useful in determining the pattern of amacrine cell distribution across the retina (39). Due to the bright fluorescent product of the "photofilling" technique, however, detailed dendritic structure was often difficult to resolve, especially among the small field neurons. In 1999 Masland and Mariani coupled their photofilling technique with the Golgi-impregnated method to produce a comprehensive anatomical study of amacrine cells in the rat retina. This study first sorted cells based on dendritic size but focused heavily on the details of dendritic stratification pattern and branching pattern in the Z-plane. Masland and Mariani identified a total of 28 amacrine cell types (38). Despite the surprising increase in estimated number of

41

anatomically distinct amacrine cell types since Kolb's seminal study, others report that the number of cell types approach 40 based on work in both the cat and rabbit retina (8).

Many of the amacrine cell types identified through anatomical studies have yet to be studied for their physiological properties. It is of great interest to determine whether the morphological cell types previously identified translate to functional cell types. There are, however, several amacrine cell types that have been characterized.

AII amacrine cell

The AII amacrine cell is an integral member of the rod circuit. It plays a throughput functional role from rod photoreceptors to the ON and OFF ganglion cells. Its participation in the rod circuit was first established using a combination of HRP staining and serial section electron microscopy. The rod ON bipolar cell terminates onto the AII amacrine cell in sublamina b of the IPL. Intracellular recordings established that the AII amacrine cell depolarizes in response to light. In addition, tracer coupling experiments using low molecular weight dyes such as Neurobiotin demonstrated that the AII amacrine cell also makes gap junction contact with the ON cone bipolar cell in sublamina b. In some mammalian retinas, for example the cat retina, the AII amacrine cell makes gap junction contact directly onto the ON ganglion cell. Application of the glycine receptor blocker, strychnine, was successful at attenuating the rod mediated OFF ganglion cell response in several studies. This evidence, in addition to anatomical and immuno-staining studies, established that the AII amacrine cell also terminates onto the OFF cone bipolar cell in a glycinergic synapse located in sublamina a of the IPL (4; 66; 68; 78; 80; 85; 91; 92; 100).

42

Anatomically, the AII amacrine cell is a narrow field cell that has a bistratified dendritic organization (Figure 1.21). Stratifying in sublamina a of the IPL, is an arrangement of thick lobular appendages responsible for the glycinergic contacts onto the OFF cone bipolar cells. Located in sublamina b of the IPL, is a radiation of thin arboreal dendrites that make gap junction contact with the ON cone bipolar cells in the rabbit retina and the ON ganglion cells in the cat retina.

The AII amacrine cells make up approximately 11% of all INL amacrine cells in rabbit retina. The dendritic field sizes and cell densities increase with eccentricity reaching a maximum of 5000 cells/mm^2 in the cat area centralis and 3000 cell/mm^2 in the visual streak of the rabbit retina (78; 80).

In addition to gap junctions with the ON cone bipolar cells, the thin arboreal dendrites of AII amacrine cells also make homologous gap junctions with other AII amacrine cells. The result of these contacts is a network of AII cells thought to alter receptive field sizes and, in some cases, amplify the rod signal. The AII homologous gap junctions are also thought to be regulated by light levels. Under dark-adapted conditions, the receptive field sizes of AII amacrine cells are only slightly larger than their dendritic field size. Under intermediate conditions the receptive field size increases six-fold; these light dependent changes are also mirrored in the observed AII coupling ratios. Because dopamine is known to uncouple homologous gap junctions between AII amacrine cells, some have suggested that dopamine may mediate the light dependent changes in receptive fields (4).

A17 Amacrine Cell

There is another well-characterized amacrine cell that is associated with the rod circuit. The A17 amacrine cell was discovered, through electron microscopy, to make reciprocal synaptic contact with the rod bipolar cell in sublamina b of the IPL. This amacrine cell was first called the A1 cell by Kolb et al (1981) in a purely anatomical study of amacrine cells (37). Using the Golgi-impregnation method, HRP staining, and electron microscopy, the A1 cell was found to correspond to the A17 amacrine cell (8).

The A17 amacrine cell is a wide-field cell; the soma gives rise to a radiation of fine bead-like dendrites that cover approximately 600-2000 μm in diameter (Figure 1.22) (8). In the Z-plane, the dendrites are diffusely spread throughout the IPL but in the distal portions of the tree, the dendrites are relatively uni-stratified deep in sublamina b. Along the length of each dendrite are small round varicosities at intervals of 10 - 50 μm that can number up to 1000 or more per cell. As early as 1974, Kolb and Famiglietti discovered that the A1 cells (A17 cells) were connected via gap junctions (36). Based on Neurobiotin injection, cell coupling observations revealed the cell densities across the retina range from 300 cells/mm^2 in the far periphery to 25000 cells/mm^2 in the are centralis of the cat retina (79). This high density results in a large degree of dendritic overlap; approximately 700 A17 amacrine cells, for example, cover each point on the cat retina (8).

In the rabbit, there are two cell types that are morphologically similar to the A17 cell observed in the cat. The S1 and the S2 amacrine cells are wide-field cells that make reciprocal synaptic contact with the rabbit rod bipolar cell. Both cell types were first identified based on their selective accumulation of indoleamines such as serotonin.

44
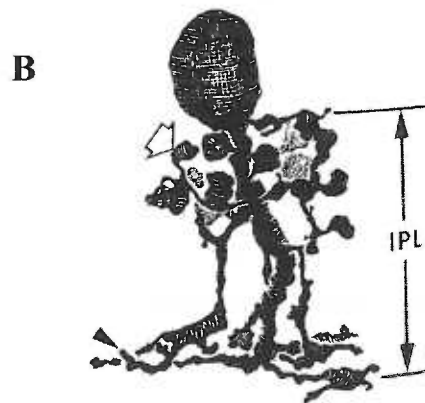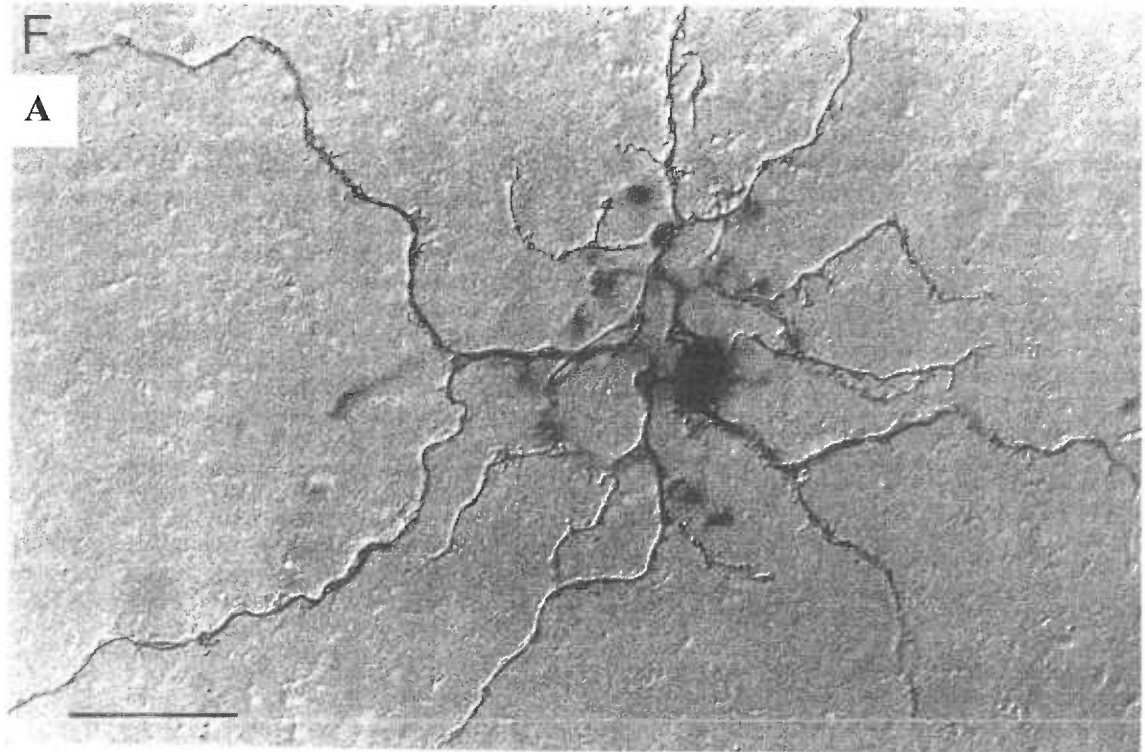
Figure 1.21. AII Amacrine Cell Anatomy – AII amacrine cell from two view points.

A. An AII amacrine cell initially injected with Lucifer yellow, then photoconverted to an opaque reaction product. Viewed in retinal wholemount (rabbit retina). Focus is on arboreal appendages located in sublamina b. Scale bar = 20μm. (83)

B. Camera Lucida drawing of an AII amacrine. (68)
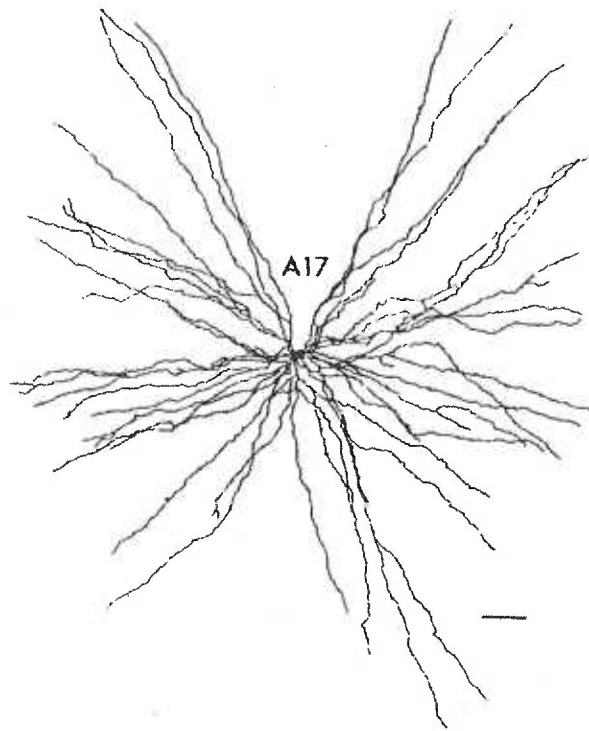
Figure 1.22. A17 Amacrine Cell Anatomy – A drawing of an A17 amacrine cell (cat retina) from intracellular iontophoresis staining with HRP. Varicosities are not visible in this drawing, but are present. Scale bar 50μm

(37)

These cell types correspond in their average dendritic extents and the presence of round varicosities along the length of each dendrite (47; 54).

The A17, S1 and S2 cells respond to light with an initial peak depolarization followed by a plateau persistent throughout the stimulus duration. The receptive field size is limited to the size of the dendritic field. These cells contain GABA and are also thought to contain serotonin. The feedback from the A17 cell onto the rod bipolar cell is thought to be excitatory at first (via serotonin), in order to quicken the time course of the rod signal, and then inhibitory (via GABA). Some believe that the inhibitory reciprocal feedback onto the rod bipolar cell underlies the surround response in the AII amacrine cell (8). This view is supported by the fact that the rod bipolar receptive field lacks a surround response, while the rod bipolar terminal possesses a surround response, which is then passed onto the AII amacrine cell. The idea that an amacrine cell can generate a surround response in higher order retinal neurons dispels the dogma that all surround responses originate at the level of the horizontal cells.

Due to the extremely large dendritic extent of the A17 amacrine cell, there were speculations that some regions of the dendritic tree were electrically isolated from the soma. Modeling studies predicted that these isolated dendritic domains could act as autonomous local modulators. Bloomfield, in 1992, tested these ideas by comparing receptive field sizes in the absence or presence of the sodium channel blocker, tetrodotoxin (TTX) (1). He found that the A17 cell relies heavily on the generation of action potentials via voltage-dependent sodium channels in order to propagate signals across its wide dendritic field. The application of tetrodotoxin reduced the size of the receptive field of A17 amacrine cell. The A17 amacrine cell therefore does not contain

47

isolated dendritic domains, but rather possessed the ability to integrate signals across the whole of its dendritic tree.

Association Amacrine Cells

Cajal in 1893 recognized a group of retinal interneurons that possessed an axon-like projection; he termed these neurons association amacrine cells. There are upwards of 10 types of association amacrine cells; two of these have been extensively studied. One cell type is the classic dopaminergic amacrine cell and the other is the polyaxonal amacrine cell (Figure 1.23) (8).

The dopaminergic amacrine cell was the first to be neurochemically identified. This cell has an unusual morphology; they are found in very low densities across the retina and possess a dendritic tree with two separate branching patterns. The dopaminergic amacrine cell gives rise to a relatively unbranched dendritic tree and an extensively branched axonal arborization, which originates from a single axon projecting from the soma (8).

The polyaxonal amacrine cell is similar in morphology to the dopaminergic amacrine cell. The cell possesses an extensive axonal arborization that originates from a single axon extending from the soma. Both cell types are known to generate large spikes in response to light and the size of their receptive fields are matched by the size of their dendritic fields but do not match the extent their axonal arborization. Both cell types have wide dendritic fields and are thought to play some sort of global regulatory function across the retina (8; 88).

48

Fountain Amacrine Cell

The fountain amacrine cell was first discovered by Masland et al 1999 in a comprehensive study of amacrine morphology using a combination of the Golgi-impregnation method and the newly developed "photofilling" method (38). The fountain amacrine cell is a small field neuron possessing a distinct "retroflexive" dendritic architecture. The cell's unique anatomy is best appreciated when viewed in the Z plane with respect to the Y plane. When viewed from this perspective, the dendritic tree has been described as resembling a fountain, with dendrites pouring down from the soma into sublamina a of the IPL and then thinly spraying up and outward into sublamina b. (99) (Figure 1.24).

Using Neurobiotin injection, fountain amacrine cells were discovered to be homologuously coupled to one another in the rabbit retina. Approximately 98% of coupled cells possessed somata located in the INL, while ≈2% were displaced to the ganglion cell layer. The density of fountain amacrine cells varied by an order of 4 from ≈ 90 cell/mm^2 in far-inferior portions of retina to ≈ 360 cells/mm^2 in the visual streak.

Due to the fountain amacrine cell's unique morphology, the dendritic field area of a given cell varied with respect to its depth in the IPL and degree of eccentricity. Fountain cells located in the visual streak of the rabbit retina had an average field area of 0.006mm^2 in sublamina a and 0.0036mm^2 in sublamina b. Among cells located in far-inferior portions of retina the average dendritic field area was 0.093mm^2 in sublamina a and 0.032mm^2 in sublamina b (99).

The fountain amacrine cell has been classified as a unique type of bistratified amacrine cell termed heteromorphically bistratified.
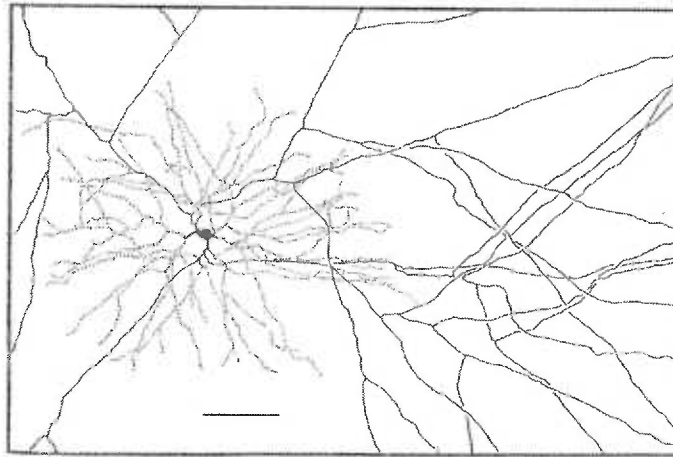
Figure 1.23. Polyaxonal Amacrine Cell - Drawing of a Polyaxonal amacrine cell from a horseradish-peroxidase-injected interstitial amacrine cell of the monkey retina. Cell as a proximal "dendritic field" (dashed processes) and a distal "axonal field" (solid processes).

scale bar − 50μm

(89)
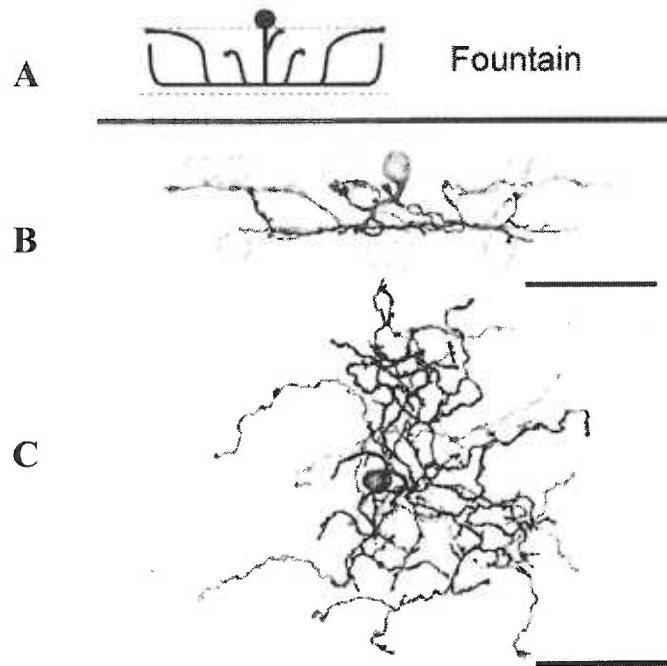
Figure 1.24. Fountain Amacrine Cell Anatomy – Fountain
amacrine cells from rabbit retina. **A.** a schematic drawing of the
fountain amacrine cell viewed in the Z-plane. **B.** A drawing from
a Golgi-stained Fountain amacrine cell viewed from the Z-plane.
C. A drawing from the same Golgi-stained fountain amacrine cell
viewed from above.

Scale bars 50μm

(38)

These cells are thought to possibly be homologous to the substance P reactive cells found in the cat retina (58; 75; 99). These two cell types have similar "retroflexive" dendritic patterns, but the fountain amacrine cell of the rabbit retina has yet to be tested for substance P immunoreactivity. Finally, the physiology of the fountain amacrine cells has also yet to be examined.

Starburst Amacrine Cell

Starburst amacrine cells are cholinergic neurons with a distinct radially symmetric morphology. There are 3-4 primary dendrites that branch out in a regular fashion with round varicosities along each dendrite, giving the cell the appearance of a "starburst" firework (18) (Figure 1.25). Starburst amacrine cells were found to colocalize GABA and acetylcholine, endowing it with both inhibitory and excitatory capabilities. There are two populations of starburst amacrine cells, one with somata located in the INL and dendrites that stratify in sublamina a of the IPL and one with somata in the GCL and dendrites that stratify in sublamina b (19; 21).

Starburst amacrine cells are thought to play a role in the formation of the receptive field properties of the direction selective ganglion cells (DSGCs). In fact, starburst amacrine cells costratify with the ON-OFF DSGCs in the rabbit retina (Figure 1.26) (20; 21). The direct mechanism by which starburst cells contribute to direction selectivity is still highly debated. Starburst amacrine cells only receive input in the proximal regions of their dendritic trees and send output signals via the distal portions.
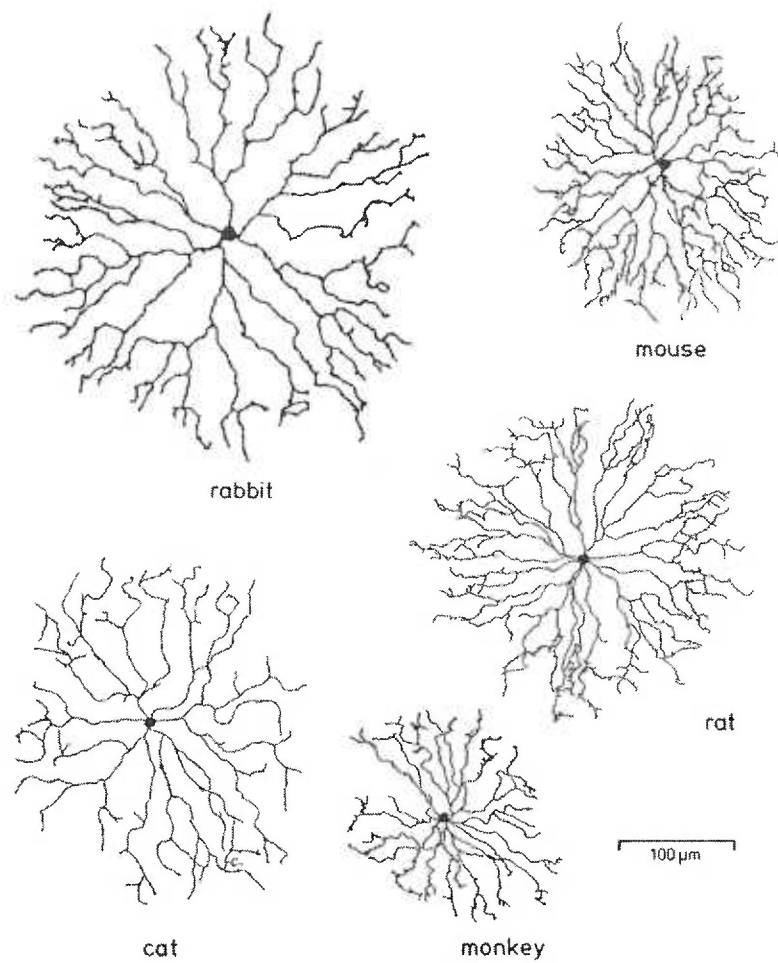
Figure 1.25. Starburst Amacrine Cell Anatomy - Drawings

from putative cholinergic amacrine cell conforming to the

starburst morphology from retinas of 5 different species.

(89)
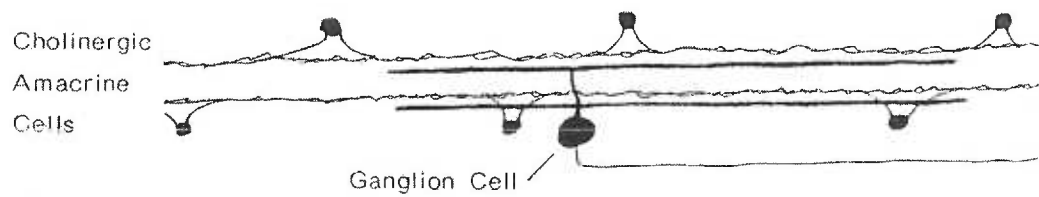
Figure 1.26. Two Populations of Starburst Amacrine Cells – Schematic drawing from rabbit retina. Two layers of spatially opposing starburst amacrine cells with costratifying DS Ganglion cells in the IPL.

(21)

The starburst cells' spatial segregation of synaptic inputs and outputs and arrangement on either side of a DSGC is thought to contribute somehow to the formation of a preferred direction in the DSGC's receptive field (8). Additionally, since starburst cells contain both acetylcholine and GABA, it is widely assumed that acetylcholine mediates the stimulation of a DSGC in its preferred direction and GABA mediates the inhibition in the null direction (8).

Amacrine Cell Functional Subtypes

With speculations on the existence of up to 40 distinct anatomical types of amacrine cells, it becomes a daunting idea that each may represent a distinct functional cell type. It may, however, be the case that there exist far fewer functional cell types that are simply morphologically heterogeneous. Masland in 1988 proposed to classify amacrine cells in to three broad functional groups based on morphology and retinal distribution. He grouped cells based on their similarity to the handful of amacrine cells that have been well characterized, the AII, A17, starburst, and the dopaminergic amacrine cell. The functional roles assigned to each new group were then based on very general descriptions of the functional properties of each well-characterized amacrine cells (41). First he introduced the densely packed, narrowly branched amacrine cells (AII). These cells were predicted to play a mostly throughput role in retinal processing similar to the one the AII amacrine cell plays. Secondly, the sparsely distributed, widely branched amacrine cells (dopaminergic), were thought to play mainly global regulatory roles across the retina. Finally, Masland described the densely overlapping amacrine cells (A17, starburst) that vary in dendritic size. The cells in this group are described as playing a mostly modulatory role, either locally or over larger sections of retina.

Although structure often predicts function, with respect to retinal neurons it is imperative that basic physiological properties be considered as well. Amacrine cells identical in morphology but dissimilar in, for example, excitable membrane properties or spontaneous membrane properties may be drastically different in function. The clearest example of this is in the case of spiking properties. Several early modeling studies performed on hippocampal neurons that elaborated the cable theory to include a more realistic multi-compartment model determined that in a non-spiking cell signal attenuation increases with respect to length and number of dendritic branch points (29; 48). Considering the often large and highly branched unmyelinated dendritic trees of several amacrine cells, spiking properties may have profound influence over function. Bloomfield in 1992 tested this idea by measuring the receptive fields of several amacrine cells before and after TTX application. He found that when action potentials were blocked, the receptive fields were reduced to less than the dendritic field (1). This indicated that the cells were indeed relying on active propagation via sodium spikes to move information across the whole of their dendritic trees. In fact, Bloomfield estimated that any amacrine cell with a dendritic diameter of more than 525 μm would require the generation of action potentials in order to maintain electrical continuity across its dendritic tree. Cells larger than 525 μm in diameter that were incapable of spiking were predicted to possess dendrites and/or dendritic domains electrically isolated from its soma and the rest of its tree. The lack of electrical continuity of an amacrine cell would have a profound impact upon its function. For example, wide field spiking amacrine cells have the logical potential to play global regulatory or modulatory roles across the retina, while non-spiking wide field cells would be confined to local effecter roles.

An amacrine cell classification scheme that considers both morphology and basic physiology has yet to be established. If our understanding of amacrine cell function is to ever be expanded beyond the handful of well-described cell types, then it is imperative that future examinations include additional relevant factors that contribute to the potential function of a given amacrine cell.

Displaced Amacrine Cells

A large population of amacrine cells is located in the ganglion cell layer of the retinas of most species. Considering the substantial population size of these displaced amacrine cells (DACs), the time devoted to studying them has historically been highly limited.

Despite the early establishment of a displaced amacrine cell (DAC) population in non-mammalian vertebrate retinas (Cajal, etc.), when observed in mammals these small cells were described, until relatively recently, as being glial cells or ectopic amacrine cells that failed to migrate to the inner nuclear layer during development. As early as 1882, Garner established that, in the cat retina, many small cell bodies survived retrograde degeneration of ganglion cells via optic nerve degeneration. Later studies utilizing retrograde HRP labeling established that these small cells do not possess axons that project to the brain and are therefore non-ganglion cells (56; 57; 76). Hughes et al demonstrated the neuronal nature of these non-ganglion cells using kainate toxicity in 1980. These neurons were subsequently named microneurons and thought to possibly represent a class of displaced amacrine cell. Their reported population size of (730,000) surprisingly outnumbers both the ganglion cell population and the number of optic nerve fibers (128-180,000) in the cat retina (31; 76).

Studies of rabbit retina uncovered a large subset of cells in the ganglion cell layer that do not project to the optic nerve and survived optic nerve transection. These cells were described as being a class of displaced amacrine cell (31; 76). Using Nissel staining, Vaney later defined a significant subset of rabbit DACs called "coronate cells" based on the shape and pattern of the basophilla staining within the cell bodies (30) (Figure 1.27). Coronate cells were later found to correspond anatomically to the starburst amacrine cell previously identified in the IPL. Starburst cells make up 85% of the DACs and 32% of the total cells in the ganglion cell layer of the rabbit retina (77; 81). The displaced starburst amacrine cells were found to have a fairly conserved anatomical structure and are reactive to cholinergic markers. In addition, the displaced starburst cells were found to stratify in the ON layer of the IPL. Subsequently, rabbit starburst amacrine cells were divided into two subtypes, *a* and *b*, that physically oppose one another in a mirror image fashion. Type (a) starburst cells have somas that lie in the INL and dendrites that stratify in the *a* sublamina of the IPL (the OFF layer). Type *b* starburst cells have somas that lie in the ganglion cell layer and dendrites that stratify in the *b* sublamina of the IPL (the ON layer). As discussed earlier, type *a* and *b* starburst cells are thought to play a roll in the OFF and ON responses, respectively, of directionally selective ganglion cells.

In the cat retina, DACs make up 80% of the neurons in the ganglion cell layer and have a topographical distribution similar to ganglion cells (96). Their density peaks near the area centralis at 4,500-7,000 cells mm^{-2} and falls to less than 1,000 cells mm^{-2} (90; 96). Investigations of cat retinal DACs utilizing immunocytochemistry and autoradiography found the presence and colocalization of several neurotransmitter markers. The uptake of H^3-muscimol labeled 75% of DACs, while antibodies against

choline-acetyl transferase labeled about 10-17%, and 25-30% took up serotonin (5-HT) (90). The morphology of DACs described in cat retina to date has been very limited and mainly focused on cell body distribution. However, some examples of DACs have been reported to have dendritic morphologies similar to cells previously identified in the IPL. For example, DACs visually corresponding to the multiple branched A17 cell , the very wide field A20, and cell the starburst amacrine cell have been observed (34; 37).

With the exception of the rabbit retina, mammalian DACs have been described to be a heterogeneous group of cells both immunohistochemically and anatomically. There has been little attempt so far to identify clear homogeneous subgroups of cells. If one's ultimate goal is to discover the functional role DACs play in retinal processing, then it is imperative to identify subgroups of cell types based on a selection criteria that is functionally relevant.

As elaborated upon in the preceding section, physiological and morphological properties must be considered when attempting to categorize amacrine cells in functional groups. A classification scheme that includes both types of properties could conceivably be applied to all amacrine cells in the retina the cells located in the INL and the cells of the GCL.

The working hypothesis, for this project, is that the morphological and physiological diversity among DACs is comparable to that observed among INL amacrine cells. We also predict that there will be relationships between morphological and physiological trends; for example DACs with large dendritic fields will be more likely to fire action potentials than small-field DACs. With that hypothesis in mind, there are several goals for the present study of the DAC population.
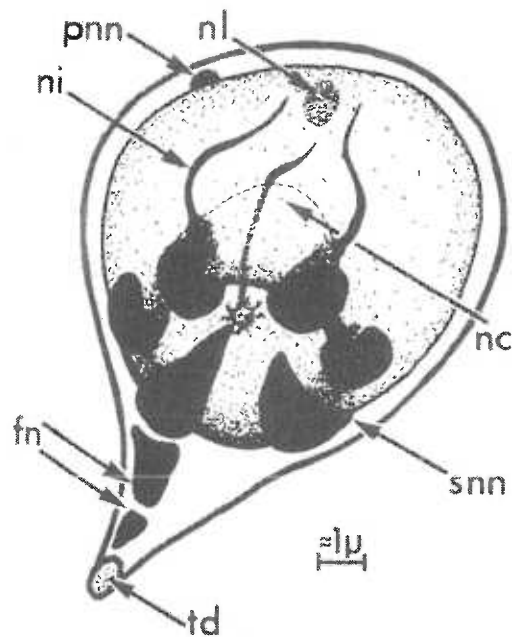
Figure 1.27. Coronate Amacrine Cells - A schematic drawing of a coronate cell from rabbit retinal showing the cupped nucleus. The rim of Nissel substance around the encapsulated cytoplasm **(nc)** is interspersed with large blocks of subnuclear Nissel substance **(snn)**. The major dendritic process **(td)** contains free Nissel material **(fn)** and a perinuclear Nissel granule is apparent **(pnn)**. Invaginations into the nucleus from the cytoplasmic cup are packed with basophil material **(ni)** and appear to approach the nucleus **(nl)**.

(30)

Because little is known about the detailed morphology of these cells and nothing is known about the extent of their physiological diversity, the first goal of this project was information gathering. We set out to learn as much as possible about the basic intrinsic membrane properties, and in the process, hoped to compare that to what we discover regarding morphology. We chose physiological properties such as input resistance, resting potential, spiking properties, and spontaneous membrane activity due to the impact these characteristics have on a cell's functional capabilities.

We also chose to examine the detailed morphology of DACs with the hope to uncover anatomical groups of based on functionally relevant characteristics. We also employed an approach to sorting DACs into morphological groups that was strongly based in statistics. Our hope was to gather morphological and physiological data for a large sample population, in order to develop a framework in which to evaluate the cells' potential for function. Although constructing such a framework turned out to be an unrealistic goal, we did discover a great deal about DACs in the ferret retina.

Several physiological groups of DACs are identified and discussed as well as several morphological groups. These groups provided many insights into the functional properties of these neurons. This study has also generated many more questions and new directions for future research in this area. DACs are certainly more than a trivial group of retinal interneurons and, as the information provided here indicates, may be present in a physiological and morphological diversity that equals amacrine cells of the INL.

CHAPTER 2:

PHYSIOLOGICAL RESPONSE PROPERTIES OF DISPLACED AMACRINE CELLS OF THE ADULT FERRET RETINA

Sally W. Aboelela and David W. Robinson

Submitted for Publication

Abstract

The ganglion cell layer (GCL) of the mammalian retina contains a large number of neurons called displaced amacrine cells (DACs) that do not project to the optic nerve. However, with the exception of the rabbit starburst amacrine cell, little is known regarding the function of this large population, due to the difficulty experienced in making physiological recordings from these neurons. We have overcome these difficulties and have used whole-cell patch-clamp techniques to examine the intrinsic membrane properties of DACs in the ferret retina. Our results indicate a large degree of diversity in the intrinsic membrane properties. In response to maintained depolarizing current injection, DACs respond with graded depolarization or by eliciting either transient or sustained bursts of spiking activity. At the resting membrane potential, 10% of the DACs generated spontaneous spikes in either an apparently random manner or at the peak of intrinsic waves of depolarization. The resting membrane activity of the remaining DACs recorded could be classified into three groups that were quiescent (28%), had robust uncorrelated synaptic activity (30%) or underwent slow waves of depolarization (42%). Diversity was also revealed in the membrane currents recorded in voltage-clamp where some DACs were quiescent (19%) or exhibited robust non-rhythmic synaptic events (42%). The remaining DACs exhibited waves oscillatory activity (39%), characterized by either rhythmic bursts of synaptic events (17%) or slow inward currents (22%). Bath application of 50 μM Biccuculine or 150 μM Picrotoxin had no effect on the waves of activity, however, the gap junction blocker, Carbenoxolone (100 μm), blocked both oscillatory patterns. By including Lucifer yellow and Biocytin in the recording pipette, it was possible to determine the morphology of recorded DACs. Based on

63

dendritic extent, neurons were classed as small, medium, or large field DACs. There were few relationships between these morphological classes and their intrinsic membrane properties. The present study provides the first in-depth examination of the intrinsic membrane properties of DACs in the ferret retina and provides new insights into the potential roles these neurons play in the processing of visual information in the mammalian retina.

Introduction

The ganglion cell layer (GCL) of the mammalian retina contains a large number of non-axon-bearing neurons called displaced amacrine cells (DACs) that do not contribute to the optic nerve (28; 30). These cells make up 35% of the neurons in the ganglion cell layer of the rabbit retina (28); (30);(81), 50% in the rat retina {Perry, 1981 40 /id}, and 80% in the cat retina (31){Wassle, 1987 34 /id}{Wong, 1987 35 /id}. DACs are extremely numerous and diverse, therefore it is imperative to identify a criteria to sort these neurons in order to understand their contribution to retinal processing.

Immunocytochemical studies have revealed a wide diversity in DAC neurochemistry. In the cat, for example, 75% of the DACs react positively for GABAergic markers, 10-17% for cholinergic markers, 25-30% for serotonin uptake, and 5% for NADPH diaphorase {Wassle, 1987 34 /id}. Such distributions clearly indicate the co-expression of neurotransmitters in a single neuron; making unambiguous functional classifications of DACs difficult based solely on their neurochemistry.

Amacrine cells have historically been to classified based on their morphology and physiology. Unfortunately, with the exception of the starburst amacrine cell, such classifications of DACs in the mammalian retina have not been possible due to a lack of detailed morphological and physiological data. With respect to amacrine cells located in the Inner Nuclear Layer (INL), despite the recognition of at least 26 morphological cell types {Kolb, 1981 KOLB1981 /id}{MacNeil, 1999 25 /id}, clear functional roles have only been demonstrated in four cell types: AII, A17, dopaminergic and starburst amacrine cell. The AII amacrine cell is a spiking narrow-field cell that links rod bipolar cells to the cone pathway (12; 68; 80; 83); the A17 is a large field spiking cell that

modulates the transmission of information from rod bipolar cells to AII amacrine cells (12; 27;54); the starburst amacrine cell is a medium field neuron involved in the formation of direction-selective receptive fields (72); and finally, the dopaminergic amacrine cell is a large field spiking neuron that contributes to the regulation retinal responses at varying levels of illumination (4; 26; 59).

Due to the paucity of methods available to pre-select cell types, the functional characterization of the remaining ~22-amacrine cell types would be a prohibitively difficult undertaking. Therefore, previous studies have defined functional groups of amacrine cells based on similarities in morphology and topography to the AII, A17, dopaminergic and starburst amacrine cell (41). However, one weakness in relying so heavily on morphology is that it ignores the critical influence intrinsic membrane properties may have on a cell's functional role. For example, crucial functional properties of the starburst and A17 amacrine cells were redefined and clarified once physiological recordings were made in these neurons. A useful approach, therefore, may be to construct general functional groups of amacrine cells based on both morphological and physiological similarities to the four well-characterized amacrine cells of the INL. The goal of this study is to apply this approach to the study of DACs and to gather the important prerequisite morphological and physiological information.

We have utilized a combination of whole-cell patch-clamp techniques, in current-clamp mode, and intracellular filling to examine the passive and excitable membrane properties of DACs in the adult ferret retina. In addition we use voltage-clamp techniques to investigate the membrane currents underlying the synaptic activity observed in our current-clamp recordings. We show that while DACs can be classified into three groups

66

based on their ability to generate spikes, there is little to no correlation between this ability and the size of their dendritic extents. In addition, we report for the first time the presence of slow oscillations in the resting membrane potential, which are blocked by the gap junction blocker, Carbenoxolone.

The present study provides the first morphological and physiological survey of DACs and serves as a first step in understanding their functional role in retinal processing.

Specific Methods

Tissue Preparation

All procedures were performed in accordance with the approved animal use protocols at the National Institute of Health (NIH) and by the institutional IUCAC committee. Ferrets (*Mustela Furo*) were given a fatal dose of sodium pentobarbital. The eyes were removed and placed in Eagle's minimum essential media (EMEM). The eyes were then hemi-sectioned and, under a dissection microscope (Leica GZ4), the retinas removed from the sclera using a periodontal elevator. The retinas were then cut into 4 quadrants and each quadrant cut in half with the peripheral and central portions segregated. Retinal sections were incubated in EMEM bubbled with 95%/5% O_2/CO_2 until they were prepared for recording.

Electrophysiological Recording

To prepare a wholemount, a retinal section was mounted on a piece of nitrocellulose filter paper with a 2-mm hole cut in it to provide access for the recording electrode. This preparation was placed, ganglion cell layer facing up, in the recording chamber, which was mounted on the stage of a Zeiss Axioskop microscope. The tissue was bathed in a solution containing (mM): 120 NaCl; 5 KCl; 3 $CaCl_2$; 10 HEPES; 10 Glucose; 1 $MgCl_2$; pH adjusted to 7.35 using NaOH (285-295 mOsm) and bubbled with 100% O_2 at room temperature. Recording electrodes with resistances between 5-7 MΩ were pulled from borosilicate glass using a Sutter Instruments model P-97 micropipette puller. The electrodes were filled with a solution containing (mM): 120 KCl; 10 NaCl; 10 HEPES; 1 $CaCl_2$; 11 EGTA; 1 $MgCl_2$; 3 ATP; 1% Biocytin (Sigma); 1% Lucifer Yellow (Molecular Probes, lithium salt); pH was adjusted to 7.35 using KOH (285-290 mOsm). Displaced

amacrine cells were exposed by manually removing portions of the basilar membrane using an empty glass electrode. Recordings were made at room temperature (~22 °C) using an Axopatch 200B amplifier controlled by pClamp8 software via a Digidata 1320 interface (Axon Instruments). Data was collected at rates between of 5 and 10 kHz and low-pass filtered at 2kHz.

Anatomical Identification

At the end of each recording, a –200 mV hyperpolarizing potential was applied to facilitate diffusion of Lucifer Yellow and biocytin into the cell. Once adequate filling was achieved, the retina was fixed in 4% paraformaldehyde for 6-8 hours at 4°C. Following fixation, retinas were processed using a standard diaminobenzidine reaction (Vectastain ABC kit). DACs judged to be fully stained by the DAB reaction were reconstructed in 3D using Neurolucida (MicroBrightField) and subsequently analyzed using NeuroExplorer (MicroBrightField).

Statistical Analysis

All values are given as the mean ± standard deviation. Significance was determined using the Student-t test.

Results

Successful patch-clamp recordings were performed on 195 amacrine cells located in the ganglion cell layer of the adult ferret retina. To ensure that recordings were not made from retinal ganglion cells, only neurons in the ganglion cell with soma diameters of less than 15 μm were selected for recording and the absence of an axon was confirmed subsequent to recording. The membrane potential at rest and its response to maintained depolarization were examined in 123 neurons using the whole-cell patch-clamp technique in current-clamp mode. To characterize the membrane currents responsible for the membrane activity at rest, voltage-clamp recordings were made in 72 DACs.

Passive Membrane Properties

On attaining the whole-cell configuration in current-clamp mode, the resting membrane potential was noted and monitored throughout the remainder of the recording. If the membrane potential became more than 10 mV more depolarized than its initial value the recording was terminated. In addition, neurons with resting potentials more depolarized than –45 mV were excluded from the study. The mean resting membrane potential obtained for every DAC included was –55 $\pm$ 6 mV (n = 100). The input resistance of each DAC was assessed by applying increasingly higher maintained current injections for 400 ms. The maximum change in membrane potential resulting from each current injection was plotted against the input current and the data were fit with a linear regression, the slope equaled the input resistance. The average input resistance of this group was 550 $\pm$ 253 MΩ (N = 70).

Excitable Membrane Properties

To assess the spike generating ability of DACs maintained, 400 ms, depolarizing currents with successively greater magnitudes were applied (Figure 2.1). About half (N = 63, 51%) of the cells studied responded to this stimulus regime with graded depolarization and were unable to generate spikes even at the most depolarized membrane potentials (Figure 2.1-A). The responses of the remaining DACs in this study (N = 60, 49%) were able to generate spikes to maintained depolarization (Figure 2.1-B and C), however the pattern of spike discharge could be grouped into two populations, transient (N = 35 or 29% of total) and sustained (N = 25 or 20% of total). Transiently firing DACs responded to maintained depolarization, above threshold, with one or two spikes at stimulus onset and the number of spikes generated did not increase with the magnitude of the depolarizing current. (Figure 2.1-B). In contrast, sustained firing DACs elicited spikes throughout the duration of the maintained depolarization (Figure 2.1-C) and there was a linear relationship between the number of spikes generated over the range of stimulus magnitudes used (Figure 2.1-D). The average spike frequency observed in sustained firing DACs was 25 ± 7 Hz (N = 25) and the average frequency response slope was 0.57 ± 0.19 Hz/pA.

Spontaneous Activity at the Resting Membrane Potential

At their resting membrane potential, DACs exhibited robust spontaneous activity characterized by a wide diversity of patterns. A small number (N = 11, 10%) of the DACs examined (N = 109) exhibited spontaneous spiking activity at the resting membrane potential. Between 12 and 60 spikes were typically observed in a one-minute recording and these spikes were either randomly (Figure 2.2-A) distributed throughout the

71

recording (N = 5) or at the peak of regular waves of depolarization (N = 6) (Figure 2.2-B). By and large, however, the spontaneous membrane activity of all the DACs examined could be separated into three general groups. The first group (N = 31, 28%) displayed little to no activity at the resting membrane potential (Figure 2.3-A), while in the second group (N = 32, 30%), robust, non-rhythmic synaptic activity could be observed (Figure 2.3-B) including the random spontaneous spiking mentioned above. The final group (N = 46, 42%) was characterized by slow (mean: 0.15 ± 0.06Hz) waves of depolarization that occurred at regular intervals (Figure 2.3-C), including those possessing spikes at the peak of many waves.

Table 1 summarizes the distribution of spiking properties with respect to spontaneous membrane activity at the resting potential. There appeared to some relationship between these activity patterns; the less active a cell was at rest, the more likely it was to also be incapable of generating action potentials.

Inducible and Spontaneous Whole Cell Currents

Using the voltage clamp method, the inducible whole cell currents were examined in a total of 76 DACs. Cells were held at –90mV and taken to 15 voltage steps exactly 1.00s apart. The first and second steps were from –90mV to –100 mV back down to –90mV in order to calculate and correct for leak current. Subsequent voltage steps were progressively depolarizing in intervals of 10mV until a peak of +40mV. In response to this protocol, DACs displayed three types of inducible whole cell currents (Figure 2.4). A total of 41% of DACs (N = 31) responded to depolarization with the activation of slow outward current; presumably K+ mediated (Figure 2.4-A). Alternatively, 21% (N = 16) of

72

the DACs responded to depolarization with the activation of a voltage-dependent inward current (at step –40 or –50mV) followed by an outward current (Figure 2.4-B). Finally, 38% of DACs (N = 29) responded to depolarizing voltage steps with a rapidly activated (at approximately step –30) transient outward current followed by a slower persistent outward current (Figure 2.4-C). When the protocol was repeated with the holding potential at –40mV instead of –90mV the transient outward current was attenuated and only the slow persistent outward current was observed.

To examine the membrane currents underlying the different patterns of spontaneous activity observed in current clamp, whole-cell voltage-clamp recordings were made while holding the cells at –90 mV (n = 72). In agreement with the recordings made in current-clamp, DACs exhibited diverse patterns of synaptic activity, which could be categorized into three groups (Figure 2.5). Approximately 19% (n = 14) of the neurons studied were quiescent at –90 mV (Figure 2.5-A), while 42% (n = 30) displayed miniature events that occurred in an apparently uncorrelated manner (Figure 2.5-B). The remaining DACs (39%, n = 28) exhibited regular waves of activity at the same frequency (mean: 0.15 ± 0.06Hz) as that observed in our current-clamp recordings (Figure 2.5-C and D). With the exception of the "quiet at rest" group, the percentage of resting activity patterns recorded in voltage clamp was similar to those recorded in current clamp (respectively, 42% vs. 32% active at rest and 39% vs. 42% oscillatory at rest). It should be strongly noted, however, that comparisons between current clamp and voltage clamp experiments should be considered gingerly due to the discrepancy between the average resting potential (-55± 6 mV) and the holding potential (–90mV).

The slow waves observed in this study were characterized by two distinct patterns of oscillatory activity. The waves in one oscillatory group (N = 12, 43% of oscillatory cells and 17% of total) were composed of correlated synaptic activity that often summated at the peak of the wave (Figure 2.5-C). We term DACs belonging to this group as summating oscillatory cells. In contrast, the second oscillatory group (N = 16, 57% of oscillatory cells and 22% of total) exhibited regular fluctuations in their baseline membrane current; neurons in this group are referred to as baseline oscillatory cells (Figure 2.5-D).

It has been reported that over 75% of all amacrine cells are GABAergic (Wassle *et al.*, 1987) and to test whether these depolarizing waves resulted from correlated GABA-mediated synaptic events, 50 μM Biccuculine or 150 μM Picrotoxin was added to the bathing solution ($Cl_{rev} = 0$ mV). In no cases (n = 15) were these GABA receptor blockers effective in reducing or abolishing the oscillatory waves of inward current (data not shown).

In order to verify that the oscillatory behavior observed in this subset of DACs was a physiologically relevant pattern of activity; the recording conditions were adapted. In order to bring the chloride reversal potential closer to physiological values (-88mV), potassium gluconate replaced potassium chloride in the bath solution. The oscillatory behavior persisted under these conditions.

The common observation of dye coupling among DACs during the anatomical processing of the tissue, lead us to examine state of electrical transmission among our cells. In contrast to the GABA blockade experiments, the potent gap junction blocker, Carbenoxolone (100 μm), was effective at either completely eliminating or greatly

74

attenuating the spontaneous oscillatory behavior (Figure 2.6) in all of the DACs tested (n = 9). This observation was consistent in both summating oscillatory cells (compare Figure 2.6-A1 with A2) and in baseline oscillatory cells (compare Figure 2.6-B1 with B2). Cells treated with Carbenoxolone still displayed random membrane activity, indicating that synaptic transmission onto the cells was still intact.

Anatomical Classification

DACs from which recordings were made exhibited a wide diversity in size and dendritic complexity (Figure 2.7, upper panel) and were grouped, based on their dendritic extent, into 3 classes: small-field (< 200 μm), medium-field (200 – 500 μm), and large-field (> 500 μm). A qualitative examination of the Lucifer yellow filled cells using epifluorescence microscopy revealed that the complexity of dendritic tree appeared to differ between the three anatomical groups; small-field cells were the most highly branched while large-field cells had the least degree of branching (c.f. Figure 2.7). Filled cells were processed through a standard DAB reaction and well-reacted neurons (n = 55) were drawn in 3D using the Neurolucida neuronal reconstruction software package and subsequently analyzed with NeuroExplorer. Of the 55 reconstructed neurons 12 (22%) were classified as small-field DACs, 18 (33%) as medium-field, and 25 (45%) as large-field. Cells stratified (lower Panel, Figure 2.7) in depths of either 15-25 μm (N = 25, 46%) or 40-60 μm (N = 30, 54%). Based on previous anatomical work on the ferret retina, the medial most margin of the ganglion cell layer (where the somas of the DACs reside) is 18-25 μm from sublamina b of the inner plexiform layer and 40-50 μm from sublamina a (Shields *et al.*, 2000).

Discussion

In the present study, we have examined the intrinsic membrane properties of amacrine cells located in the ganglion cell layer of the ferret retina. We show that while the input resistance and resting membrane potential were similar across all of the neurons examined, there were marked differences in the ability of DACs to generate spikes and certain spiking patterns in response to maintained depolarization. DACs were also found to exhibit a wide diversity in membrane activity at rest with one population exhibiting an oscillatory behavior that has not previously been described. Utilizing intracellular filling, we show that DACs have similarly diverse morphologies as those described for amacrine cells of the INL. Table 2.2 summarizes the distribution of physiological properties with respect to dendritic field size. There appeared to be no correlation between either spiking properties or spontaneous membrane activity and dendritic field size. A more detailed morphological analysis may be necessary in order to resolve relationships between physiology and anatomy. Such an in-depth morphological study would be a useful future direction.

Relationship Between Spiking Ability and Dendritic Morphology

The ability to generate spikes would permit a neuron to rapidly transmit information across the whole of its arbor. Based on the observations made in the rabbit starburst amacrine cell (1; 3), one would expect that the receptive field sizes of spiking DACs would equate with the size of their dendritic extent. In contrast, the receptive field size of non-spiking DACs would be limited by the neuron's morphology and its passive cable properties. It is important to note however, that the receptive fields of the spiking-axon-

76

bearing amacrine cells, such as the Polyaxonal cell type, have been demonstrated to be as large as their dendritic field but not as large as their axon arborization. (71; 87) Although electrical continuity is intact by virtue of their spiking ability, the extensive axon arborization in these cells seem specialized not for receiving inputs but rather for the projection of synaptic outputs. These axon-bearing amacrine cells do however; serve as an important example of the care that must be taken when speculating on electrical continuity based on receptive field size. The interaction, however, between spiking ability and morphology clearly determines a cells electrical continuity and therefore limits its potential functional role in retinal processing. By combining spike generating ability - or inability - with the dendritic extent of recorded neurons, three functionally relevant groups begin to emerge in our study: i) spiking cells of any dendritic size; ii) non-spiking, large-field cells; and iii) non-spiking, small- and medium-field, cells.

Spiking DACs can be thought of in two general ways with regards to their putative roles in any given retinal circuit. These cells would be electrically continuous and capable of conveying signals either vertically in a retinal circuit (similar to the narrow–field AII) or by laterally modulating many parallel retinal circuits (like the wide-field A17) (41). The spiking cells we observed exhibited a wide variety of dendritic extents, which may help determine which of these two functional roles any given spiking neuron might play. Furthermore, the spike pattern may serve to provide additional information regarding the light stimulus. Continuously spiking DACs displayed a positive linear relationship between injected current and spike frequency, indicating the potential to convey information about signal intensity, while transiently spiking cells would be limited to conveying signal onset. It is notable to mention that the large-field group had the largest

portion of continuously spiking cells (45%, compared to 13 and 16% in small and medium field respectively), while the small-field group had the most transiently spiking cells (46% compared to 19 and 21% in medium and large field respectively; Table 2.2).

Another functional group, consisting of non-spiking-large-field DACs will have electrically-isolated domains that are autonomous from the rest of the cell. Individual dendrites or dendritic domains located on the same cell could independently modulate several different retinal circuits. These cells would be ideal for local modulation and could play dynamic but spatially resolved roles in multiple circuits (41).

Finally, the electrical continuity of non-spiking, small- and medium-field, DACs as a group is difficult to resolve because the attenuation of a signal is determined not only by length but also by the complexity of dendritic branching (15; 48). The more highly branched a cell is, the more quickly signal attenuation occurs. Based on our observations, small- and medium-field DACs were more highly branched than large-field neurons (visual observation, Figure 2.7). Therefore, it is likely that at least some portion of small- and medium-field non-spiking DACs will also have electrically-isolated dendritic domains suitable for local modulation. The remainder would be electrically continuous and more suited to participate in either the rapid vertical transmission of information through the retina or lateral modulation of retinal circuits within the confines of its entire dendritic arbor.

Functional Implications of Oscillatory Membrane Activity

The most surprising pattern of spontaneous activity we observed was the presence of low frequency (0.15 ± 0.06Hz) waves of excitatory activity. Similar waves of activity

have been extensively reported in the developing ferret retina (45; 94; 95; 97; 98). During development, retinal ganglion cells undergo synchronized bursts of spontaneous action potentials, driven by oscillatory cholinergic amacrine cells located in the GCL (104). This pattern of activity is thought to be crucial in the segregation of retinogeniculate afferents (95) and ceases in both ganglion and amacrine cells by eye opening, P10 (45; 94; 104). Since the age of ferrets used in this study was from P46 and older, the oscillations reported here are assumed to be a previously unreported feature of the adult ferret retina.

Oscillatory neuronal activity of varying frequencies is common in many regions of the CNS (43; 74; 103). Based on both empirical work and computer simulations, it has been shown that networks formed exclusively from interneurons are capable of generating rhythmic oscillatory activity (65; 74; 103). For example, large numbers of oscillatory GABAergic interneurons in the hippocampus are heavily interconnected in distinct networks capable of generating coherent rhythms in principal neurons (projection neurons) (103). Considering that 75% of DACs are GABAergic interneurons (96), the oscillatory neurons observed in this study could represent a network of cells analogous to those observed in the CNS.

The oscillatory waves of activity were resistant to GABA blockade in the form of bath-applied Biccuculine and Picrotoxin, indicating that the waves were not GABAergically driven. However, often during anatomical processing of Biocytin-filled DACs, we observed a high degree of cell coupling, implying gap junction connections and therefore electrical coupling. The low frequencies of the oscillations observed in DACs (0.15 ± 0.05 Hz) are also consistent with a gap junction mechanism. Transmission

efficacy through gap junctions is highly frequency-dependent; lower frequencies result in higher coupling ratios and lower phase-lag allowing gap junctions to act as "Low Pass" filters (43). Application of Carbenoxolone (a gap junction blocker) successfully attenuated the oscillatory waves of activity in 10 out of 10 cells, supporting a role for gap junctions. Spontaneous synaptic activity was persistent during Carbenoxolone application, indicating that chemical transmission onto these neurons was intact and only electrical transmission was disrupted.

It is also intriguing to note the presence of two activity patterns among oscillatory DACs: the "summating oscillatory cells" (Figure 2.5-C) and the "baseline oscillatory cells" (Figure 2.5-D). The activity pattern in summating cells is most consistent with periodic input possibly via a chemical synapse, while the activity pattern in baseline oscillatory cells is most similar to rhythmical electrical synaptic communication. It is possible that baseline oscillatory cells make up a network of electrically coupled cells in the retina; while summating cells are indirectly connected to this network via chemical synaptic input (Figure 2.8).

The model, of an oscillatory amacrine cell network in the retina, is an intriguing one that leads to many further questions. Several brain regions employ synchronous inhibitory activity by GABAergic interneuronal networks onto principal neurons, the result of which is often synchronized oscillatory electrical activity (46). Could oscillatory GABAergic DACs be organized into a network across the retina in order to impose some synchronized input onto ganglion cells? If so, what purpose does such input serve with respect to visual coding?

In conclusion, the present study identifies several morphologically and physiologically distinct groups of DACs in the ferret retina. When these groups were examined with respect to each other, several functionally relevant groups of DACs emerged. In addition, we report a previously unidentified pattern of spontaneous activity (oscillatory DACs) that may be a novel physiological and/or functional cell type. These findings provide crucial insight into the possible roles played by DACs in retinal processing.

Figure 2.1
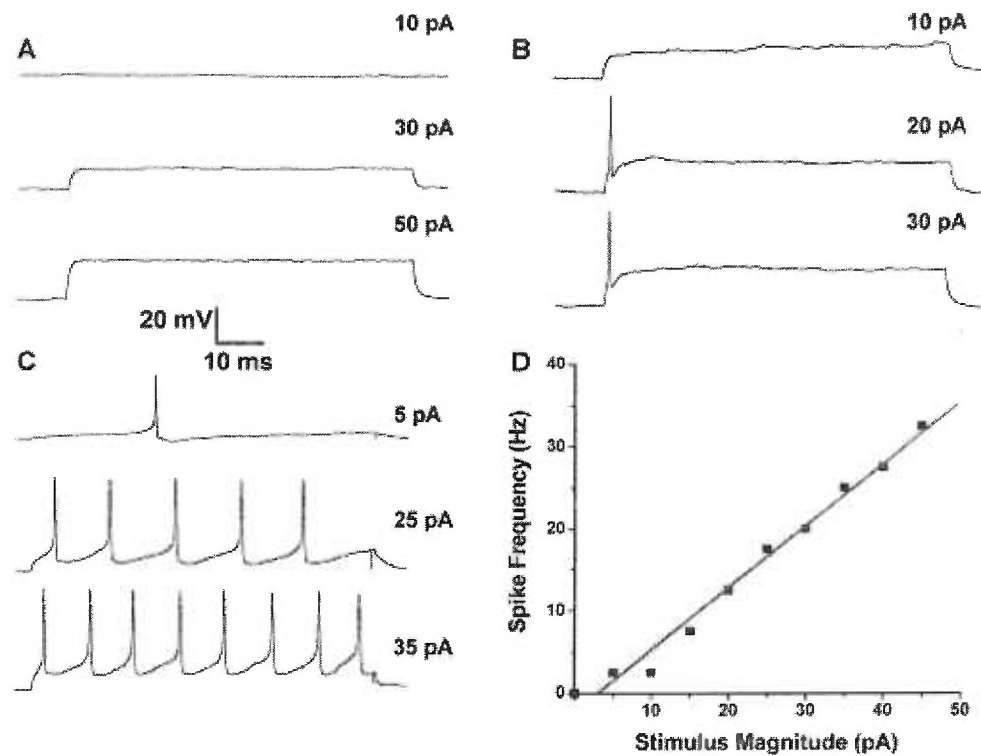
Figure 2.1. Response to Maintained Depolarization. (A) In response to maintained depolarization, 51% of the DACs examined responded in a graded manner. Of the remaining DACs, 29% responded with a transient burst of spikes (B), while the rest (20%) elicited sustained trains of spikes (C). The stimulus magnitude used to elicit each response shown is indicated on the right of each trace. In DACs that generated sustained firing patters, there was a linear relationship between frequency of spike output and the stimulus amplitude. (D) A plot of the response frequency as a function of the stimulus magnitude. The straight line was iteratively fit and has a slope of 0.75 Hz/pA

Figure 2.2
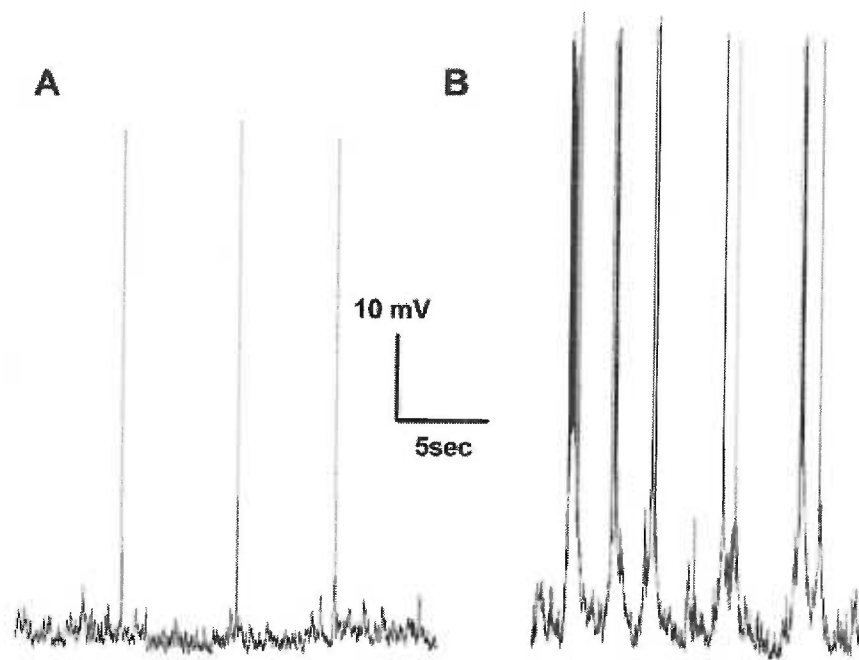
Figure 2.2. Spontaneous Spiking - At the resting membrane potential 10% of the DACs examined exhibited spontaneous spikes. The pattern of this spontaneous spiking activity fell into two groups. In the first group (A), spikes were randomly distributed, while in the second group (B), spikes occurred at the crest of waves of depolarization. In the second group, spikes were rarely seen between the waves of depolarization resting membrane potential.
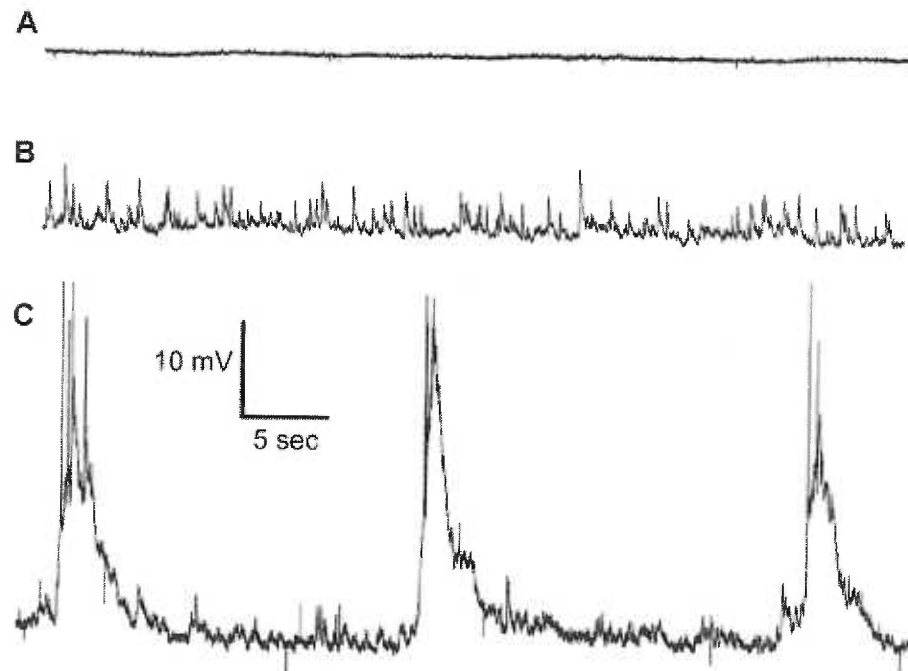
Figure 2.3

Figure 2.3. Spontaneous Activity in the Resting Membrane Potential - In DACs that did not exhibit spiking activity at rest, the pattern of activity in the resting membrane potential could be classified into 3 groups. DACs belonging to the first group (28%) were quiescent at rest (A), while cells belonging to the second group (30%) exhibited robust uncorrelated synaptic activity (B). The final group (42%) was characterized by slow regular waves of depolarization (C).

Figure 2.4
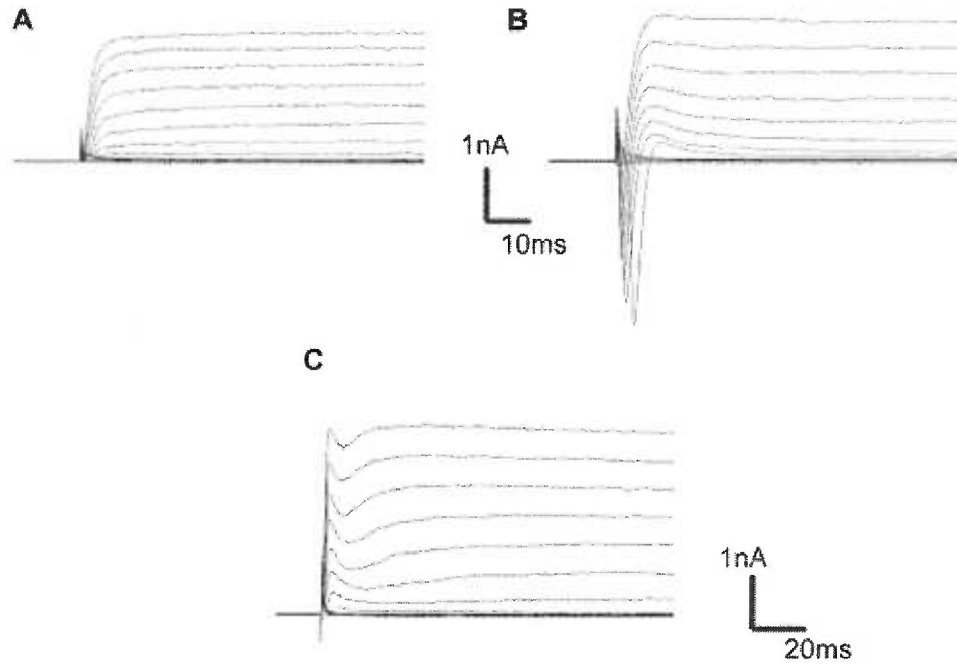
Figure 2.4. Whole Cell Currents – Three General types of whole cell currents observed in DACs under voltage clamp conditions. Voltage steps were in increments of 10mV beginning at –90mV, cells were initially stepped to –100 and back to –90mV to calculate leak current. A total of 15 voltage steps were applied, peaking at 40mV. **A.** Traces from a representative cell from a population of DACs that only displayed a slow outward current upon depolarization. **B.** Traces from a representative cell of a population of DACs that displayed a voltage dependent inward current followed by an outward current in response to depolarization. **C.** Traces from a representative cell of a population of DACs that displayed a rapidly activated transient outward current followed by a slower outward current in response to depolarization.

Figure 2.5
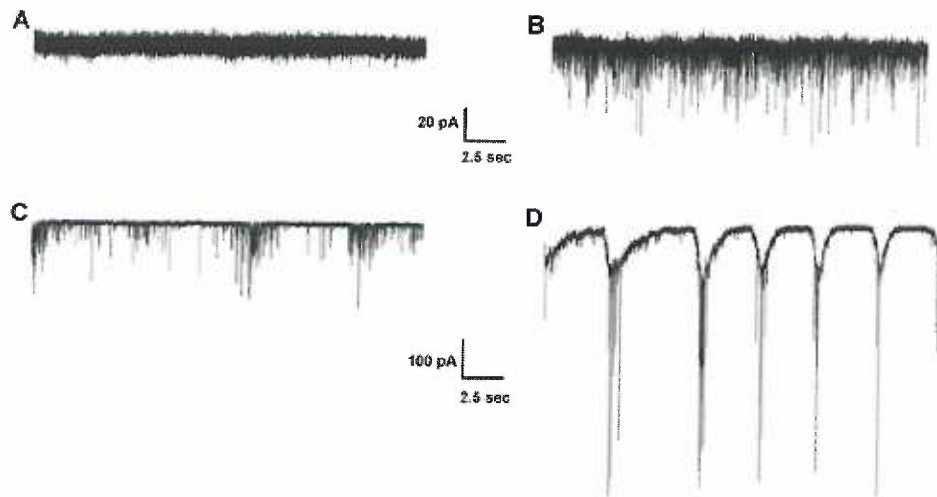
Figure 2.5. Spontaneous Membrane Currents - Whole-cell voltage-clamp

techniques were utilized to examine the currents underlying the different patterns

of activity observed in the resting membrane potential. Approximately 19% of the

DACs examined did not show any synaptically driven membrane currents (A).

Non-rhythmic patterns of synaptic events were observed in 42% of the DACs (B).

Of the remaining 39% of DACs, approximately half exhibited waves of correlated

activity that comprised of bursts of synaptic activity (C), while the rest had regular

waves of inward current (D).

Figure 2.6
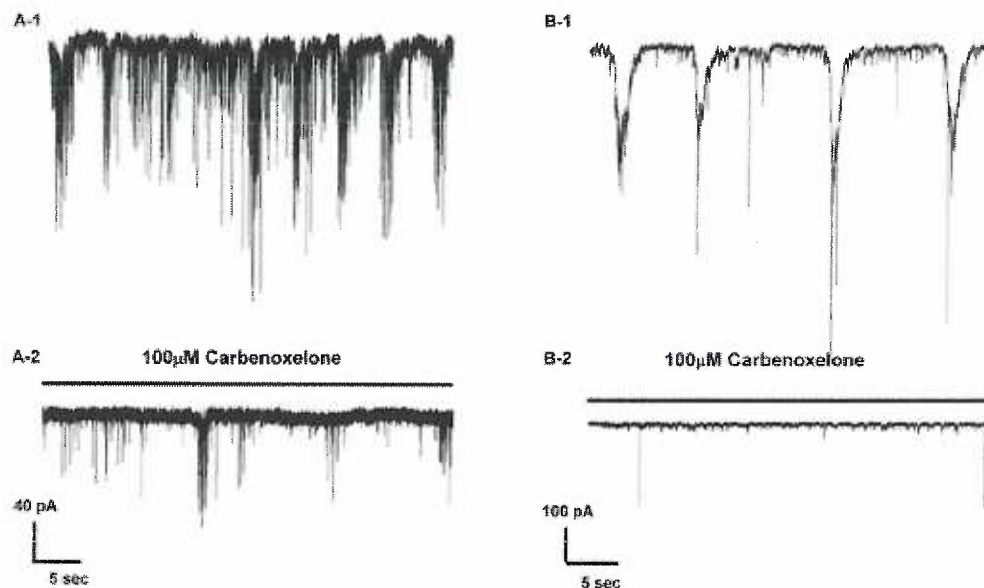
Figure 2.6. Effects of Carbenoxolone on Oscillatory Behavior - Bath application of the gap junction blocker Carbenoxolone (100µM) was utilized to determine whether the oscillatory behavior observed in the membrane potential of some DACs was driven by a network of interconnected neurons. In all cases, Carbenoxolone was successful in blocking the spontaneous oscillatory waves of activity whether they were characterized by correlated bursts of synaptic activity (compare A1 with A2) or waves of inward current (compare B1 with B2).

Figure 2.7
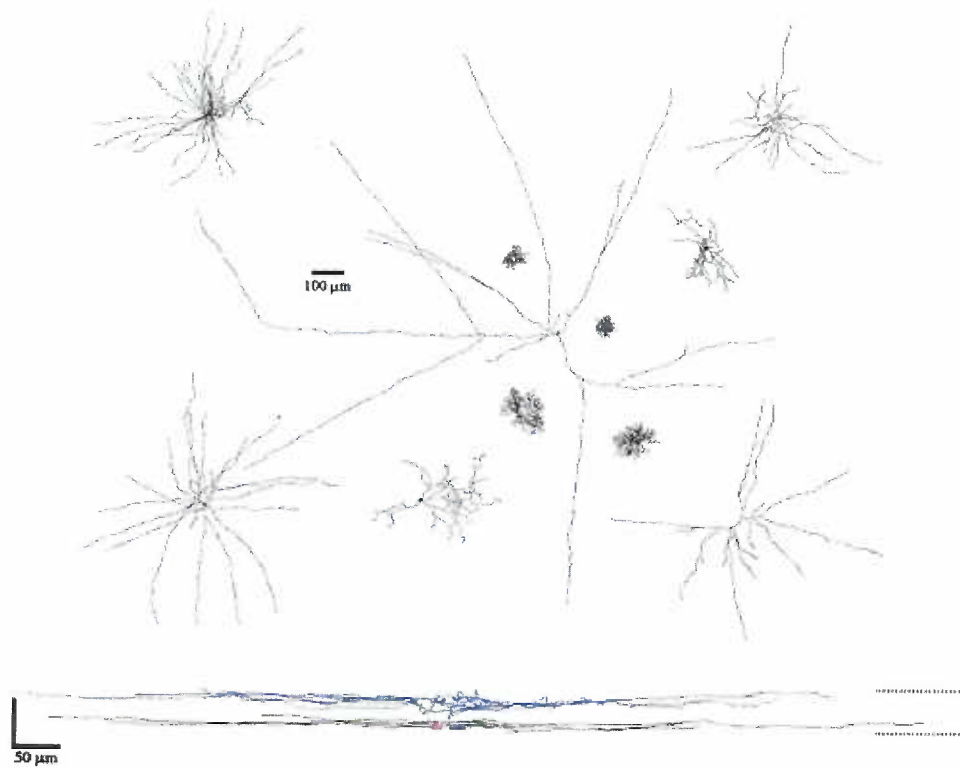
Figure 2.7. Anatomical Diversity of DACs - Shown are Neurolucida reconstructions of successfully processed DACs that illustrate the diverse morphology observed in this population of neurons. Based on the extent of their dendritic arbor, cells could be classified into small-field (<200 μm), medium-field (200 – 500 μm) and large-field (>500 μm). It was generally the case that small-field cells had many more branches in their dendritic tree giving them a more "bushy" appearance. Medium-field neurons also tended to have a much greater degree of branching than large-field DACs. Scale bar is 100 μm. The lower panel shows two representative neurons chosen to illustrate the stratification patterns observed in DACs. One (blue) stratified near sublamina b of the INL whereas the other (black) stratified in sublamina a.

Figure 2.8
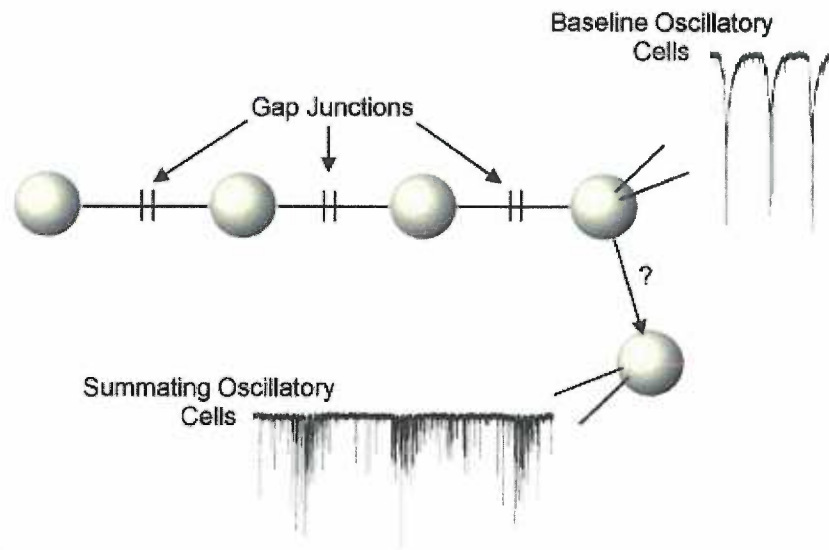
Figure 2.8. Model of Oscillatory Behavior - Model Explaining the Correlated Patterns of Spontaneous Membrane Activity. The different patterns of correlated membrane activity and their sensitivity to Carbenoxolone, could be explained by a network of gap junction coupled neurons ("baseline oscillatory cells") that make synaptic contact with other DACs ("summating oscillatory cells").

Tables

Table 2.1

	Quiet at Rest (%)	Active at Rest (%)	Oscillatory at Rest (%)
Non-Spiking	68	47	41
Spiking	32	53	59
Transient	26	19	35
Sustained	6	34	24

Comparisons of Membrane Activity at Resting Potential and Spiking Activity

Table 2.2

	Small-Field (%)	Medium-Field (%)	Large-Field (%)
Non-Spiking	41	65	34
Spiking	59	35	66
Transient	46	19	21
Sustained	13	16	45
Quiet at Rest	31	38	25
Active at Rest	30	20	30
Oscillatory	39	42	45

Comparison of the functional properties of DACs with the extent of their dendritic arbor.

CHAPTER 3:

MORPHOLOGICAL CHARACTERIZATION OF MAMMALIAN DISPLACED AMACRINE CELLS

Sally A. Aboelela[1], Michael R. Lasarev[2] and David W. Robinson[1*]

Abstract

In the present study, we have conducted a detailed morphological analysis of displaced amacrine cells (DACs) in the ferret retina in attempt to identify groups defined by robust statistical procedures. A total of 55 neurons were filled with Biocytin and, following processing, were reconstructed in three dimensions using the Neurolucida neuronal reconstruction package. Six morphological parameters were chosen, based on their functional relevance: dendritic extent, number of dendritic nodes, area of influence, dendritic distribution index, depth of stratification, and degree of dendritic symmetry. The data for each parameter were then fitted with a mixture of the appropriate number of Gaussian distributions to determine the number of statistically significant groups within each dataset. Neurons within each of these groups were then further analyzed to determine if they were further characterized by any of the other five remaining parameters.

A total of eight morphological groups are discussed in the present study. We discuss six novel groups emerging primarily from combinations of the parameters examined. These cells are termed *small-circular-complex* DACs (~30% of population), *large-noncircular-simple* DACs (~ 40% of population), *radially symmetric* and *non-radially symmetric DACs*, *"ON"* layer stratifying and *"OFF"* layer stratifying DACs. Two more groups were identified based on anatomical similarities to previously described functional INL amacrine cell types; these are the *orientation-biased* and *approach/direction biased* DACs.

Introduction

There is a large population of amacrine cells located in the ganglion cell layer (GCL) of the mammalian retina commonly referred to as displaced amacrine cells (DACs). These cells make up 35% of the neurons in the ganglion cell layer of the rabbit retina (28); (30); (81), 50% in the rat retina (57), and 80% in the cat retina (31). Although the prevalence of this population of amacrine cell across mammalian species is well established, their anatomical diversity and functional role in retinal processing remain largely unknown.

Previous morphological studies of DACs have concentrated on characterizing neurons with similar morphologies to those observed in the inner nuclear layer (INL). For example, in the rabbit retina, 85% of the cells that make up the DAC population have starburst amacrine cell morphology (77). Likewise, amacrine cells have been observed in the GCL of cat retina that morphologically resemble the multiple branched A17 (54), the very wide field A20 (52), and the starburst amacrine cell (60).

Although the presence of amacrine cells in the GCL has been known for more than 20 years (57), there has yet to be a wide-scale study of their morphology similar to that performed on amacrine cells in the INL (52; 38). These past studies utilized the Golgi-staining (57) and a photochemical "Photo-filling" method (38) to survey the detailed morphology of a large sample of INL amacrine cells in an attempt to establish a comprehensive catalog of these neurons. Morphological categorization in these studies relied heavily on dendritic characteristics that were visually apparent. For example, both studies used dendritic extent to initially sort neurons into groups named narrow-field, small-field, medium-field, and wide/large-field. Further sorting was then accomplished

93

using patterns of stratification and specific details of their dendritic architecture (38). The methods used to define the number of groups and their boundaries (e.g. narrow-field vs. small field) were somewhat subjective and lacked rigorous statistical support.

The purpose of the present study is to use the ferret retina to examine the degree of anatomical diversity in mammalian DACs and to provide a detailed structural analysis of these neurons. In addition, we sought to determine the presence of statistically definable groups based on morphological characteristics chosen for their potential influence on neuronal function. The morphological characteristics chosen in this study are concerned with aspects of the dendritic tree such as extent, area, number of nodes, degree of symmetry, and depth of stratification. The functional relevance of these anatomical characteristics is clear when considering several well-defined cells types such as the AII (a small bushy neuron), A17 (a large non bushy neuron), and starburst amacrine cells (a symmetrical neuron whose function changes drastically based on depth of stratification).

To our knowledge, this is the first study to present morphological groups of mammalian DACs defined through rigorous statistical analysis. It is our hope that this examination serves as a starting point to the functional characterization of DACs and a better understanding of their role in retinal processing.

Specific Methods

Tissue Preparation

All procedures were performed in accordance with the approved animal use protocols at the National Institute of Health (NIH) and by the institutional IUCAC committee. Ferrets (Mustela Furo) were given a fatal dose of sodium pentobarbital. The eyes were removed and placed in Eagle's minimum essential media (EMEM). The eyes were then hemi-sected and, under a dissection microscope (Leica GZ4), the retinas removed from the sclera. The retinas were then cut into 4 quadrants and each quadrant cut in half with the peripheral and central portions segregated. Retinal sections were incubated in EMEM bubbled with 95%/5% O_2/CO_2 until they were prepared for filling.

MORPHOLOGICAL ANALYSIS

A −200 mV hyperpolarizing potential was applied to facilitate diffusion of Lucifer Yellow and biocytin into the cell. Once adequate filling was achieved, the retina was fixed in 4% paraformaldehyde for 6-8 hours at 4°C. Following fixation, retinas were processed using a standard diaminobenzidine (DAB) reaction (Vectastain ABC kit). DACs judged to be fully stained by the DAB reaction were analyzed using the Neurolucida neuronal reconstruction system (MicroBrightField). The **dendritic field areas (areas of influence)** were calculated using the area of a complex polygon that encompasses the ends of the dendrites. The software application ImageJ (http: //rsb.info.nih.gov/ij/) was used to calculate the area of this polygon as well as its **circularity** (4π * [area of influence/perimeter^2]).

In-house software routines were used to convert the 2D structure of the neuron into polar coordinates to assess **dendritic extent, dendritic distribution index**, and the **dendritic polarity index**. These routines analyzed a black and white 2D image of a

neuron (1600 x 1200 pixels) and calculated the polar coordinates for each black pixel that made up the soma and dendrites using the center of the soma as the origin (0,0). Therefore, thicker dendrites had a larger number of polar coordinates per unit length of dendrite than did finer ones. The **dendritic extent** was determined by summing the lengths of the longest dendrites in symmetrically opposite 30° ($\pi/6$ radians) regions of the dendritic field.

The **dendritic distribution index** was calculated by dividing the polar plot into 16 equal regions ($\pi/8$ radians), determining the number of black pixels contained in each region, and normalizing these values by the total number of pixels in the whole neuronal structure. The **distribution index** is the minimum number of whole regions required to account for 80% of the total dendritic structure. A value close to 1 indicates that the dendritic mass of a cell is evenly distributed around the soma, while a value close to 0 indicates that the majority of dendrites are restricted to single region. This value does not account for the distance of a particular part of the dendritic field from the soma, or the relationship between the dendritic masses of neighboring regions, but merely gives an indication of how tightly clumped dendrites are in regions of space around the soma.

The **dendritic normalized vector sum (VS_N)** is a form of polarity index and provides a quantitative analysis of how symmetrically distributed the dendritic tree is around the soma. In contrast to the **distribution index**, the VS_N takes into account both the location and the distance of each dendrite with respect to the soma. However, the **polarity index** does not give any information regarding the degree of dendritic clumping that may exist within the whole arbor. To calculate the polarity index, the polar coordinate of each pixel that comprises the dendritic tree was converted into a vector, with a distance and angle

relative to the center of the soma. A **vector sum** was then calculated to determine the resultant vector length and angle. This method cancels symmetrically opposed parts of the dendritic tree and the resultant vector length indicates the degree of polarity within the dendritic arbor. The resultant angle indicates the direction of polarization. By normalizing the resultant vector length by the sum of the lengths of all the vectors, it was possible to compare the degree of polarity across cells with different sizes of dendritic arbor. A neuron with a symmetrical dendritic tree, such as a starburst amacrine cell, would have a VS_N close to 0, whereas a very polarized cell, such as a cortical pyramidal neuron, would have a VS_N closer to 1. While the resultant angle provides information regarding the direction of polarity, the orientation of each neuron analyzed, and its location within the retina, was unknown. Therefore, in the present study a comparison of resultant vector angles across neurons was not meaningful.

Statistical Analysis

Definition of Groups

The distinct groups contained within the observed values for each morphological characteristic were represented by separate Gaussian components. The appropriate number of Gaussian components for each morphological characteristic was determined by increasing the number of components and running successive likelihood ratio tests (25). Fitting was halted when inclusion of an additional Gaussian component failed to significantly increase the log-likelihood. The adequacy of our mixture model (mixture of components) for each morphological characteristic was tested again by comparing the actual percentiles of the data set to the values predicted by our model. In all cases, the correlation was in excess of 0.995. Parameter estimates for each Gaussian component,

such as the mean and standard deviation, were determined using the E-M algorithm (10). This algorithm simultaneously calculated the proportion of data points for a given characteristic that make up each component (i.e. relative contribution of each component to the overall mixture); this proportion is termed the prior probability of group membership.

Graphing the Resulting Distributions

The predicted mixture model for each morphological characteristic is plotted as a smooth continuous line and the data are then added to the graph as a histogram. In these graphs, density is used instead of frequency or count due to the nature of our mixture model. The predicted mixture models had different standard deviations for each component, thereby requiring unequal bin-widths to adequately display the fits. It was therefore necessary to normalize frequency with respect to bin-width; density is equal to frequency divided by the interval (bin-width). Hence, the area of the corresponding rectangles on the histogram represents the relative frequency (proportion) and the combined area of all rectangles equal 100%.

Determining Which Group a Cell Belongs

After calculating the number of Gaussian components contained within each morphological characteristic, we determined which component each cell belonged. This was accomplished by calculating posterior probability - the probability that a given cell belongs to a given component. For every morphological characteristic, the posterior probability is calculated for each cell by dividing its density in each component by its overall density for the mixture model. Posterior probabilities equal to or greater than 0.85 were used to determine the most likely Gaussian component to which a cell belonged.

Cells that did not have a posterior probability of at least 0.85 to any component were described as unclassifiable.

When groups were examined for similarities in other morphological characteristics, significance ($p < 0.05$) was determined using the unpaired Student-t test and values are given as the mean $\pm$ S.D.

Results

A total of 55 DACs were successfully filled, reconstructed and morphologically characterized to determine their dendritic extent, number of dendritic nodes, dendritic distribution index, normalized vector sum (VS_N), dendritic area, and dendritic depth of stratification. The values obtained for each characteristic were fitted with a mixture of an appropriate number of Gaussian components as described in the Methods. To determine which component a particular value was a member, the posterior probability that a given value belonged to a specific Gaussian component was calculated for each data point (c.f. Methods). Neurons with observations that could not be placed into any of the distributions were termed unclassifiable. A summary of the statistical analysis that we conducted on the morphological characteristics of DACs is shown in Table 3.1. The analysis for number of dendritic nodes was best fit with a single Gaussian distribution. The mean number of nodes for the 55 DACs studied was 38 ± 33. Clearly the number of nodes in a neuron's dendritic tree is not an appropriate characteristic on which to base a classification scheme. The suitability of using the remaining morphological characteristics as a basis for grouping DACs is described below.

Morphological Groups based on Dendritic Extent

The values for dendritic extent obtained from the 55 analyzed DACs were best fit by two Gaussian components (Figure 3.1). The first group consisted of 24 cells (44%) and had a relatively small average dendritic extent of $200 \pm 82.8\mu m$. The second group (N = 25, 45%) had a larger average dendritic extent of $1125 \pm 455\mu m$. Finally, 6 (11%)

100

of the DACs did not fit into either group. The average dendritic extent of these unclassifiable cells was 411 ± 60 μm.

The DACs in each of the groups based on dendritic extent also exhibited a number of other significantly different morphological characteristics. The dendritic distribution (9.6 ± 1.6), number of nodes (57.4 ± 35.5) and circularity (0.81 ± 0.07) of the neurons in the first group were significantly higher ($p<0.05$) than those measured in neurons belonging to the second group (7.0 ± 2.3; 20.4 ± 17.8; and 0.62 ± 0.15, respectively). Therefore, DACs with the smallest extent values also tended to have dendritic arbors that were more circular in shape, more evenly distributed around the soma, and more highly branched than those observed in DACs with the largest extents.

Morphological Groups based on Area of Influence

Due to the extremely large range in the calculated areas of influence (3146 to 2.5 x 10^6 μm^2) the log of the area was used to aid the fitting of the mixture of Gaussian components to the data. The areas of influence were best fit with three components (Figure 3.2) with means of 4400 ± 1004 μm^2 (N=5, 9%), 29535 ± 13197 μm^2 (N = 19, 35%) and 622072 ± 563891 μm^2 (N=20, 36%). Of the total population, 11 cells (20%) did not fit into any of the 3 distributions with a certainty greater than 85%.

The average dendritic distribution and extent were significantly different between all three groups (c.f. Table 3.1). The average circularity index and number of nodes was significantly greater ($p < 0.05$) in neurons belonging to the first group (0.82 ± 0.04; 51 ± 14, respectively) than the third (0.65 ± 0.1; 22 ± 19, respectively). Neurons belonging to the second group had significantly ($p < 0.05$) greater circularity (0.77 ± 0.1), number of

nodes (56 ± 41), and normalized vector sum (0.44 ± 0.2) than neurons belonging to the third group (0.65 ± 0.1, 22 ± 19, 0.31 ± 0.2, respectively).

Morphological Groups based on Dendritic Distribution Index

The calculated dendritic distribution indices for the population of DACs examined were best fit by 2 Gaussian components (Figure 3.3). The first group consisted of 23 DACs (41%) and had a dendritic distribution index of 6.5 ± 2.2. The second group (N = 24, 49%) had a dendritic distribution index of 9.9 ± 0.9. There were 5 DACs (10%) for which it was not possible to determine to which group they belonged. These unclassifiable cells all had dendritic distribution indices of 8. The number of nodes in neurons belonging to the first group was 20.4 ± 16 compared with 53.4 ± 37.3 in the second group ($p < 0.05$). The circularity index was lower in the first group (0.64 ± 0.17) than in the second (0.76 ± 0.13), while the dendritic extent was greater in neurons belonging to first group (950 ± 575 μm) than those in the second (370 ± 320 μm). DACs belonging to the group with the highest distribution indices also tended to be more circular and have smaller extents than DACs belonging to the group with the lowest distribution indices.

Morphological Groups based on Dendritic Stratification

The depths of stratification observed in 51of the 55 reconstructed DACs fit into two statistical groups with only one neuron being unclassified (Figure 3.4). With respect to the distal border of their somas, dendritic trees stratified to an average depth of either 23 ± 4μm (N = 24 or 47%) or 43 ± 8μm (N = 26 or 52%). The two groups based on depth of stratification did not differ significantly in any other morphological parameter.

102

Dendritic Groups Based on Normalized Vector Sum

The normalized vector sum (VS_N) gives a quantitative measure of the degree of

symmetry in the dendritic tree with respect to the cell soma (c.f. Methods). For the 55

DACs in the present study, a mixture of three Gaussian components best fit the

normalized vector sum (Figure 3.5). The first group (0.27 ± 0.1) based on these

distributions contained 58% (N = 32) of the DACs analyzed. Group 2 comprised 13 cells

(24%) with a mean VS_N of 0.53 ± 0.03 and the final group (0.72 ± 0.06) contained 7

DACs (13%). Only three cells could not be placed into a group with any certainty.

DACs belonging to the first group represented those neurons with the highest degree

of symmetry. By comparing the dendritic distribution index of these cells, it was possible

to further subdivide this group into neurons exhibiting **radial** and **non-radial** symmetry

(Figure 3.5-A 1 and 2). DACs within the first group with dendritic distributions greater

than 9 were termed radially symmetric because their dendritic tree was distributed evenly

around the soma giving rise to a low VS_N (Figure 3.5-A1). Radially symmetric cells

comprised 50% (N = 16) of the neurons in the first group and had a mean VS_N of $0.25 \pm$

0.13 and an average dendritic distribution index of 10.5 ± 0.7. A total of 10 (33% of

Group 1) DACs had a distribution index value of less than 9 and were considered to be

non-radially symmetric with respect to their cells bodies (Figure 3.5-A2). Non-radially

symmetric DACs had a mean VS_N of 0.27 ± 0.08 and a mean distribution index of

6.3 ± 1.2. The remaining 6 (17%) group 1 cells had a pattern of symmetry that was not

easily classifiable as either radial or non-radial symmetric. All three subgroups differed

significantly ($p < 0.05$) in their number of nodes and their circularity index

(c.f. Table 3.1). Radial symmetric cells had 55.2 ± 16.9 nodes and a circularity index of

0.77 ± 0.12. Non-radially symmetric cells had 16.9 ± 13.9 nodes and a circularity index of 0.55 ± 0.081.

Discussion

Similar to amacrine cells in the INL, the present study shows that the morphology of DACs is extremely diverse. The approach we adopted statistically sorted cells based on several functionally relevant morphological characteristics and compared similarities between emerging groups. The data collected for each morphological characteristic could be fitted by one, two, or three Gaussian distributions. The number of distributions within each parameter data set formed the basis for defining morphological groups. Several of these groups had additional morphological characteristics that differed significantly. After considering these differences, a number of cell types began to emerge based a combination of several morphological characteristics.

Small-Circular-Complex DACs

Statistical sorting of dendritic extent, dendritic distribution index, and dendritic area revealed a common trend. Three lines of evidence painted a picture of a cell type that is small-field, with dendrites that are circular or evenly distributed about the soma, and branch into a complex dendritic tree (c.f. Figures 3.1-A, 3.2-A and 3.6-A). First, DACs with the smallest extents also had the greatest number of nodes, distribution index (most evenly distributed), and circularity index (most circular) (c.f. Table 3.1). Second, DACs with the greatest distribution indices also had smaller extents and significantly more dendritic nodes than the rest of the sample population. Finally, cells with the smallest areas also had the smallest extents, greatest number of nodes, and largest distribution indices. This type of cell, termed here as **"small-circular-complex"**, comprised approximately 30% percent of the total DACs studied.

105

Previous studies performed on INL amacrine cells used dendritic extent to initially sort cells (37; 38). The narrow and small field amacrine cells described in these studies are the most similar to our small-circular-complex DACs. We have encountered cells within the **"small-circular-complex"** category that morphologically resemble Kolb's (1981) A1-A6, A9, and A11 in addition to MacNeil's (1999) Narrow S1, A8, and AB diffuse cells.

There are many functional implications for a neuron with such a morphological profile. For example, electrical continuity across a neuron's dendritic arbor is more likely for small-field cells (1; 3). Bloomfield (1996) estimated that a cell with a dendritic extent greater than 525μm would require active propagation via voltage-dependent-sodium channels for a signal originating in the soma to reach the distal ends of the dendritic tree. The range of extent diameters for **"small-circular-complex"** cells (81.3 – 335.3 μm) is well under this estimated value. It is important to consider, however, that signal attenuation increases with the number of branch points as well as with extent. The electrical continuity, therefore, is still unclear in these small but highly branched neurons. DACs with the **"small-circular-complex"** morphology may achieve electrical continuity by balancing their extent size and degree of branch with their excitable membrane properties; cells that are too complex to passively propagate signals across even their small extents may employ active propagation.

Large-Noncircular-Simple DACs

In addition to uncovering the **"small-circular-complex cells"**, comparison of groups based on dendritic extent, dendritic distribution index, and dendritic area also

106

uncovered a second cell type that we call **"large-noncircular-simple"** DACs (c.f. Figures 3.1-B, 3.2-C, 3.5-A1 and 3.5-C and 3.6-B). Cells with the largest extents also had the fewest number of nodes and lowest distribution and circularity indices of the neurons studied. Similarly, when cells were sorted by distribution index, the least evenly distributed cells also had the largest extents and least number of dendritic nodes. Finally, DACs with the greatest areas also had the largest extents and the fewest nodes (c.f. Table 3.1). Taken together, this information indicates the existence of a DAC type that is large-field, sparsely branched, with an irregularly distributed dendritic tree. This cell group represents approximately 40% of the total population of DACs studied.

The **"large-noncircular-simple"** DACs comprise a cell type that correlates best with Kolb (1981) and MacNeils's (1999) medium and wide field amacrine cells. Inclusive within the **large-noncircular-simple** population we studied were neurons resembling the A15, A17, A22 (37), and the WF3-2 (38) amacrine cell types.

If **"large-non-circular-simple"** cells (or a subset) were capable of generating spikes, it would permit integration of signals over a larger dendritic area than non-spiking cells. These spiking neurons would then possibly play global regulatory or modulatory functional roles across the large areas of retina that their dendrites span (41). In the case of non-spiking **"large-non-circular-simple"** cells, although the low number of dendritic nodes prevalent in this cell type would aid in signal propagation, the inability to generate spikes would preclude signals from reaching the more distal regions of the dendritic tree. This would create dendritic domains that are electrically isolated from the soma and each other. These isolated domains could act autonomously as local modulators in nearby retinal circuits (41).

107

DACs Grouped Based on Pattern of Symmetry

When the dendritic arbors of DACs were examined for their degree of symmetry with respect to the soma (VS_N), the data was best fit by three distributions. The first of these distributions represents cells with the highest degree of symmetry and lowest VS_N. Further analysis of this group of neurons revealed two cell types based on the pattern of symmetry. A total of 50% of the cells in the first distribution VS_N had a dendritic tree that was evenly distributed and had a high circularity index (c.f. Table 3.1). We term this group **"radially symmetric"** (Figure 3.5-A1). In contrast to the **"small-circular-complex cells"**, which also had evenly distributed, circular dendritic trees, the dendritic extents of **"radially symmetric"** DACs were significantly larger and more variable.

From a functional perspective, radial symmetry has the potential to endow a cell with specialized integrative capabilities. The ability to receive symmetrical and equivalent input radially across the dendritic tree could be used to ensure that no orientation bias is imposed on the signal. However, the excitatory vs. inhibitory nature of the synaptic input can be varied across the cell to select for a preferred direction. The starburst amacrine cell, for example, uses its radially symmetric dendritic tree to receive uniform yet functionally opposing light stimulations that move in opposite directions across the cell's dendritic tree (18; 20; 21; 82).

The second cell type to emerge from further analysis of neurons with a high degree of symmetry had low distribution indices indicating spatially confined patterns of symmetry that were not radial about the soma (Fig 3.5-A2). This cell type made up 31% of the DACs in the first distribution of VS_N. These cells also had a significantly lower number of nodes and circularity indices than the **"radially symmetric"** cells. With the

exception of the high degree of symmetry, **"non-radially symmetric"** DACs have many features in common with the **large-noncircular-simple** cells described above: low number of nodes, large dendritic extents, low distribution indices, and low circularity indices. It is possible that the non-radial cells are actually a symmetrical subset of the more encompassing large-non-circular-simple group of cells.

Functionally, **"non-radially symmetric"** cells have much of the same integrative potential as the **"radially symmetric"** cells. The **"non-radially symmetric"** cells, however, have dendritic trees that are far more restricted spatially. Uniform but spatially opposing synaptic input would be confined to the cell's natural axis of symmetry. This feature endows the **"non-radially symmetric cells"** with a natural orientation bias that is not present in the **"radially symmetric"** cells.

DACs Grouped on their level of Stratification

After examining the depths of stratification observed in the sample population of DACs, 47% stratified near the "ON" layer and 52% in the "OFF" layer of the IPL. A subset of the neurons (bistratified) with dendrites terminating in the OFF lamina also had dendrites stratifying in the ON lamina (5/51). In addition, two cells with dendrites terminating in the ON lamina had multiple levels of stratification within this layer. The location of the ON and OFF layers were based on previous estimations in the ferret retina (Shields *et al.*, 2000).

Our results provide strong evidence that DACs are involved in both the ON and OFF circuits within the retina. The only previously studied DAC for which stratification pattern is known is the displaced starburst amacrine cell, which in contrast only projects to the ON lamina of the IPL (19).

109

Previous studies relied heavily on stratification pattern as an additional sorting tool (37; 38). This is especially true for the MacNeil (1999) study, where careful attention was paid to the details of dendritic morphology in the z plane. In agreement with this previous study, we found DACs that were "narrowly-stratified", "diffusely-stratified", and "bistratified". However, when the morphological and physiological parameters of neuronal groups based on stratification were compared, no statistically significant differences were observed. Therefore we found that using the depth of stratification alone was not a useful tool with which to group DACs.

Orientation-Biased and Direction/Approach-Biased Cells

Bloomfield has previously described a group of amacrine cells he termed **"orientation-biased"** based on the distribution of their dendritic arbor (2). These cells were **"orientation-biased"** because a maximal response was only obtained when the light stimuli was oriented with the spatially restricted dendritic tree. In the present study, 11% of DACs possessed dendritic patterns that were spatially restricted to similar regions of space on either side of the soma (Figure 3.6). These neurons morphologically resemble the **"orientation-biased"** neurons described by Bloomfield and presumably have similar response properties.

In 13% of the DACs studied, the dendritic tree was spatially confined to one 180° arc with respect to their somas (Figure 3.6). With respect to a moving light stimulus, such cells would require light to travel in the specific direction or from the specific approach that corresponds to the 180° arc containing 100% of the dendritic density. These cells were categorized as **"direction/approach-biased"** DACs.

Summary

The present study shows that there is an extremely high degree of diversity in the dendritic structure of DACs. However, by using statistical methods, it is possible to sort this diverse population of neurons into clearly defined groups based on a number of functionally relevant morphological parameters. Previous studies took the approach of cataloging amacrine cells based on every permutation of morphology encountered. Although such a catalog can be extremely useful, the purpose of the present study was to identify statistically significant morphological cell types that are most likely to translate into functional groups.

The present study discusses eight groups of DACs, six of which are novel based on our statistical approach and two are based on anatomical similarities to previously described functional cell types. The "*small-circular-complex*" (30% of population) DACs have small, evenly distributed, and bushy dendritic trees while the "*large-noncircular-simple*" (40% of population) cells have larger, irregular, and sparsely branched dendritic trees. As with any statistical trend within a population, there are outliers to both of the above-mentioned groups; for example, there are a few DACs with very large and evenly distributed dendritic trees (Figures 3.3-B and 3.5-A1). We also encountered "*radially symmetric*", "*non-radially symmetric*", "*ON*" layer stratifying, and "*OFF*" layer stratifying DACs. Finally, the last two DAC types (the "*orientation-biased*" and the "*approach/direction biased*" cells) were the only cells to be chosen based on previous accounts and without statistical support.

None of the cell types described above differed significantly in their basic physiological properties. For example, all cell types had similar proportions of spiking

versus non-spiking cells. The functional role of a given DAC must therefore depend upon not only its morphological group but also its distinct physiological properties and pattern of synaptic input.

Figure 3.1
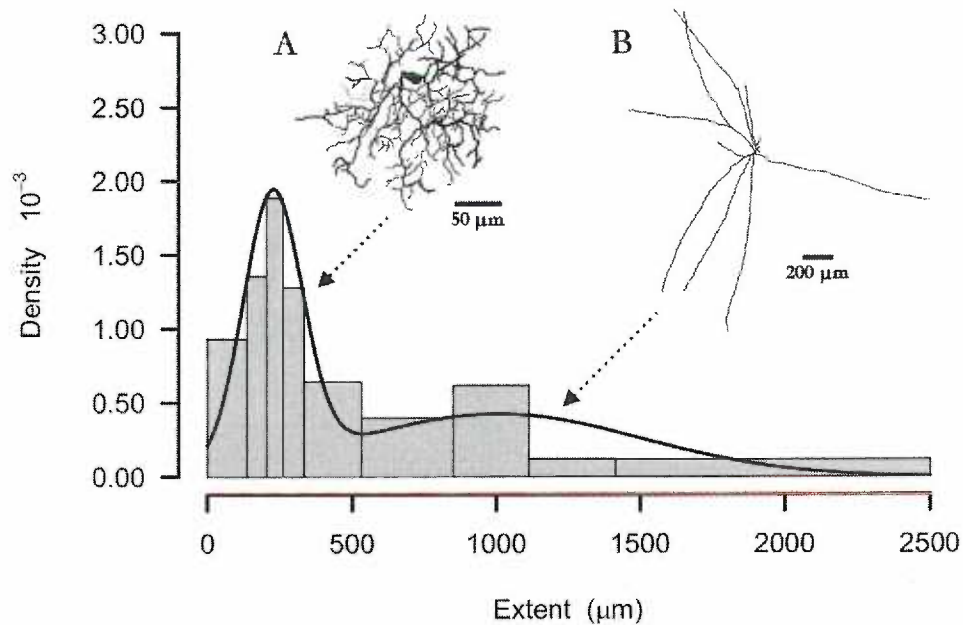
Figure 3.1. Dendritic Extent – The values for dendritic extent for the 55 reconstructed DACs are plotted in a histogram and were best fit with a mixture of 2 Gaussian distributions (solid line; Pearson correlation: 0.993). The measure of density is defined as the relative frequency (proportion) divided by the length of the interval. The mean and standard deviation of the first distribution was 226 and 101 μm, while those of the second distribution were 1004 and 502 μm, respectively. The group to which each DAC belonged was determined by examining the probability of it residing in either the first or second distribution. Of the total population, 24 cells were grouped together with a dendritic extent of 200 ± 82.8μm. A second group comprised 25 cells with a dendritic extent of 1125 ± 455μm. For 6 DACs it was not possible to determine with any degree of certainty which group they belonged. Panels A and B show the morphology of representative cells from the first and second groups, respectively.

Figure 3.2
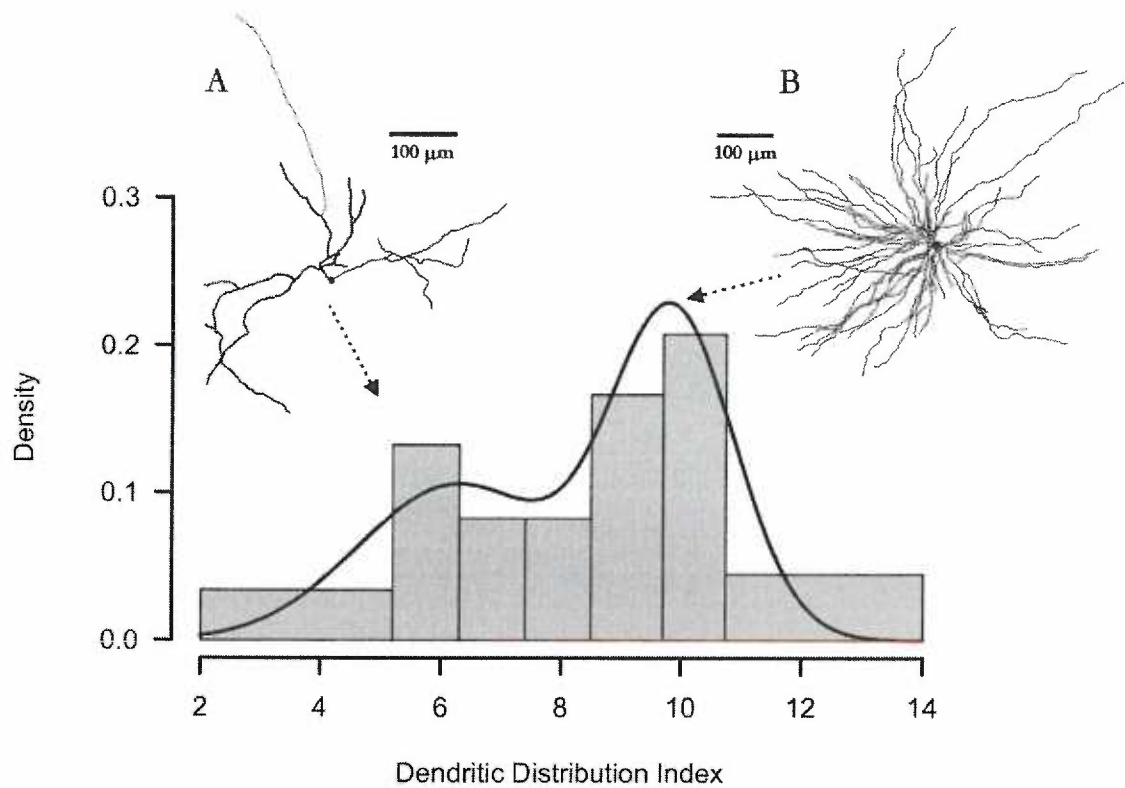
Figure 3.2. Dendritic Distribution Index – The dendritic distribution index gives a

quantitative measure of how regularly the dendritic tree is distributed around the cell soma.

The dendritic distribution indices for 55 DACs are plotted as a histogram and the data were

best fit by a mixture of 2 Gaussian distributions (solid line; Pearson correlation: 0.998). The

mean and standard deviation of the first distribution were 6.2 and 1.6, while for the second

distribution they were 9.8 and 1, respectively. Neurons belonging to the first and second

groups had dendritic distributions of 6.5 ± 2.2 (N=23) and 9.9 ± 0.9 (N=24), respectively.

There were five DACs that could not be placed in one of these two groups with any

certainty. Panels A and B show the morphology of DACs representative of those belonging

to the first and second group, respectively.

Figure 3.3
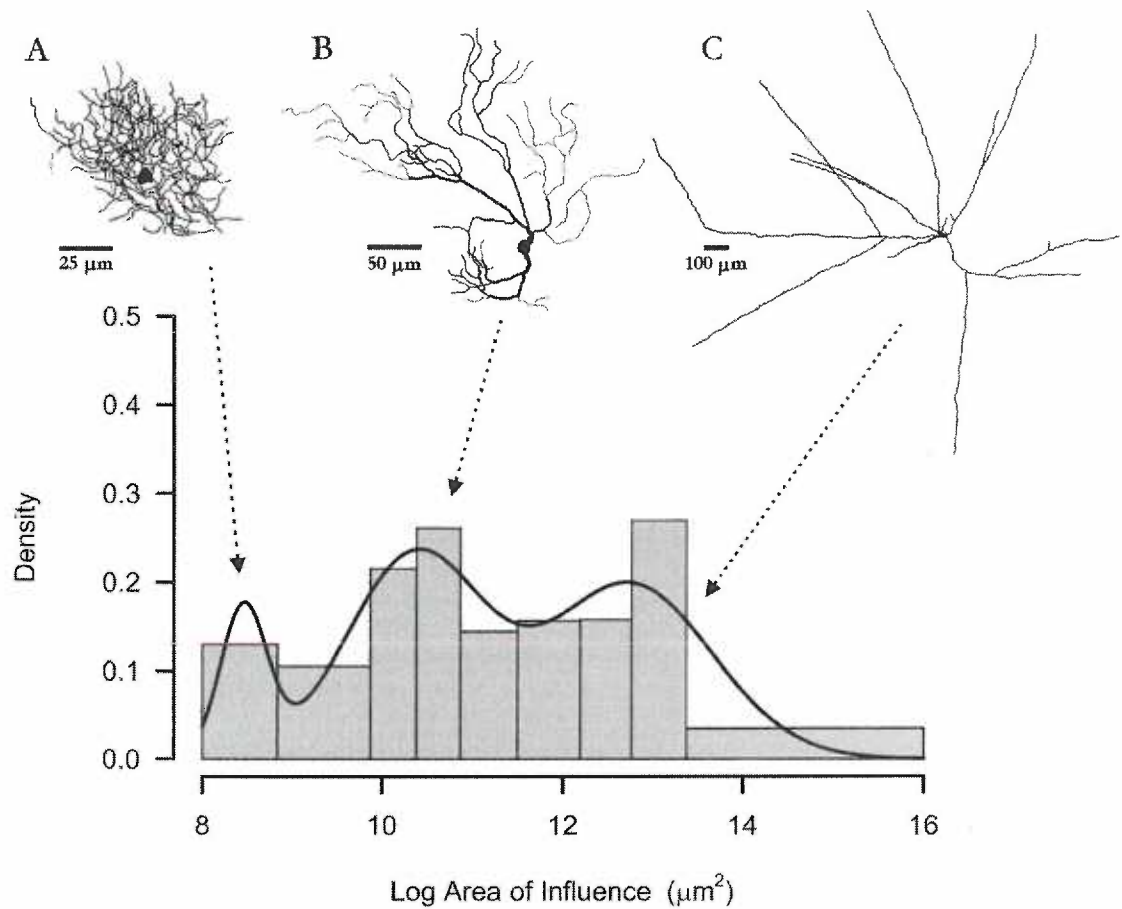
Figure 3.3. Dendritic Area of Influence – The logarithm of the area of influence determined in 55 DACs is plotted in a histogram and the data were best fit with a mixture of 3 Gaussian distributions (solid line; Pearson correlation: 0.999). The mean and standard deviation for each distribution were: 8.5 and 0.3 (first); 10.4 and 0.8 (second); and 12.7 and 0.9 (third), respectively. Neurons were grouped based on the probability of them belonging to one of these three distributions. Neurons belonging to the first, second and third groups had area of influences of $4400 \pm 1004 \ \mu m^2$ (N=5), $29535 \pm 13197 \ \mu m^2$ (N = 19) and $622072 \pm 563891 \ \mu m^2$ (N=20). In total, 11 DACs could not be placed in one of the three groups with any certainty. Panels A, B and C show the morphology of representative cells from the first, second and third groups, respectively.

Figure 3.4
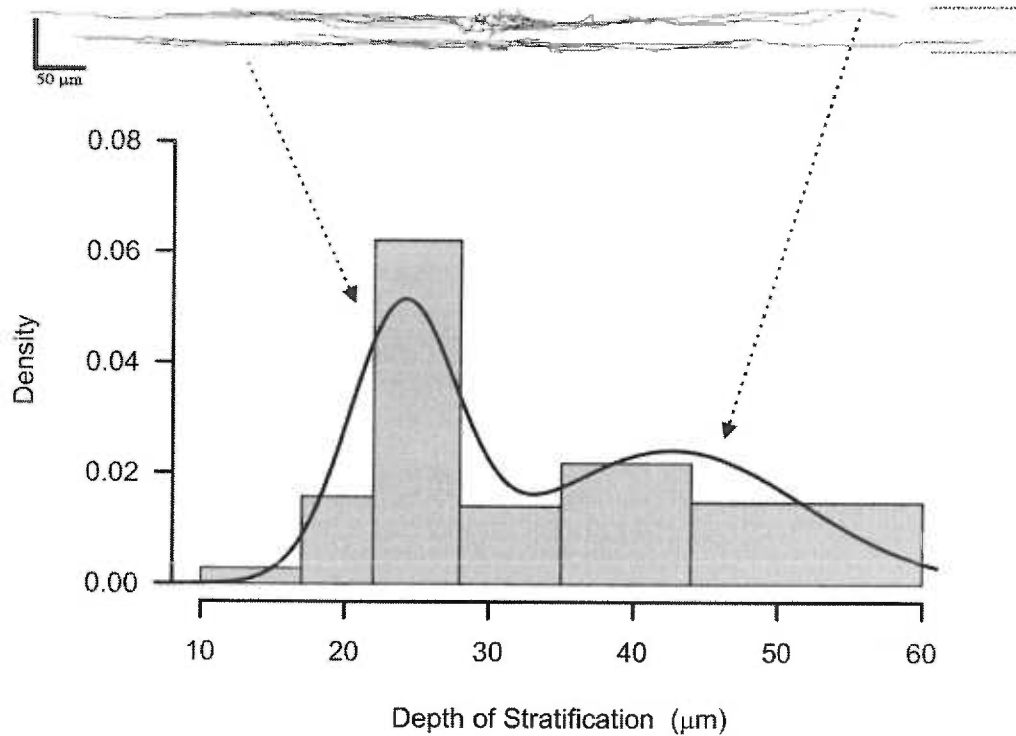
Figure 3.4. Dendritic Stratification - The depth of stratification within the IPL was determined by measuring the distance that the deepest dendrite of each DAC terminated within the IPL. The values obtained are plotted in a histogram and were best fit with a mixture of 2 K Gaussian distributions (solid line; Pearson correlation: 0.995). The mean and standard deviations of the first distribution was 24.4 and 3.7 μm, respectively. For the second distribution the mean and standard deviation were 42.32 and 9.1 μm, respectively. Neurons were grouped based on the probability of them belonging to one of these distributions. There were 24 neurons that could be grouped into the first distribution and these had a mean depth of stratification of 23 ± 4μm and 26 placed into the second group with a mean depth of stratification of 43 ± 8μm. Only one neuron could not be placed with certainty into one of the two groups. Above the histogram a panel shows the stratification pattern of 2 DACs belonging to the first and second groups to illustrate the boundaries to which they project within the IPL.

Figure 3.5
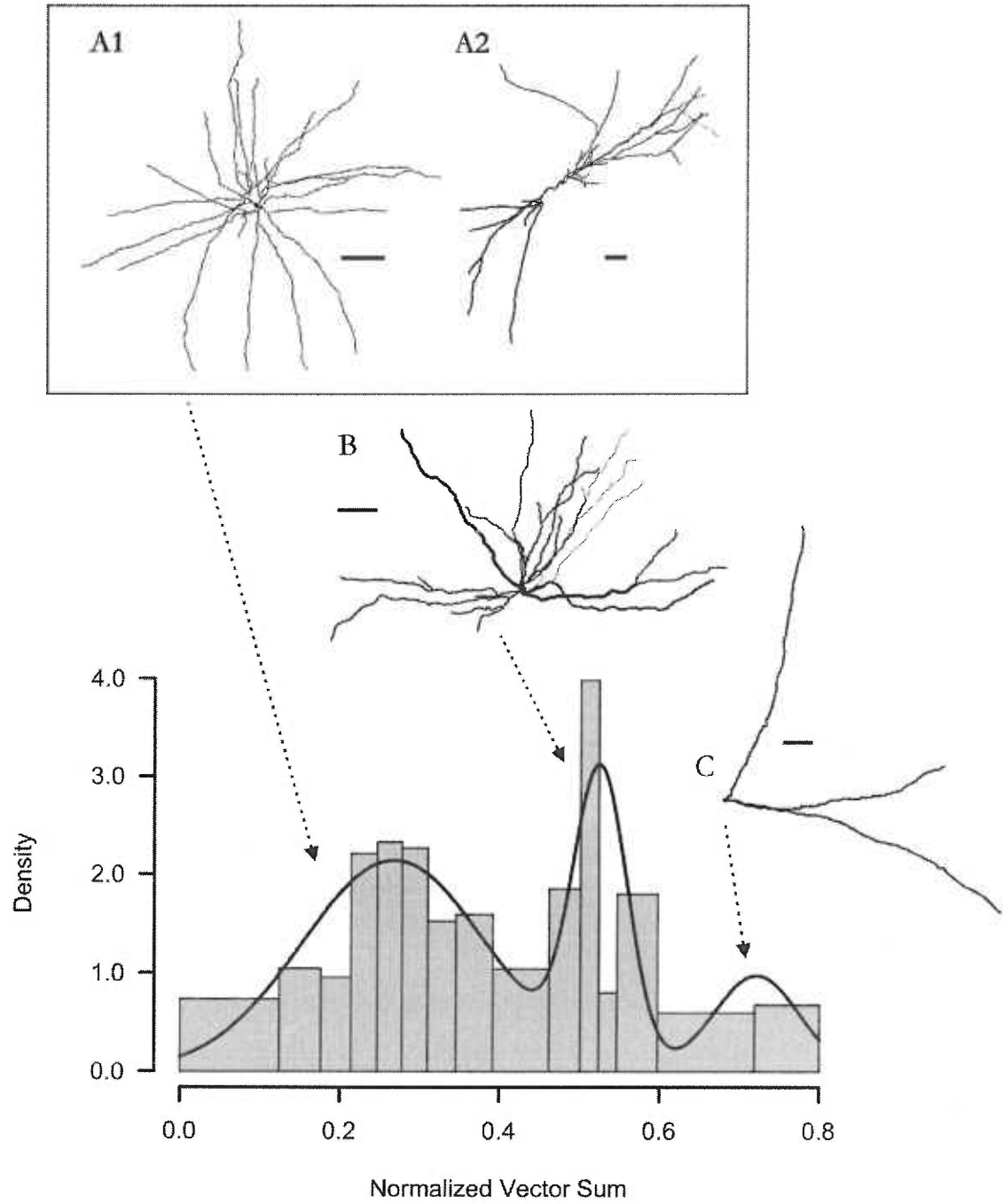
Figure 3.5. Degree of Symmetry **(VS$_N$)** – The normalized vector sum gives a quantitative measure of the degree of symmetry within the dendritic arbor with respect to the cell soma. The values of VS$_N$ for 55 DACs are plotted in a histogram and the data were best fit by a mixture of 3 Gaussian distributions (solid line; Pearson correlation: 0.998). The mean and standard deviation for each distribution were:0.27 and 0.1 (first); 0.52 and 0.03 (second); and 0.72 and 0.05 (third), respectively. Neurons were grouped based on the probability of them belonging to one of these distributions. The first group comprised 32 DACs with a VS$_N$ of 0.27 ± 0.1, while the VS$_N$ of the second (13 DACs) and third groups (7 DACs) were 0.53 ± 0.03 and 0.72 ± 0.06, respectively. Only three cells could not be placed into a group with any certainty. Panels A, B and C illustrate the cells with morphologies representative of neurons belonging to first, second and third groups, respectively. The neurons in the first group have the highest degree of symmetry in their dendritic trees. On closer examination it became clear that neurons in this group were either radially symmetric (A1) or non-radially symmetric (A2). Scale bar = 100 μm.
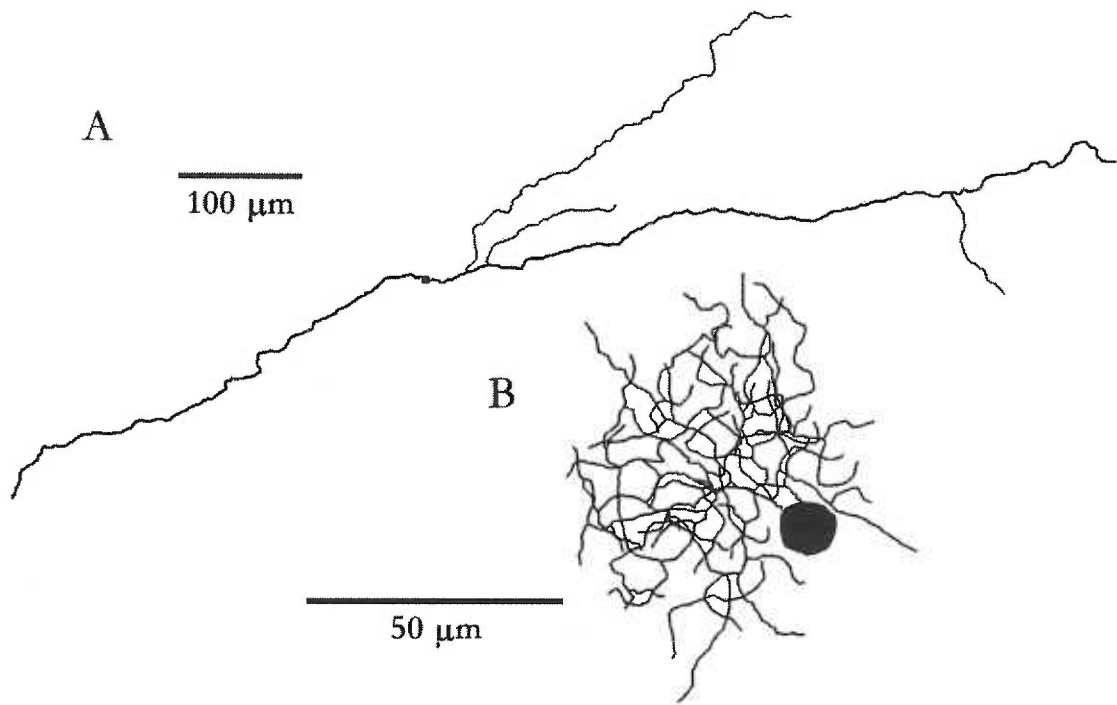
Figure 3.6

Figure 3.6. Orientation-Biased and Direction/Approach-Biased Cells – In the present study, 11% of DACs possessed dendritic patterns that were spatially restricted to similar regions of space on either side of the soma (Panel A). In addition, 13% of the DACs studied had a dendritic tree that was spatially confined to one 180° arc with respect to their somas (Panel B).

Table 3.1

Parameter	Cell Groups	Extent (µm)	Nodes	Distribution	VS_N	Area (µm²)	Stratification (µm)	Circularity
Dendritic Extent	1	200 ± 82.8	57.4 ± 35.5	9.6 ± 1.6				0.81 ± 0.07
	2	1125 ± 455	20.4 ± 17.8	7.0 ± 2.3				0.62 ± 0.15
Dendritic Nodes	1		38 ± 33					
Dendritic Distribution	1	950 ± 575	20.4 ± 16	6.5 ± 2.2				0.64 ± 0.17
	2	370 ± 320	53.4 ± 37.3	9.9 ± 0.9				0.76 ± 0.13
Normalized Vector Sum (VS_N)	1				0.25 ± 0.1			
	Radially Symmetric		55.2 ± 16.9	10.5 ± 0.7	0.25 ± 0.1			0.77 ± 0.12
	Non-Radially Symmetric		16.9 ± 13.9	6.3 ± 1.2	0.27 ± 0.1			0.55 ± 0.081
	Miscellaneous		21.2 ± 9.7	9 ± 0	0.24 ± 0.1			0.65 ± 0.1
	2				0.53 ± 0.03			
	3				0.72 ± 0.06			
Area of Influence	1	94 ± 16	51 ± 14.3	10.8 ± 1.7		4400 ± 1004		0.82 ± 0.04
	2	253 ± 69	56.2 ± 40.5	9.3 ± 1.2	0.44 ± 0.2	29535 ± 13197		0.77 ± 0.1
	3	1240 ± 430	22.1 ± 19	7.3 ± 2.3	0.31 ± 0.2	622072 ± 563891		0.65 ± 0.1
Stratification	1		29.9 ± 29.7				25 ± 2.2	
	2		46.5 ± 36.4				41. ± 8	

120

Chapter 4:

Discussion

The purpose of my thesis was two-fold: to uncover as much as possible about the anatomy and physiology of DACs in the ferret retina and to identify as many functionally relevant groups as possible based of the information I found. To accomplish this goal, I made electrophysiological recordings from a large sample of DACs in both current and voltage clamp mode. Cells were examined for their passive and excitable membrane properties as well as their spontaneous membrane activity. Lucifer yellow and biocytin were included in the recording pipette in order to resolve the anatomy.

Based on my investigation, six physiological and eight morphological groups of DACs were identified. My goal from the outset was to compare the physiological groups to the morphological groups in order to obtain complete cell profiles that could be used to predict functional roles. In reality, comparisons were not possible due to the difficulty of obtaining both reliable physiological recordings and detailed anatomical structure in the same neuron. The number of cells successfully processed for anatomy was 55 out of 195. Among those 55 neurons, the sample sizes for each of the physiological group were too few to draw conclusions any more reliable than pure speculation.

Spiking Ability and Morphology

It would be of great interest to know what proportion of the "small-circular-complex" versus the "large-noncircular-simple" DACs have spiking capabilities. If one were to make the teleological assumption that any given DAC employs strategies to increase the likelihood of its electrical continuity, then several predictions could be made. Electrical continuity allows a neuron to integrate signals across its entire dendritic tree and therefore play a homogenous functional role. One would expect that there would be a greater proportion of spiking cells among the "large-noncircular-simple" compared to the

122

"small-circular-complex" DACs. The average dendritic extent size of neurons comprising the "large-noncircular-simple" anatomical group was 1126 ± 455 μm; cells of this size would require the ability to generate action potentials to maintain electrical continuity across its entire dendritic tree. Out of a total of 10 "large-noncircular-simple" DACs, 40% were non-spiking cells, 30% were transiently spiking cells, and 30% were continuously spiking cells. The preceding observation was surprising; we did not expect to encounter so many non-spiking amacrine cells of that dendritic size. Non-spiking cells of that size would be incapable of maintaining electrical continuity across its entire dendritic tree. The functional implications for this are discussed in greater detail below.

One would also suspect that, among the "small-circular-complex" DACs, cells with the greatest degree of dendritic complexity would have a greater proportion of spiking cells. This prediction is due to the fact that neurons with a highly branched and complex dendritic tree have a more rapid rate of signal attenuation than do cells of the same extent size and fewer dendritic nodes. Although the neurons comprising the "small-circular-complex" anatomical group have the smallest average dendritic extent sizes, they also have the greatest average number of nodes (57 ± 36), which stands to compromise electrical continuity. Interestingly, within the "small-circular-complex" group, the non-spiking neurons had a significantly smaller average dendritic extent size $(171 \pm 103, N = 8)$ than did the spiking neurons $(214 \pm 73, N = 10)$. It's possible that each "small-circular-complex" DAC possesses the proper balance of the two factors that influence signal attenuation the most, extent size and number of nodes, to optimize electrical continuity.

Using Morphological or Physiological Groups To Evaluate Functional Role

The Morphological and Physiological groups of DACs presented in this study all have important implications for function. We hoped to use the morphology and the physiology discovered in this study as a means to identify potential functional groups of DACs. Although rigorously quantitative comparisons were difficult to make with all the groups identified in this study, as explained above, qualitative comparisons did result in some intriguing ideas regarding potential functional roles.

One of the morphological groups described in this study was particularly appropriate for this type of qualitative examination. Approximately 40% of the DACs analyzed for anatomy had the largest average dendritic extent sizes, low average number of dendritic nodes, and circularity index values. These cells, termed "large-non-circular-simple" DACs have morphological characteristics most similar to the A17 amacrine cell, a large dendritic field composed of very thin sparsely branched dendrites. In the case of the A17 amacrine cell, the general functional role is to provide lateral modulation to numerous parallel retinal circuits over a large receptive field. The A17 amacrine cell is capable of generating action potentials and therefore has a receptive field that is at least as large as its dendritic field. Interestingly, nearly half of the DACs conforming to the "large-non-circular-simple" morphology, which were also evaluated for excitable membrane properties, were incapable of generating action potentials. Considering that the average extent size of cells in this morphological group is 1126 ± 455 μm, without the ability to generate action potentials, a cell of that size would have a receptive field far smaller than its dendritic field. In this type of large field non-spiking amacrine cell some or all of its distal sites would most probably be electrically isolated from the soma and the

124

rest of the dendritic tree. Without electrical continuity, these large field amacrine cells would be incapable of engaging in a functional role analogous to the A17 amacrine cell. Instead, these cells could have a very different function that includes an important role for its spatially confined autonomous sites.

Considering that amacrine cells are one of the first cell types to appear during development, these isolated distal regions could play an important developmental role by releasing factors that influence the synaptic organization within its retinal area. Alternatively, these autonomous sites could be acting as local modulators for neighboring retinal circuits, unencumbered by propagation to the soma and therefore capable of responding very rapidly. The advantage of having a large field amacrine cell with multiple electrically isolated distal regions as opposed to several small cells performing the same function is the possibility for more long-term regulation. Functional properties of these distal regions such as neurotransmitter content or presynaptic receptor up/down regulation could be regulated by the soma on a slower time scale in these large field amacrine cells.

It would be of great interest to study these "large-non-circular-simple" DACs further. Examining characteristics such as receptive field size with respect to spiking ability would be useful in determining the accuracy of the speculations made above. As I discuss later however, there are many challenges that need to be addressed before a thorough study of the "large-non-circular-simple" DACs is accomplished.

Oscillatory DACs

The most intriguing physiological cell type to emerge from this investigation was the spontaneously oscillatory DAC. Observed in voltage clamp, there were two general

125

patterns of oscillatory behavior: the "baseline" oscillatory pattern, composed of fluctuations in baseline current, and the "summating" pattern, composed of unitary synaptic events that often summate at peak. It would be of great interest to discover whether members of this physiological cell type share a common anatomy, or if the two subgroups are morphologically distinct. A total of 18 spontaneously oscillatory DACs were analyzed for anatomy. A total of 56% of that sample population possessed the "summating" oscillatory pattern, while 44% displayed the "baseline" oscillatory pattern. As a whole the, standard deviations for all the anatomical characteristics were large. This may indicate a degree of anatomical diversity among this physiological cell type. A larger sample must be taken, however, to confirm this observation. It is possible that oscillatory cells are an anatomically heterogeneous population, but if even one of the oscillatory subgroups share a common morphology, the implications for future study are significant. The likelihood is great that if even some oscillatory DACs share a common physiology and morphology, they may actually represent a single functional amacrine cell group. And not since the "ON" layer stratifying starburst cell has a functionally distinct amacrine cell type been discovered in the Ganglion Cell Layer.

Challenges to Present and Future Study

As illustrated by this body of work, there are inherent difficulties in attempting to investigate a single physiological and/or morphological type of DAC. The present study identified four physiological groups and four anatomical groups (using strictly statistical measures) of DACs in the adult ferret retina. One of the initial goals for this study was to compare the morphological groups to the anatomical groups in order to identify potential functional groups. Several factors contributed to the low sample sizes within each

morphological/physiological group (e.g. non-spiking small-circular-complex DACs). These factors included, the success rate of the physiological determination, the abundance of the morphological and/or physiological cell type, and the success rate of the anatomical staining technique. I calculated the initial sample size of random DACs that would be required to ensure (within a 95% confidence interval) that the final sample size of each morphological/physiological group was reasonably large (e.g. $N = 30$, in statistics the number 30 is the boundary for assuming a normal distrobution). These values were determined by first creating a probability tree (example below) then, using the probability values, constructing a 95% confidence interval to determine the initial sample size required to ensure a final sample size of at least 30.

Probability Tree for Spiking Activity and Degree of Symmetry

Radially Symmetric (28% x 30 % x 51% x 93%) = 4%

30%   Non-Radially (18% x 30% x 51% x 93%) = 2.6% Symmetric

Non-Symmetric (54% x 30% x 51% x 93%) = 7.7%

Non-Spiking 51%

Transiently Spiking

Radially Symmetric (28% x 30% x 29% x 93%) = 2.3%

93%   29%   30%   Non-Radially (18% x 30% x 29% x 93%) = 1.5% Symmetric

Non-Symmetric (54% x 30% x 29% x 93%) = 4.4%

Continuously Spiking 20%

Radially Symmetric (28% x 30% x 20% x 93%) = 1.6%

Non-Radially (18% x 30% x 20% x 93%) = 1% Symmetric

30%

Non-Symmetric (54% x 30% x 20% x 93%) = 3%

The probability of obtaining a successful recording of a morphological/ physiological DAC cell type was calculated by the product of all the methodological success rates and the abundances of each trait. The success rate of determining the spiking properties of a given DAC was 93% and the success rate of determining the anatomy of a given DAC was 30%. A total of 28% of all DACs were Non-spiking, while 29% were transiently spiking and 20% were continuously spiking.

A similar tree was constructed for each of the sets of morphological/ physiological DAC cell groups. Once the probabilities were calculated a 95% confidence interval was performed on each. These are the resulting initial sample sizes required to get a final sample size of at least 30 for each of the possible morphological/ physiological cell types.

Spiking vs. Degree of Symmetry:

Non-spiking/ Radially Symmetric: N = 524 – 1073
Non-spiking/ Non-radially Symmetric: N = 823 – 1683
Transiently Spiking/ Radially Symmetric: N = 927 – 1879
Transiently Spiking/ Non-Radially Symmetric: N = 1454 – 2945
Continuously Spiking/ Radially Symmetric: N = 1373 – 2759
Continuously Spiking/ Non-Radially Symmetric: N = 2107 – 4280

Spiking vs. Small-complex and Large-simple:

Non-spiking/ Small-circular-complex: N = 337 – 678
Non-spiking/ Large-noncircular-simple: N = 337 – 689
Transiently Spiking/ Small-circular-complex: N = 586 – 1207
Transiently Spiking/ Large-noncircular-simple: N = 586 – 1186
Continuously Spiking/ Small-circular-complex: N = 855 – 1724
Continuously Spiking/ Large-noncircular-simple: N = 835 – 1694

Spiking vs. ON-OFF Layer Stratifying:

Non-spiking/ ON: N = 306 – 616
Non-spiking/ OFF: N = 275 – 555
Transiently Spiking/ ON: N = 544 – 1093
Transiently Spiking/ OFF: N = 503 – 999
Continuously Spiking/ ON: N = 772 – 1590
Continuously Spiking/ OFF: N = 731 – 1496

Spontaneous Activity vs. Degree of Symmetry:

Quiet at Rest/ Radially Symmetric: N = 1082 – 2149
Quiet at Rest/ Non-Radially Symmetric: N = 1662 – 3370
Active (Synaptically) at Rest/ Radially Symmetric: N = 990 – 2003
Active (Synaptically) at Rest/ Non-Radially Symmetric: N = 1558 – 3142
Oscillatory at Rest/ Radially Symmetric: N = 710 – 1445
Oscillatory at Rest/ Non-Radially Symmetric: N = 1114 – 2241

Spontaneous Activity vs. Small-Circular and Large-Simple:

Quiet at Rest/ Small-circular-complex: N = 678 – 1393
Quiet at Rest/ Large-noncircular-simple: N = 658 – 1341
Active (Synaptically) at Rest/ Small-circular-complex: N = 627 – 1279
Active (Synaptically) at Rest/ Large-noncircular-simple: N = 616 – 1248
Oscillatory at Rest/ Small-circular-complex: N = 461 - 907
Oscillatory at Rest/ Large-noncircular-simple: N = 1807 – 3680

Spontaneous Activity vs. ON-OFF Layer Stratifying:

Quiet at Rest/ ON: N = 627 – 1269
Quiet at Rest/ OFF: N = 586 – 1186
Active (Synaptically) at Rest/ ON: N = 586 – 1175
Active (Synaptically) at Rest/ OFF: N = 524 - 1093
Oscillatory at Rest/ ON: N = 420 – 844
Oscillatory at Rest/ OFF: N = 378 – 782

As expected the sample sizes were prohibitively large. The morphological/ physiological group that required the largest initial sample was the Continuously spiking/ non-radially symmetric DACs. Among these cells, in order to ensure a sample size of at least 30 (with 95% confidence) one must record from between 2107 – 4280 random DACs. The single value for the initial sample size required to ensure that all of the morphological/ physiological groups listed above would contain an N of at least 30 would be 4280; the upper limit. It is important to note that the expectation that each morphological/ physiological group will have a sample size of at least 30, is based on the assumption that each group exists. If some groups turned out to have N values that were far fewer than 30, maybe even zero, then it is possible that they are not naturally occurring combinations of morphology and physiology.

As these calculations illustrate, the current approach is not a realistic method of making statistically rigorous comparisons between physiological and morphological groups of DACs. This fact is made even clearer if one were to consider the rate at which an individual can acquire successful recordings of DACs. I averaged 2-3 successful recordings per animal, per recording day. At that rate one would have to sacrifice 1,712 animals and put in a total of 5 years of recording days. The greatest limiting factor in this process was the anatomical processing which had a success rate of 30%. The best way to improve the approach and lower the initial sample size is to find an anatomical method that has a better success rate. One could also reevaluate the wide-scale nature of the approach taken in this study, although, the alternatives are limited.

The most formidable difficulty in studying DACs is the lack of adequate pre-selection methods. Among DACs, for example, there is no way of knowing whether the cell you are about to patch is a "small-circular-complex" cell, a "large-noncircular-simple" cell, or any other anatomical cell type. And, not until a neuron is successfully recorded from can you determine what physiological cell type.

Using the techniques commonly available, the morphology can only be resolved well after the recording, once the retina has been processed. These techniques are also usually cytotoxic and make subsequent recordings impossible. The pre-selection methods that are currently available are limited to a handful of amacrine cell types that express a few neuropeptides such as serotonin, and acetylcholine. Masland and MacNeil (1999) developed a visualization method that is not cytotoxic, the "photofilling" technique. Unfortunately, this method causes the cell to radiate brightly making it often difficult to resolve detailed dendritic anatomy, especially in smaller field cells. There is another

130

technique that may be useful in morphological pre-selection, but that has only been applied to the retina in a few cases. Lipophillic dies such as DiI or DiO can be globally applied to whole-mount retina using a gene gun (24; 70). Sun et al (2002) used this technique to label 520 ganglion cells with DiI in the mouse retina. In that study, tungsten particles coated with DiI were propelled into whole-mount retina using a Bio-Rad PDS-1000/He Biolistic particle delivery system (gene gun), which employs a gas (helium) pressure "trigger". This technique can completely visualize a very large number of cells residing at the surface. If there was a way to differentiate the die-filled ganglion cells from die-filled amacrine cells, one could selectively record from the DACs that possessed any morphological profile of interest.

Pre-selecting for a specific physiological trait, alternatively, is labor-intensive but possible. As was accomplished in this study for oscillatory DACs, one can patch a DAC, immediately determine if it has the desired physiological trait, and either discard the cell if it does not or proceed if it does. The time required for such an approach depends on the prevalence of the physiological trait of interest. For example, oscillatory DACs made up, on average, 39% of all DACs; so for every 10 DACs successfully patch –clamped only three to four cells were oscillatory and could be included. The further difficulty of resolving the morphology of a physiological DAC type depends greatly on the success rate of the staining method. If the success rate is 50%, for example, then for every 10 cells patched and three to four oscillatory cells recorded from, only one to two cells will be successfully stained and reconstructed. This process is not impossible, but certainly laborious and time consuming at the least.

131

Despite the paucity of rigorous data comparing the physiology and morphology of the DACs examined in this study, numerous novel physiological findings were discovered. These exciting findings have lead to many unanswered questions. For example, what mechanisms underlie the various patterns of excitable membrane properties? It is possible that non-spiking cells lack a voltage gated inward current that is present in both the transient and continuously spiking DACs. This question can be resolved by switching from current to voltage clamp recording modes in the same cell to determine the underlying currents. Also, what determines whether a cell is transiently or continuously spiking? Transiently spiking cells may express a strong Ca^{2+} activated potassium channel, K(Ca), that would extend the after-hyperpolarization (AHP) and prevent the neuron from repolarizing firing further action potentials. If that were true, then application of the K(Ca) blocker, Apamin, would abbreviate the AHP and cause a transiently spiking DAC to spike continuously in response to injected current.

Much of the model proposed at the end of the physiological chapter also still stands to be tested. The nature of the junction between oscillatory cells (baseline oscillatory cells in the model) still needs to be unequivocally resolved. This can be done by several methods. Although the blockade of oscillatory behavior by bath application of Carbenoxolone was strong evidence for electrical junctions between oscillatory DACs, the experiment can be repeated with the blocker in the recording pipette. An attenuation of oscillatory behavior under those conditions would rule out the possibility that the previous results were the result of an upstream blockade. Additionally, it would be interesting to include a low molecular weight tracer such as neurobiotin in the recording pipette to determine the presence of cell coupling and, if so, observe the coupling ratios.

If oscillatory cells were demonstrated to be tracer-coupled to other DACs and intracellular Carbenoxolone was successful at blocking oscillations, then that would be strong evidence indicating these cells are electrically coupled and propagate rhythmic activity through those junctions.

The proposed model also suggests that the "summating oscillatory" cells receive input from the primary network via a putative chemical synapse. If Carbenoxolone, present in the recording pipette, is unsuccessful at blocking oscillatory behavior in summating DACs, that would suggest that electrical junctions do not propagate oscillatory behavior in "summating" cells. This would support the proposed model.

Classification Scheme and an Alternate Approach

An important goal of this study was to develop an appropriate classification scheme in which to manage the extreme diversity of this cell group. As more was discovered, that task proved to be a formidable one. There may be much to learn about attempts to classify any group of amacrine cells from the extensive research done on interneurons in other regions of the CNS. Similar efforts have been put forth to manage the diversity of interneurons, including an attempt to come up with morphological categories. Very few relationships have been found between any morphological and physiological category of central interneurons. Those who study interneurons have been faced with the possibility that there may exist a "staggering number of cell types" (43). This statement adequately describes the current state of amacrine cell research including DACs.

The most promising method of meaningfully categorizing interneurons has been based on the type of synaptic input a cell receives. Specifically, there has been an interest

in the proportion of excitatory versus inhibitory inputs a given interneuron receives. This is accomplished by analyzing the temporal profile of a cell's spontaneous synaptic events. Excitatory events decay far more rapidly than do inhibitory events. Specialized algorithms have been developed to detect and sort spontaneous events based on their decay times. Selective excitatory and inhibitory blockers can then be applied to verify the proportion of inputs. This method is not only a means of sorting interneurons using a criteria that is functionally relevant, but has also been found to be fairly successful. This method can be easily applied to amacrine cell research and may prove to be as useful as it is in interneurons populations.

Conclusion

Despite the passing of decades since the first investigation into DACs, the present study is the first physiological and detailed morphological look at these neurons as a population. Much like the amacrine cells whose somata are located in the INL, DACs are rich in their physiological and anatomical diversity. Five of the six physiological DAC types (non-spiking, transiently spiking, continuously spiking cells, cells that are quiet at rest, and active at rest) have counterparts in the INL. The oscillatory DACs discovered in this study, however, are a novel population in the adult ferret retina. These cells are sure to spark great interest and further study.

The goal to devise a model by which to sort and categorize DACs in a meaningful way was met in an unexpected fashion. Despite the lack of rigorous comparisons between the morphological and physiological data presented here, there did emerge very clear and relevant DAC cell types. The morphological data, for example, successfully sorted DACs using rigorous statistics to produce several visually apparent cell types. All of the

identified cell types identified serve as an initial framework by which further

characterizations and comparisons can be made. The information presented here is an

important foundation for the discovery of potential function cell types of DACs. The

identification of functional groups of will lead to a better understanding of the

contribution DACs make to the various retinal circuits and in-turn retinal processing.

References

1. Bloomfield SA. Relationship between receptive and dendritic field size of amacrine cells in the rabbit retina. *J Neurophysiol* 68: 711-725, 1992.

2. Bloomfield SA. Orientation-sensitive amacrine and ganglion cells in the rabbit retina. *J Neurophysiol* 71: 1672-1691, 1994.

3. Bloomfield SA and Miller RF. A functional organization of ON and OFF pathways in the rabbit retina. *J Neurosci* 6: 1-13, 1986.

4. Bloomfield SA, Xin D and Osborne T. Light-induced modulation of coupling between AII amacrine cells in the rabbit retina. *Vis Neurosci* 14: 565-576, 1997.

5. Bolz J, Wassle H and Thier P. Pharmacological modulation of on and off ganglion cells in the cat retina. *Neuroscience* 12: 875-885, 1984.

6. Boycott B and Wassle H. Parallel processing in the mammalian retina: the Proctor Lecture. *Invest Ophthalmol Vis Sci* 40: 1313-1327, 1999.

7. Boycott BB and Wassle H. The morphological types of ganglion cells of the domestic cat's retina. *J Physiol* 240: 397-419, 1974.

8. Chalupa LM WJ. *The Visual Neurosciences*. MIT Press, 2003.

9. Chun MH, Han SH, Chung JW and Wassle H. Electron microscopic analysis of the rod pathway of the rat retina. *J Comp Neurol* 332: 421-432, 1993.

10. D.M.Titterington AFSUEM. *Statistical Analysis of Finite Mixture Distributions.* John Wiley & Sons, 1986.

11. Dacheux RF and Raviola E. The rod pathway in the rabbit retina: a depolarizing bipolar and amacrine cell. *J Neurosci* 6: 331-345, 1986.

12. Daw NW, Jensen RJ and Brunken WJ. Rod pathways in mammalian retinae. *Trends Neurosci* 13: 110-115, 1990.

13. de l, V, Kurahashi T and Kaneko A. L-glutamate-induced responses and cGMP-activated channels in three subtypes of retinal bipolar cells dissociated from the cat. *J Neurosci* 15: 3571-3582, 1995.

14. DeVries SH and Baylor DA. An alternative pathway for signal flow from rod photoreceptors to ganglion cells in mammalian retina. *Proc Natl Acad Sci U S A* 92: 10658-10662, 1995.

15. Ellias SA and Stevens JK. The dendritic varicosity: a mechanism for electrically isolating the dendrites of cat retinal amacrine cells? *Brain Res* 196: 365-372, 1980.

16. Enroth-Cugell C, Lennie P and Shapley RM. Surround contribution to light adaptation in cat retinal ganglion cells. *J Physiol* 247: 579-588, 1975.

17. Euler T, Schneider H and Wassle H. Glutamate responses of bipolar cells in a slice preparation of the rat retina. *J Neurosci* 16: 2934-2944, 1996.

18. Famiglietti EV, Jr. 'Starburst' amacrine cells and cholinergic neurons: mirror-symmetric on and off amacrine cells of rabbit retina. *Brain Res* 261: 138-144, 1983.

19. Famiglietti EV, Jr. On and off pathways through amacrine cells in mammalian retina: the synaptic connections of "starburst" amacrine cells. *Vision Res* 23: 1265-1279, 1983.

20. Famiglietti EV. Starburst amacrine cells: morphological constancy and systematic variation in the anisotropic field of rabbit retinal neurons. *J Neurosci* 5: 562-577, 1985.

21. Famiglietti EV. Dendritic co-stratification of ON and ON-OFF directionally selective ganglion cells with starburst amacrine cells in rabbit retina. *J Comp Neurol* 324: 322-335, 1992.

22. Fukuda Y, Hsiao CF, Watanabe M and Ito H. Morphological correlates of physiologically identified Y-, X-, and W-cells in cat retina. *J Neurophysiol* 52: 999-1013, 1984.

23. Fukuda Y and Stone J. Retinal distribution and central projections of Y-, X-, and W-cells of the cat's retina. *J Neurophysiol* 37: 749-772, 1974.

24. Gan WB, Grutzendler J, Wong WT, Wong RO and Lichtman JW. Multicolor "DiOlistic" labeling of the nervous system using lipophilic dye combinations. *Neuron* 27: 219-225, 2000.

25. George Casella RLB. *Statistical Inference*. Brooks Cole, 2001.

26. Hampson EC, Vaney DI and Weiler R. Dopaminergic modulation of gap junction permeability between amacrine cells in mammalian retina. *J Neurosci* 12: 4911-4922, 1992.

27. Hartveit E. Reciprocal synaptic interactions between rod bipolar cells and amacrine cells in the rat retina. *J Neurophysiol* 81: 2923-2936, 1999.

28. Hayden SA, Mills JW and Masland RM. Acetylcholine synthesis by displaced amacrine cells. *Science* 210: 435-437, 1980.

29. Holmes WR and Rall W. Estimating the electrotonic structure of neurons with compartmental models. *J Neurophysiol* 68: 1438-1452, 1992.

30. Hughes A and Vaney DI. Coronate cells: displaced amacrines of the rabbit retina? *J Comp Neurol* 189: 169-189, 1980.

31. Hughes A and Wieniawa-Narkiewicz E. A newly identified population of presumptive microneurones in the cat retinal ganglion cell layer. *Nature* 284: 468-470, 1980.

32. John E.Dowling. *The Retina: An Approachable Part of the Brain*. Belknap Pr, 2003.

33. Kolb H. The organization of the outer plexiform layer in the retina of the cat: electron microscopic observations. *J Neurocytol* 6: 131-153, 1977.

34. Kolb H. The inner plexiform layer in the retina of the cat: electron microscopic observations. *J Neurocytol* 8: 295-329, 1979.

35. Kolb H. The architecture of functional neural circuits in the vertebrate retina. The Proctor Lecture. *Invest Ophthalmol Vis Sci* 35: 2385-2404, 1994.

36. Kolb H and Nelson R. Rod pathways in the retina of the cat. *Vision Res* 23: 301-312, 1983.

37. Kolb H, Nelson R and Mariani A. Amacrine cells, bipolar cells and ganglion cells of the cat retina: a Golgi study. *Vision Res* 21: 1081-1114, 1981.

38. MacNeil MA, Heussy JK, Dacheux RF, Raviola E and Masland RH. The shapes and numbers of amacrine cells: matching of photofilled with Golgi-stained cells in the rabbit retina and comparison with other mammalian species. *J Comp Neurol* 413: 305-326, 1999.

39. MacNeil MA and Masland RH. Extreme diversity among amacrine cells: implications for function. *Neuron* 20: 971-982, 1998.

40. Marc RE. Neurochemical stratification in the inner plexiform layer of the vertebrate retina. *Vision Res* 26: 223-238, 1986.

41. Masland RH. Amacrine cells. *Trends Neurosci* 11: 405-410, 1988.

42. Masland RH. Processing and encoding of visual information in the retina. *Curr Opin Neurobiol* 6: 467-474, 1996.

43. McBain CJ and Fisahn A. Interneurons unbound. *Nat Rev Neurosci* 2: 11-23, 2001.

44. McNaughton PA. Light response of vertebrate photoreceptors. *Physiol Rev* 70: 847-883, 1990.

45. Meister M, Wong RO, Baylor DA and Shatz CJ. Synchronous bursts of action potentials in ganglion cells of the developing mammalian retina. *Science* 252: 939-943, 1991.

46. Mellon D, Jr. and Wheeler CJ. Coherent oscillations in membrane potential synchronize impulse bursts in central olfactory neurons of the crayfish. *J Neurophysiol* 81: 1231-1241, 1999.

47. Menger N and Wassle H. Morphological and physiological properties of the A17 amacrine cell of the rat retina.

48. Miller RF and Bloomfield SA. Electroanatomy of a unique amacrine cell in the rabbit retina. *Proc Natl Acad Sci U S A* 80: 3069-3073, 1983.

49. Mills SL and Massey SC. Differential properties of two gap junctional pathways made by AII amacrine cells. *Nature* 377: 734-737, 1995.

50. Muller F, Wassle H and Voigt T. Pharmacological modulation of the rod pathway in the cat retina. *J Neurophysiol* 59: 1657-1672, 1988.

51. Nawy S. The metabotropic receptor mGluR6 may signal through G(o), but not phosphodiesterase, in retinal bipolar cells. *J Neurosci* 19: 2938-2944, 1999.

52. Nelson R. AII amacrine cells quicken time course of rod signals in the cat retina. *J Neurophysiol* 47: 928-947, 1982.

53. Nelson R and Kolb H. Amacrine cells in scotopic vision. *Ophthalmic Res* 16: 21-26, 1984.

54. Nelson R and Kolb H. A17: a broad-field amacrine cell in the rod system of the cat retina. *J Neurophysiol* 54: 592-614, 1985.

55. Neves G and Lagnado L. The retina. *Curr Biol* 9: R674-R677, 1999.

56. Perry VH. The ganglion cell layer of the retina of the rat: a Golgi study. *Proc R Soc Lond B Biol Sci* 204: 363-375, 1979.

57. Perry VH. Evidence for an amacrine cell system in the ganglion cell layer of the rat retina. *Neuroscience* 6: 931-944, 1981.

58. Pourcho RG GD. Substance P-like immunoreactive amacrine cells in the cat retina. *Journal of Comparative Neurology* 275: 542-552, 1988.

59. Pourcho RG. Dopaminergic amacrine cells in the cat retina. *Brain Res* 252: 101-109, 1982.

60. Sandell JH and Masland RH. A system of indoleamine-accumulating neurons in the rabbit retina. *J Neurosci* 6: 3331-3347, 1986.

61. Santiago Ramon y Cajal SATaMG. *The Structure of The Retina*. Springfield, Illinois: Charles C. Thomas, 1972.

62. Schiller PH. The ON and OFF channels of the visual system. *Trends Neurosci* 15: 86-92, 1992.

63. Shapley R. Retinal physiology: adapting to the changing scene. *Curr Biol* 7: R421-R423, 1997.

64. Sharpe LT and Stockman A. Rod pathways: the importance of seeing nothing. *Trends Neurosci* 22: 497-504, 1999.

65. Skinner FK, Zhang L, Velazquez JL and Carlen PL. Bursting in inhibitory interneuronal networks: A role for gap- junctional coupling. *J Neurophysiol* 81: 1274-1283, 1999.

66. Smith RG and Vardi N. Simulation of the AII amacrine cell of mammalian retina: functional consequences of electrical coupling and regenerative membrane properties. *Vis Neurosci* 12: 851-860, 1995.

67. Strettoi E, Dacheux RF and Raviola E. Synaptic connections of rod bipolar cells in the inner plexiform layer of the rabbit retina. *J Comp Neurol* 295: 449-466, 1990.

68. Strettoi E, Raviola E and Dacheux RF. Synaptic connections of the narrow-field, bistratified rod amacrine cell (AII) in the rabbit retina. *J Comp Neurol* 325: 152-168, 1992.

69. Stryer L. Cyclic GMP cascade of vision. *Annu Rev Neurosci* 9: 87-119, 1986.

70. Sun W, Li N and He S. Large-scale morphological survey of mouse retinal ganglion cells. *J Comp Neurol* 451: 115-126, 2002.

71. Taylor WR. Response properties of long-range axon-bearing amacrine cells in the dark-adapted rabbit retina. 1996.

72. Taylor WR and Vaney DI. Diverse synaptic mechanisms generate direction selectivity in the rabbit retina. *J Neurosci* 22: 7712-7720, 2002.

73. Tian N and Slaughter MM. Functional properties of a metabotropic glutamate receptor at dendritic synapses of ON bipolar cells in the amphibian retina. *Vis Neurosci* 12: 755-765, 1995.

74. Traub RD, Kopell N, Bibbig A, Buhl EH, LeBeau FE and Whittington MA. Gap junctions between interneuron dendrites can enhance synchrony of gamma oscillations in distributed networks. *J Neurosci* 21: 9478-9486, 2001.

75. Vaney DI WGYH. The morphology and topographic distributions of substance-P-like immunoreactive amacrine cells in the cat retina. *Proc R Soc Lond B Biol Sci* 237: 471-488, 1989.

76. Vaney DI. A quantitative comparison between the ganglion cell populations and axonal outflows of the visual streak and periphery of the rabbit retina. *J Comp Neurol* 189: 215-233, 1980.

77. Vaney DI. 'Coronate' amacrine cells in the rabbit retina have the 'starburst' dendritic morphology. *Proc R Soc Lond B Biol Sci* 220: 501-508, 1984.

78. Vaney DI. The morphology and topographic distribution of AII amacrine cells in the cat retina. *Proc R Soc Lond B Biol Sci* 224: 475-488, 1985.

79. Vaney DI. Neuronal coupling in rod-signal pathways of the retina. *Invest Ophthalmol Vis Sci* 38: 267-273, 1997.

80. Vaney DI, Gynther IC and Young HM. Rod-signal interneurons in the rabbit retina: 2. AII amacrine cells. *J Comp Neurol* 310: 154-169, 1991.

81. Vaney DI, Peichi L and Boycott BB. Matching populations of amacrine cells in the inner nuclear and ganglion cell layers of the rabbit retina. *J Comp Neurol* 199: 373-391, 1981.

82. Vaney DI and Taylor WR. Direction selectivity in the retina.

83. Vaney DI, Young HM and Gynther IC. The rod circuit in the rabbit retina. *Vis Neurosci* 7: 141-154, 1991.

84. Vardi N, Matesic DF, Manning DR, Liebman PA and Sterling P. Identification of a G-protein in depolarizing rod bipolar cells. *Vis Neurosci* 10: 473-478, 1993.

85. Veruki ML and Hartveit E. AII (Rod) amacrine cells form a network of electrically coupled interneurons in the mammalian retina. *Neuron* 33: 935-946, 2002.

86. Victor JD and Shapley RM. Receptive field mechanisms of cat X and Y retinal ganglion cells. *J Gen Physiol* 74: 275-298, 1979.

87. Volgyi B. Morphology and physiology of the polyaxonal amacrine cells in the rabbit retina. 2001.

88. Volgyi B, Xin D, Amarillo Y and Bloomfield SA. Morphology and physiology of the polyaxonal amacrine cells in the rabbit retina. *J Comp Neurol* 440: 109-125, 2001.

89. Wassle H and Boycott BB. Functional architecture of the mammalian retina. *Physiol Rev* 71: 447-480, 1991.

90. Wassle H, Chun MH and Muller F. Amacrine cells in the ganglion cell layer of the cat retina. *J Comp Neurol* 265: 391-408, 1987.

91. Wassle H, Grunert U, Chun MH and Boycott BB. The rod pathway of the macaque monkey retina: identification of AII-amacrine cells with antibodies against calretinin. *J Comp Neurol* 361: 537-551, 1995.

92. Wassle H, Grunert U and Rohrenbeck J. Immunocytochemical staining of AII-amacrine cells in the rat retina with antibodies against parvalbumin. *J Comp Neurol* 332: 407-420, 1993.

93. Wassle H, Yamashita M, Greferath U, Grunert U and Muller F. The rod bipolar cell of the mammalian retina. *Vis Neurosci* 7: 99-112, 1991.

94. Wong RO. Retinal waves and visual system development. *Annu Rev Neurosci* 22: 29-47, 1999.

95. Wong RO, Chernjavsky A, Smith SJ and Shatz CJ. Early functional neural networks in the developing retina. *Nature* 374: 716-718, 1995.

96. Wong RO and Hughes A. The morphology, number, and distribution of a large population of confirmed displaced amacrine cells in the adult cat retina. *J Comp Neurol* 255: 159-177, 1987.

97. Wong RO and Oakley DM. Changing patterns of spontaneous bursting activity of on and off retinal ganglion cells during development. *Neuron* 16: 1087-1095, 1996.

98. Wong WT, Myhr KL, Miller ED and Wong RO. Developmental changes in the neurotransmitter regulation of correlated spontaneous retinal activity. *J Neurosci* 20: 351-360, 2000.

99. Wright LL VD. The fountain amacrine cells of the rabbit retina. *Visual Neuroscience* 17: 1145R-1156R, 1999.

100. Xin D and Bloomfield SA. Comparison of the responses of AII amacrine cells in the dark- and light-adapted rabbit retina. *Vis Neurosci* 16: 653-665, 1999.

101. Yamashita M and Wassle H. Responses of rod bipolar cells isolated from the rat retina to the glutamate agonist 2-amino-4-phosphonobutyric acid (APB). *J Neurosci* 11: 2372-2382, 1991.

102. Young HM and Vaney DI. Rod-signal interneurons in the rabbit retina: 1. Rod bipolar cells. *J Comp Neurol* 310: 139-153, 1991.

103. Zhang Y, Perez Velazquez JL, Tian GF, Wu CP, Skinner FK, Carlen PL and Zhang L. Slow oscillations (</=1 Hz) mediated by GABAergic interneuronal networks in rat hippocampus. *J Neurosci* 18: 9256-9268, 1998.

104. Zhou ZJ. Direct participation of starburst amacrine cells in spontaneous rhythmic activities in the developing mammalian retina. *J Neurosci* 18: 4155-4165, 1998.